**Institute of Chemistry**
Graduate Program in Biological Sciences (Biochemistry)

# How do antimicrobial peptides destroy membranes?

A Molecular Dynamics perspective

**PhD Thesis**

To obtain the degree of PhD from the
**University of São Paulo**

by

**Peter Park**

Original version of the corrected thesis

**São Paulo**
Date of deposit at the SPG:
09-03-2023

**Universidade de São Paulo**
**Instituto de Química**
Programa de Pós-Graduação em Ciências Biológicas
(Bioquímica)

# Peter Park

## Como os peptídeos antimicrobianos destroem membranas?

Uma perspectiva sob o olhar da Dinâmica Molecular.

Versão original da tese corrigida

**São Paulo**
2023

Ficha Catalográfica elaborada eletronicamente pelo autor, utilizando o programa desenvolvido pela Seção Técnica de Informática do ICMC/USP e adaptado para a Divisão de Biblioteca e Documentação do Conjunto das Químicas da USP

Bibliotecária responsável pela orientação de catalogação da publicação:
Marlene Aparecida Vieira - CRB - 8/5562

Park, Peter
P235h How do antimicrobial peptides destroy membranes? A Molecular Dynamics perspective / Peter Park. - São Paulo, 2023.
142 p.

Tese (doutorado) - Instituto de Química da Universidade de São Paulo. Departamento de Bioquímica.
Orientador: Cuccovia, Iolanda Midea
Coorientador: Lima, Filipe da Silva

1. Peptídeos Antimicrobianos. 2. Dinâmica Molecular. 3. Simulação computacional. 4. Membranas. 5. Vesículas. I. T. II. Cuccovia, Iolanda Midea, orientador. III. Lima, Filipe da Silva, coorientador.

# Contents

# Abstract

Park, P. **How do antimicrobial peptides destroy membranes? A Molecular Dynamics perspective**. 2023. 147p. PhD Thesis – Graduate program in Biochemistry. Institute of Chemistry, University of São Paulo, São Paulo.

Cationic alpha-helical antimicrobial peptides (CHAMP) are potential candidates as novel drugs against resistant bacteria. CHAMPs are short amphipathic, membrane-active peptides in many organisms as part of their innate immune defense system. CHAMPs spark interest in pharmaceutical applications due to their ability to bear less risk of inducing bacterial resistance than conventional antibiotics, selectivity towards bacteria and fungi, and fast antimicrobial action. Their detailed mechanism of action on membranes needs to be clarified. Elucidating CHAMPs' mode of action can provide relevant information that can be used to better design new CHAMPs with higher efficacy and selectivity. Here, we used Molecular Dynamics (MD) simulations to investigate the detailed mode of action of BP100 (H-KKLFKKILKYL-$NH_2$), a promising CHAMP, on membranes. We characterized the initial interaction between a single BP100 and membranes using atomistic simulations. We described peptide flip, a dynamic phenomenon in which BP100 binds to the membranes, rotates and penetrates the membrane core, and causes local membrane effects, such as thinning, negative curvature, and a decrease in lipid lateral diffusion. We show peptide flip is a common step in the CHAMP/membrane interaction, using other similar CHAMPs: Decoralin, Neurokinin-1, and Temporin-L. Using coarse-grained MD, we studied the CHAMPs peptide concentration effect on vesicles, showing CHAMP-induced membrane budding at highly curved regions of negatively charged vesicles at a high peptide:lipid ratios. Our results suggest that the carpet mode of action fits the description of CHAMPs lysis activity, and we discuss the importance of significant hydrophobic residues in CHAMPs design and activity.

**Key words:** Antimicrobial peptides; antibiotics; Molecular Dynamics; drug design; mechanism of action; Coarse-graining MD.

# Resumo

Park, P. **Como os peptídeos antimicrobianos destroem membranas? Uma perspectiva sob o olhar da Dinâmica Molecular.** 2023. 147p. Tese de Doutorado – Programa de Pós-graduação em Bioquímica. Instituto de Química, Universidade de São Paulo, São Paulo.

Peptídeos antimicrobianos catiônicos helicoidais (CHAMP) são moléculas promissoras a serem utilizadas como novos antibióticos contra bactérias resistentes. CHAMPs são peptídeos de sequência curta, anfipáticos, possuem atividade em membranas e podem ser encontrados em muitos organismos fazendo parte do sistema imune inato. Os CHAMPs despertam interesse em aplicações farmacêuticas por terem menos risco de induzir resistência bacteriana em comparação a antibióticos convencionais, seletividade contra bactérias e ação rápida. Contudo, o seu mecanismo de ação detalhado ainda é desconhecido. Neste trabalho, utilizamos simulações de Dinâmica Molecular (MD) para investigar o modo de ação detalhado do BP100 (H-KKLFKKILKYL-$NH_2$), um promissor CHAMP, em membranas. Utilizando simulações atomísticas, caracterizamos a interação inicial entre um monômero do BP100 e membranas. Descrevemos o "peptide flip", um fenômeno dinâmico onde o peptídeo BP100 se liga às membranas, gira e penetra no interior da membrana e causa efeitos locais, como afinamento da membrana, curvatura negativa e diminuição na difusão lateral lipídica. Demonstramos que o "peptide flip" é uma etapa em comum na interação entre CHAMP e membranas, utilizando outros CHAMPs: Decoralin, Neurokinin-1 e Temporin-L. Utilizando coarse-grained MD, investigamos o efeito da concentração de peptídeo em vesículas-modelo de fosfolipídios, mostrando que CHAMPs induzem a protrusão de membranas em regiões de alta curvatura de vesículas negativas em altas concentrações de peptídeo. Nossos resultados sugerem que o modo de ação de carpete melhor descreve atividade de lise dos CHAMPs e discutimos a importância de aminoácidos hidrofóbicos volumosos no design e atividade de CHAMPs.

**Palavras-chave:** Peptídeos antimicrobianos; antibióticos; Dinâmica Molecular; mecanismo de ação, Coarse-graining MD.

# Chapter 1

# Introduction

## 1.1. Sepsis and Antimicrobial Resistance

Sepsis is a life-threatening organ dysfunction caused by a dysregulated host response to infection[1]. In 2020, the World Health Organization (WHO) published its first ever global report on sepsis, calling for global action[2]. It has been estimated that 49 million cases of sepsis and 11 million sepsis-related deaths occurred worldwide in 2017, accounting for approximate 20% of all-cause annual deaths globally[3]. While sepsis can affect any individual worldwide, the highest rates of incidence and mortality of sepsis exist in lower-middle-income countries[3]. In Brazil, for example, it has been estimated that one third of intensive care unit (ICU) beds are occupied by patients with severe sepsis and septic shock, with an overall lethality of 55%[4]

Sepsis treatment consists in using broad-spectrum antibiotics which in turn contributes to the global threat of antimicrobial resistance (AMR). The use of antibiotics in agricultural practices is also a major accelerator in the spread of AMR[5]. In the 2020 Global Antimicrobial Resistance Surveillance System (GLASS) report by WHO[6], it was reported the high median resistance of *Acinetobacter spp.*, a common cause of hospital infections: 41.2% and 63.2% of the isolates were resistant to aminoglycosides and carbapenems respectively, with some countries already reporting 90% to 100% resistance. The most frequently reported

pathogens were, in order, *E. coli, K. pneumoniae, Salmonella spp., Acinetobacter spp., S. aureus, S. pneumoniae, N. gonorrhoeae* and *Shigella spp*[6]. All 8 of them are bacteria and 6 of them are Gram-negative.

Prevention and treatment are strategies to combat AMR. Prevention strategies include public awareness, access to sanitation, increased vaccine coverage, reduction in the misuse of antibiotics in agriculture[7,8] and clinical practices[9], and rapid diagnostics[10]. However, in the treatment front, new antibacterials are urgently needed.

## 1.2. Antimicrobial Peptides

Almost 100 years ago, Alexander Fleming first noticed the presence of a soluble antimicrobial substance in humans[11]. Fleming observed that the nasal secretions from a patient suffering from acute coryza had bactericidal and bacteriostatic properties on bacterial culture plates. He named this new compound as lysozyme because of its capacity to ''lyse'' fully grown bacterial plate cultures. Subsequently, he found lysozyme activity in various human physiological fluids and tissues of animals, as well as egg whites. In 1928, Fleming subsequently discovered that penicillin extracted from the culture of green mold, *Penicillium notatum,* stopped the growth of various bacteria[12].

In 1939, René Dubos isolated from *Bacillus brevis*, a soil bacillus, another antimicrobial substance and named gramicidin and reported that several Gram-positive bacteria underwent lysis when incubated with gramicidin *in vitro* and *in vivo*[13,14]. In the following year it was shown that gramicidin was a heterogeneous mixture of six antimicrobial peptides (AMPs) with alternating L- and D-amino acids[15–17]. Gramicidin displayed antiseptic activity in the treatment of infected wounds on guinea pigs[18], and was the first antibiotic to be manufactured commercially and is available today as an over-the-counter topical antibiotic.

Antimicrobial peptides (AMPs) surged as a promising category of potent antimicrobials that can kill or stall growth of drug resistant

bacteria[19]. The majority of AMPs have the ability to kill microbial pathogens directly, whereas others act indirectly by modulating immunological activities[19]. The majority of AMPs are short (from 10 to 50 amino acids), cationic, and amphiphilic molecules that are found in the innate immune system of virtually all living organisms as integral defense components against pathogenic organisms[20,21]. The ubiquity of AMPs in living organisms shows the virtual endless source of novel antibiotic agents. As of now, a total of 19,896 antimicrobial peptides (February 2023) have been cataloged in the database of antimicrobial activity and structure of peptides (DBAASP v3)[22].

AMPs can be classified based on their secondary structure: the α-helical, β-sheet and extended AMPs[21,23]. Amphiphilic α-helical AMPs usually have no secondary structure in water whereas in non-polar environments, such as membranes, they adopt α-helical conformation. β-sheet AMPs usually contain cysteine residues with disulfide bonds that stabilize their structure[23,24]. Lastly, extended AMPs are peptides that do not possess a specific structural motif but rather are defined by a high content of specific residues, such as histidine, arginine, proline, glycine or tryptophan[21,25].

## 1.3. Mechanism of action

AMPs can display bacteriostatic or bactericidal activity via two different pathways: outer membrane-disruption or targeting intracellular components[19]. However, for either cases, the initial interaction with bacterial membranes or outer bacterial cell wall is a key factor in AMP activity[26].

Bacteria are most commonly categorized in 2 subgroups, Gram positive and Gram-negative bacteria, according to their cell envelope structure. Gram-positive bacteria possess a single thick outer peptidoglycan layer and Gram-negative bacteria are surrounded by two thin peptidoglycan layers and an extra outer layer, rich in lipopolysaccharides (LPS), phospholipids, and proteins[27].

Generally, AMPs display a net positive charge and bacterial membranes are rich in negatively charged LPS (Gram-negative), teichoic acid (Gram-positive) and lipids, such as phosphatidylglycerol, phosphatidylserine, and cardiolipin[28]. The electrostatic interaction between AMPs and bacterial membranes conveys a selective binding of AMPs to bacterial membranes rather than to predominantly neutral eukaryotic membranes[26].

In the intracellular mode of action, AMPs penetrate cells without causing membrane lysis and inhibit directly or indirectly various cytoplasmic components, such as nucleic acids, ribosomes, enzymes, and cell-wall synthesis-related molecules[19]. For example, it was shown that pleurocidin and dermaseptin block ($^3$H)thymidine, ($^3$H)uridine and ($^3$H)leucine uptake in E. coli, showing that they inhibit DNA, RNA and protein synthesis[29]. Both AMPs do not cause damage to the cytoplasmatic membrane at their minimal inhibitory concentrations[29].

In the outer membrane-disruption mode of action, peptides target mainly the phospholipid membrane of bacteria in a peptide:lipid (P/L) ratio dependent manner[30]. It is suggested that at low P/L, AMP are bound parallel to the membrane and as P/L increases, AMPs adopt a perpendicular orientation in relation to the membrane and at higher P/L,

AMPs would form transmembrane pores[19,30]. However, such explanation is too simplistic and cannot accommodate the wide diversity of AMPs and their particular binding modes and membrane permeabilizing actions.

Three models[19] were proposed to explain membrane permeabilization by AMPs. In the barrel-stave model, peptides helices bundle as staves, forming a barrel-like structure with a central lumen. The peptide hydrophobic moiety aligns with the membrane core region while the hydrophilic moiety of the peptide helix faces the central lumen, hydrated with water.

In the toroidal-pore model, alpha-helical AMPs bind and insert into the membrane and bend both monolayers, connecting both leaflet headgroups and creating a pore lined by the lipid headgroups and AMPs. In both models, the formation of pores promotes cell death through bacteria inner content leakage or osmotic shock and lysis.

In the carpet model, cationic AMPs bind parallel to the anionic membrane surface. At higher concentrations, peptides cover the membrane surface in a carpet-like manner and disrupt the membrane in a detergent-like fashion, eventually leading to the formation of micelles. At a threshold P/L, AMPs form toroidal transient holes in the membrane, allowing additional peptides to access the membrane. Finally, the membrane disintegrates and forms micelles after disruption of the bilayer curvature.

## 1.4. Molecular Dynamics

The full understanding of AMPs mode of action on membranes would permit the rational design of new derivatives with higher selectivity and efficacy.

A variety of experimental techniques have been used to assess the mechanism of AMPs activity and their structural properties. For example, microscopy assays reveal how AMPs damage the cell surface of bacteria, shedding light to AMPs targets and modes of membrane permeabilization[31]. Vesicle leakage assays can reveal the critical P/L ratios for membrane disruption and the necessary anionic composition in membranes for AMP permeabilizing activity[32]. Circular dichroism[32,33] and solid-state NMR spectroscopy[34] are used to assess the secondary structure of AMPs in polar and non-polar environments, which provides relevant information on the structure/activity relationship of AMPs.

However, experimental techniques provide macroscopic-averaged insights on a mesoscopic scale. They provide little information on the transition between initial AMP binding to membranes to membrane permeabilization. In order to study the detailed mechanism of AMPs, a detailed description of peptide/membrane interactions at the atomic scale is necessary, focusing on its early and medium stages in the AMP/membrane interaction.

Molecular Dynamics (MD) simulations are invaluable computational tools to study molecular systems in atomistic detail. Their applications cover a wide range of scientific fields, such as Chemistry, Biology, and Material Science, since they combine two features that cannot be captured by experimental methods at the same time, information in atomistic detail and dynamic behavior of the system under study. In MD simulations, atoms are treated as single points with unique properties, such as mass, size, charge, etc. Atoms and molecules can then interact and affect the environment around them.

The position, velocity, and acceleration of atoms are calculated by solving Newton's equations of motion and obtaining the forces acting upon every atom (Eq 1).

$$F_i = m_i a_i = m_i \frac{\partial^2 r_i}{\partial t^2}$$

$$i = 1 \ldots N$$

$F_i$ is the force acting on atom $i$, $m_i$ corresponds to the atom's mass and $a_i$ is the acceleration, which can be obtained by the second derivative of the position $r_i$, as a function of time. $N$ is the total number of atoms in the system.

The time-dependent integration of the classical equations of motion provides a sequence of molecular coordinates with the trajectory of the atoms. Kinetic theory and statistical mechanics are employed to extract thermodynamic properties for the systems under study and to obtain macroscopic data from the microscopic world.

The force that acts on each atom can be calculated from the negative derivative of the potential energy (U).

$$F = -\nabla U$$

The potential energy (U) is the sum of all pair-interactions between atoms. Most commonly, the functional form for U includes two types of terms: interactions between covalently bonded atoms (bonds, angles, and dihedrals) and interactions between non-bonded atoms (Coulomb and van der Waals interactions).

$$U = U_{bonded} + U_{non-bonded} =$$

$$U_{bonded} = \sum_{bonds} \frac{a_i}{2}(l_i - l_{eq})^2 + \sum_{angles} \frac{b_i}{2}(\theta_i - \theta_{eq})^2 + \sum_{torsion-angles} \frac{c_i}{2}[1 + \cos(n\,\omega_i - \gamma_i)]$$

$$U_{non-bonded} = \sum_{Lennard-Jones} 4\varepsilon_{ij}\left[\left(\frac{\sigma_{ij}}{r_{ij}}\right)^{12} - \left(\frac{\sigma_{ij}}{r_{ij}}\right)^{6}\right] + \sum_{Coulomb} \frac{1}{4\pi\varepsilon_0}\frac{q_i q_j}{e_r r_{ij}}$$

Bonds and angles are treated as harmonic oscillators with specific force constants ( $a_i$ , $b_i$ , respectively) and equilibrium values ( $l_{i_0}$ , $\theta_{i_0}$ , respectively). Dihedral angles are represented as periodic functions with specific periodicity determined by $n$, and heights of rotational barriers defined by $c_i$. The van der Waals repulsive and attractive (dispersion) interatomic forces are typically modelled using the Lennard Jones 12-6 potentials and electrostatics forces are computed with Coulomb potentials.

The collection of potential energy equations, parameters, and constants is named forcefield[35]. Forcefields components can be obtained from experimental data and/or quantum mechanical calculations and equations can be adjusted and customized by the user with the goal of achieving parity between simulation and experimental data.

Therefore, the forcefield is pivotal to obtain accurate data from MD simulations. AMBER[36], CHARMM[37], GROMOS[38], OPLS[39] and MARTINI[40] are examples of widely used forcefield families. The parameters of each forcefield are usually specific for discrete types of systems (lipids, proteins, peptides, nucleic acids, polymers, etc).

Major challenges in MD simulations are related to the size of the system and the time scale. A common way to reduce the computational cost is decreasing the level of complexity of a system. Forcefields be then classified in 3 groups: all-atom (AA) forcefields, in which the interaction of every atom is computed; united-atom (UA) forcefields treat non-polar hydrogens implicitly and coarse-grained forcefields clusters groups of atoms into one interaction site, called as bead. As the complexity level decreases, so does the computational cost thus allowing to simulate larger systems for longer time scales.

## 1.5. Objective of this work

This thesis aimed to elucidate how short cationic alpha-helical amphiphilic antimicrobial peptides (CHAMPs) destroy membranes. CHAMPs are widely present in nature and also can be synthesized. They are shorter than most commonly known AMPs, such as melittin, gramicidin, and human defensins, which are known to permeabilize membranes through the toroidal pore model. However, due to CHAMPs shorter size span, transmembrane pore formation would be highly improbable.

We chose BP100 (H-KKLFKKILKYL-$NH_2$) as our model to investigate CHAMPs mechanism of action on model membranes, due to its high selectivity against Gram-negative bacteria, rapid action, and ample experimental description. We used all-atom simulations to study in detail the first steps of BP100 interaction with model membranes and using coarse-grained simulations, we were able to describe how CHAMPs permeabilize membranes.

## 1.6. Thesis outline

**Chapter 1** introduces the reader to the subject this thesis addresses.

**Chapter 2** presents BP100 as the model to study CHAMPs mechanism of action on membranes. Using all-atom simulations, we described peptide flip, a key event for peptide binding on membranes.

**Chapter 3** deals with the membrane outcomes upon peptide binding. We describe in detail the local activity of BP100 on membranes.

In **Chapter 4** we demonstrate that other CHAMPs share similar binding steps and cause membrane alterations as BP100. And by using coarse-graining simulations, we describe the effect of peptide concentration in CHAMPs membrane perturbing action, showing evidence that the carpet mechanism model better describes CHAMPs activity.

Finally, **Chapter 5** shows additional projects in which contributions were made using Molecular Dynamics simulations.

# 1.7. References

1. Singer, M. *et al.* The third international consensus definitions for sepsis and septic shock (sepsis-3). *JAMA - Journal of the American Medical Association* vol. 315 801–810 Preprint at https://doi.org/10.1001/jama.2016.0287 (2016).
2. *Current evidence, identifying gaps and future directions GLOBAL REPORT ON THE EPIDEMIOLOGY AND BURDEN OF SEPSIS.* (2020).
3. Rudd, K. E. *et al.* Global, regional, and national sepsis incidence and mortality, 1990–2017: analysis for the Global Burden of Disease Study. *The Lancet* **395**, 200–211 (2020).
4. Machado, F. R. *et al.* The epidemiology of sepsis in Brazilian intensive care units (the Sepsis PREvalence Assessment Database, SPREAD): An observational study. *Lancet Infect Dis* **17**, 1180–1189 (2017).
5. Reardon, S. Antibiotic use in farming set to soar despite drug-resistance fears. *Nature* (2023) doi:10.1038/D41586-023-00284-X.
6. *Global Antimicrobial Resistance and Use Surveillance System (GLASS) Report.*
7. Mann, A., Nehra, K., Rana, J. S. & Dahiya, T. Antibiotic resistance in agriculture: Perspectives on upcoming strategies to overcome upsurge in resistance. *Current Research in Microbial Sciences* vol. 2 Preprint at https://doi.org/10.1016/j.crmicr.2021.100030 (2021).
8. O'Neill, J. Tackling drug-resistant infections globally: final report and recommendations. Preprint at (2016).
9. Morris, S. & Cerceo, E. Trends, epidemiology, and management of multi-drug resistant gram-negative bacterial infections in the hospitalized setting. *Antibiotics* vol. 9 Preprint at https://doi.org/10.3390/antibiotics9040196 (2020).
10. Bush, K. *et al.* Tackling antibiotic resistance. *Nature Reviews Microbiology* vol. 9 894–896 Preprint at https://doi.org/10.1038/nrmicro2693 (2011).
11. Fleming, A. On a remarkable bacteriolytic element found in tissues and secretions. *Proceedings of the Royal Society of London. Series B, Containing Papers of a Biological Character* **93**, 306–317 (1922).
12. Fleming, A. On the Antibacterial Action of Cultures of a Penicillium, with Special Reference to their Use in the Isolation of B. influenzæ. *Br J Exp Pathol* **10**, 226 (1929).
13. Dubos, R. J. Studies on a bactericidal agent extracted from a soil bacillus: I. Preparation of the agent. Its activity in vitro. *J Exp Med* **70**, 1–10 (1939).
14. Dubos, R. J. Studies on a bactericidal agent extracted from a soil bacillus: II. Protective effect of the bactericidal agent against experimental pneumococcus infections in mice. *Journal of Experimental Medicine* **70**, 11–17 (1939).
15. Sarges, R. & Witkop, B. GRAMICIDIN A. V. THE STRUCTURE OF VALINE- AND ISOLEUCINE-GRAMICIDIN A. *J Am Chem Soc* **87**, 2011–2020 (1965).
16. Sarges, R. & Witkop, B. Gramicidin. VII. The Structure of Valine-and Isoleucine-gramicidin B. *J Am Chem Soc* **87**, 2027–2030 (1965).
17. Sarges, R. & Witkop, B. Gramicidin. VIII. The Structure of Valine- and Isoleucine-Gramicidin C. *Biochemistry* **4**, 2491–2494 (1965).

18. Gause, G. F. & Brazhnikova, M. G. Gramicidin S and its use in the Treatment of Infected Wounds. *Nature 1944 154:3918* **154**, 703–703 (1944).
19. Brogden, K. A. Antimicrobial peptides: Pore formers or metabolic inhibitors in bacteria? *Nature Reviews Microbiology* vol. 3 238–250 Preprint at https://doi.org/10.1038/nrmicro1098 (2005).
20. Mahlapuu, M., Håkansson, J., Ringstad, L. & Björn, C. Antimicrobial peptides: An emerging category of therapeutic agents. *Frontiers in Cellular and Infection Microbiology* vol. 6 Preprint at https://doi.org/10.3389/fcimb.2016.00194 (2016).
21. Zhang, L. J. & Gallo, R. L. Antimicrobial peptides. *Current Biology* **26**, R14–R19 (2016).
22. Pirtskhalava, M. *et al.* DBAASP v3: Database of antimicrobial/cytotoxic activity and structure of peptides as a resource for development of new therapeutics. *Nucleic Acids Res* **49**, D288–D297 (2021).
23. Bahar, A. & Ren, D. Antimicrobial Peptides. *Pharmaceuticals* **6**, 1543–1575 (2013).
24. Nakatsuji, T. & Gallo, R. L. Antimicrobial peptides: Old molecules with new ideas. *Journal of Investigative Dermatology* vol. 132 887–895 Preprint at https://doi.org/10.1038/jid.2011.387 (2012).
25. Izadpanah, A. & Gallo, R. L. Antimicrobial peptides. *J Am Acad Dermatol* **52**, 381–390 (2005).
26. Epand, R. M. & Epand, R. F. Bacterial membrane lipids in the action of antimicrobial agents. *Journal of Peptide Science* **17**, 298–305 (2011).
27. Silhavy, T. J., Kahne, D. & Walker, S. The bacterial cell envelope. *Cold Spring Harbor perspectives in biology* vol. 2 Preprint at https://doi.org/10.1101/cshperspect.a000414 (2010).
28. Sohlenkamp, C. & Geiger, O. Bacterial membrane lipids: diversity in structures and pathways. *FEMS Microbiol Rev* **008**, 133–159 (2016).
29. Patrzykat, A., Friedrich, C. L., Zhang, L., Mendoza, V. & Hancock, R. E. W. Sublethal concentrations of pleurocidin-derived antimicrobial peptides inhibit macromolecular synthesis in Escherichia coli. *Antimicrob Agents Chemother* **46**, 605–614 (2002).
30. Wimley, W. C. Describing the mechanism of antimicrobial peptide action with the interfacial activity model. *ACS Chemical Biology* vol. 5 905–917 Preprint at https://doi.org/10.1021/cb1001558 (2010).
31. Kalfa, V. C. *et al.* Congeners of SMAP29 kill ovine pathogens and induce ultrastructural damage in bacterial cells. *Antimicrob Agents Chemother* **45**, 3256–3261 (2001).
32. Manzini, M. C. *et al.* Peptide:Lipid ratio and membrane surface charge determine the mechanism of action of the antimicrobial peptide BP100. Conformational and functional studies. *Biochim Biophys Acta Biomembr* **1838**, 1985–1999 (2014).
33. Avitabile, C., D'Andrea, L. D. & Romanelli, A. Circular Dichroism studies on the interactions of antimicrobial peptides with bacterial cells. *Sci Rep* **4**, (2014).
34. Misiewicz, J. *et al.* Action of the multifunctional peptide BP100 on native biomembranes examined by solid-state NMR. *J Biomol NMR* **61**, 287–98 (2015).
35. Allen, M. P. Introduction to Molecular Dynamics Simulation Introduction. *Computational Soft Matter: From Synthetic Polymers to Proteins, Lecture Notes* **23**, 1–28 (2004).
36. Ponder, J. W. & Case, D. A. Force Fields for Protein Simulations. *Adv Protein Chem* **66**, 27–85 (2003).
37. Brooks, B. R. *et al.* CHARMM: The biomolecular simulation program. *J Comput Chem* **30**, 1545–1614 (2009).
38. Hermans, J., Berendsen, H. J. C., van Gunsteren, W. F. & Postma, J. P. M. A consistent empirical potential for water–protein interactions. *Biopolymers* **23**, 1513–1518 (1984).

39. Jorgensen, W. L., Maxwell, D. S. & Tirado-Rives, J. Development and testing of the OPLS all-atom force field on conformational energetics and properties of organic liquids. *J Am Chem Soc* **118**, 11225–11236 (1996).
40. Vries, A. H. de. The MARTINI Force Field: Coarse Grained Model for Biomolecular Simulations. 7812–7824 (2007) doi:10.1021/jp071097f.

# Chapter 2

# Binding and flip as initial steps for BP100 antimicrobial actions

This chapter is a slightly modified version of a published article
https://doi.org/10.1038/s41598-019-45075-5

## 2.1. Abstract

BP100 is a short antimicrobial peptide and can also act as a molecule-carrier into cells. Like with other antimicrobial peptides, the precise mechanism of membrane disruption is not fully understood. Here we use computer simulations to understand, at a molecular level, the initial interaction between BP100 and zwitterionic/negatively charged model membranes. In agreement with experimental results, our simulations showed BP100 folded into an alpha helix when in contact with negatively charged membranes. BP100 binding induced the aggregation of negatively charged lipids on mixed membranes composed of zwitterionic and anionic lipids. The peptide in alpha-helix conformation initially interacts with the membrane via electrostatic interactions between the negatively charged lipids and the positively charged residues of the peptide. At that point the peptide flips, burying the hydrophobic residues into the bilayer highlighting the importance of the hydrophobic effect contribution to the initial interaction of cationic antimicrobial peptides with membranes.

## 2.2. Introduction

Cationic antimicrobial peptides (CAMPs) are short-length, amphiphilic, rich in basic residues of the innate immune system of complex organisms, serving as the first defense line against pathogens. CAMPs can potentially give rise to a new generation of drugs due to their broad spectrum of antimicrobial activity against bacteria, rare cases of the appearance of AMP-resistant bacteria, selectivity, and rapid effects. Due to their potential advantage as antimicrobials, new AMPs are increasingly being isolated or synthesized and their properties investigated. Although increasing evidence shows that some AMPs may also act intracellularly, inhibiting proteins[1], nucleic acids[1–4] and cell-wall synthesis[1–5] and inducing cell apoptosis[1,3,5], most of them kill cells by disturbing the membrane's integrity[1,2,6,7]. Several CAMPs seem to disturb the membrane of cells by self-aggregation on the membrane and forming pores beyond a certain peptide/lipid (P/L) ratio threshold[1,2].

BP100 (H-KKLFKKILKYL-$NH_2$), is a hybrid CAMP synthesized by combinatorial chemistry involving parts of two natural AMPs, melittin, and cecropin A [8]. BP100 shows high antimicrobial activity and selectivity against some Gram-negative bacteria, with a promising minimal inhibitory concentration ranging from 2.5 to 5 µM and low cytotoxicity against mammalian cells making this peptide an exciting candidate for therapeutic use[8]. BP100 conformation and activity on model membranes have been extensively analyzed with experimental techniques[9–13]. BP100 has a random coil conformation in solution and zwitterionic bilayers but acquires predominantly alpha-helical and amphipathic conformation in the presence of negatively charged membranes. BP100 is highly mobile on the membrane surface and orients parallel in predominantly negatively charged vesicles[9,10]. BP100 secondary structure formation and bacteria killing performance seem to be directly related to negative charge content in membranes, thus explaining its high selectivity towards negative bacterial membrane and low cytotoxicity against predominantly less negatively charged mammalian cell membranes[11,14].

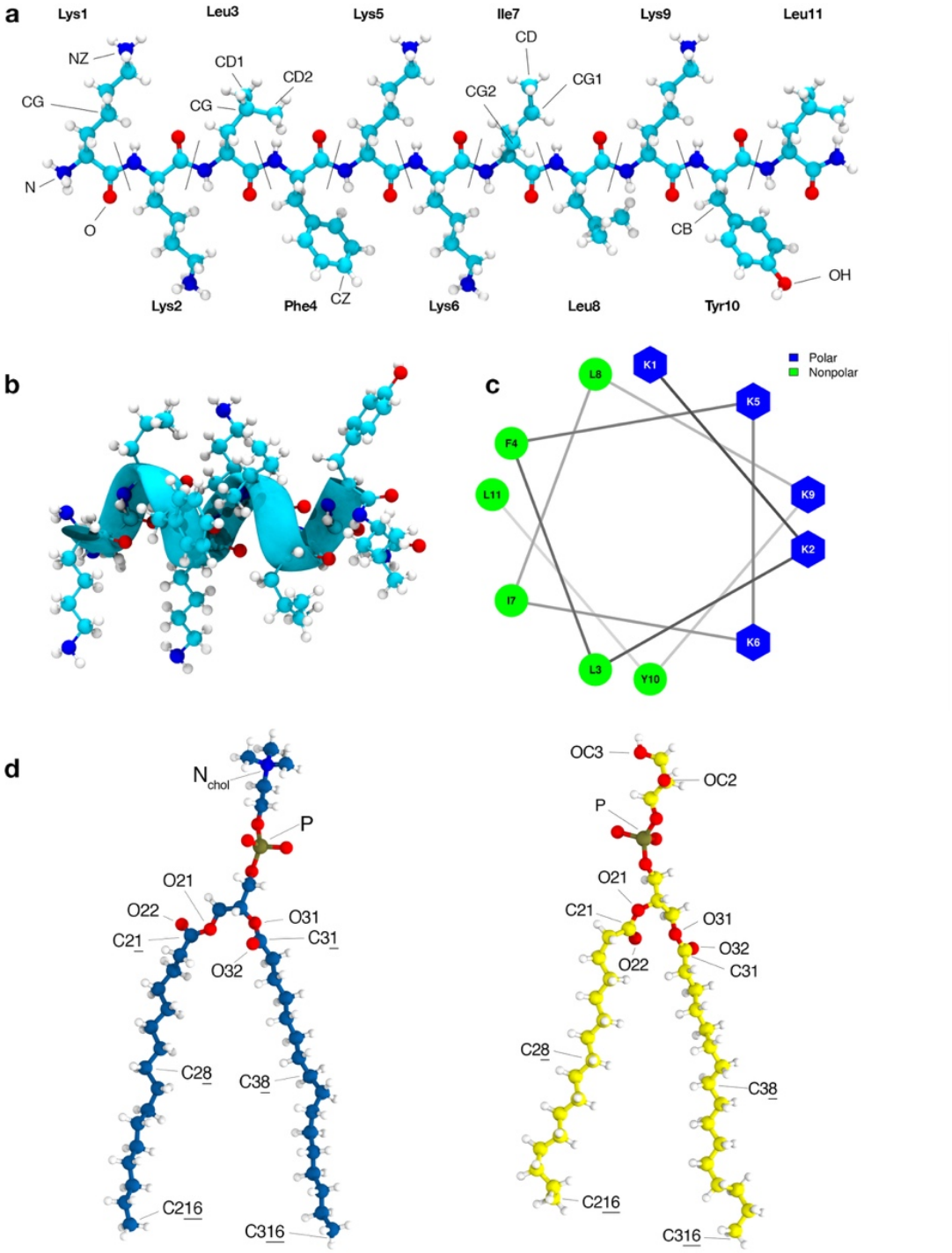


Figure 1. BP100 initial structures: random coil **L**-BP100 (a) and alpha-helical **α**-BP100 (b). Helical wheel projection (c), Lys5 and Ile7 were used as representative residues of polar and apolar moieties, respectively. In (d) DPPC (in blue) and DPPG (in yellow). Atom names are shown for peptide and lipids; they were used in our peptide-lipid pair analysis.

Experimental approaches to investigate peptide/membrane interactions mainly focus macroscopic-averaged insight on a mesoscopic scale. A detailed description of peptide/membrane interactions at the atomic scale may help to gain information on CAMPs disruption mechanisms, permitting the rational design of new derivatives and, therefore, the better therapeutic use of these novel antimicrobials.

Molecular Dynamics (MD) simulations provide atomic-level insights and have been widely used to study the interaction of AMPs with membranes[15–18] . MD simulations were also utilized to study BP100's structure and activity: Wang Y. et al.[17] performed an 8 µs-long MD simulation of BP100 in DMPC bilayer and found that BP100 remained in the surface-bound-state inserting through its C-terminus. They also reported the unfolding of BP100 N-terminus (Lys1 and Lys2) after 1.5 µs, resulting in a tilt angle of 97° and 81% helicity[10,17]. In a study with Brownian Dynamics simulations with a coarse-grained peptide model, Alves et al.[18] simulated BP100 confined in model membranes at 293 K for 1 µs each and reported the high stability of BP100 pre-folded alpha helix and a threefold decrease in its lateral diffusion in POPC: POPG membranes relative to that in POPC membrane[18].

In this work we report simulations, in solution and membranes, extending for more than 25 µs of BP100 and membranes of 1,2-dipalmitoyl-sn-glycerol-3-phosphocholine (DPPC), 1,2-dipalmitoyl-sn-glycerol-3-phosphoglycerol (DPPG), and DPPC: DPPG mixtures (1:1). We systematically investigated the dependence of BP100 secondary structure on DPPG lipids which agrees with experimental findings[11] . We also analyzed the contribution of PG-containing lipid rafts on BP100 conformation and behavior. In most simulations containing DPPG lipids, we observed the occurrence of a dynamic transition of the peptide adsorbed at the membrane interface, where the apolar facet of the BP100 (Fig. 1c), initially exposed to water, rotates toward the membrane interior, leaving the polar facet of the peptide exposed to water. This process, defined here as peptide flip, could be part of CAMPs primary antimicrobial mechanism. Constraining four residues of the peptide into an alpha helix

turn, we observed that the unconstrained regions of the peptide rapidly acquired an alpha-helix conformation in DPPG-containing membranes, suggesting that the formation of these small alpha-helical nuclei in peptide/membrane interactions may be the initial step for the peptide insertion into the hydrophobic core of the membranes.

## 2.3. Methods

All simulations sets were assembled, carried out and analyzed using GROMACS 5.0.2 software package. For trajectories visual inspections and image rendering, VMD 1.9.2 software was used. Table 1 shows all simulation systems and its simulation time. The program used to analyze the hydration shell of the peptide using the Minimum Distance Distribution Function was developed in our group.

### 2.3.1. Lipid bilayers

We used Slipids forcefield[19] parameters were chosen to simulate DPPC, DPPG, and DPPC/DPPG mixed bilayers. 64-lipids-per-monolayer DPPC and DPPG pure membrane topologies were taken from the Slipids developer group website (http://www.fos.su.se/~sasha/SLipids/Downloads.html).

Mixed bilayers of DPPC and DPPG containing 32 DPPCs and 32 DPPGs in each leaflet were constructed using the PACKMOL[20] software. One membrane was composed of randomly distributed lipids (PCPG-NR) on both leaflets and the other, a 4 x 4 DPPG raft was placed in the center of both monolayers (PCPG-R) and the remaining 48 lipids were randomly distributed (Fig. 2).

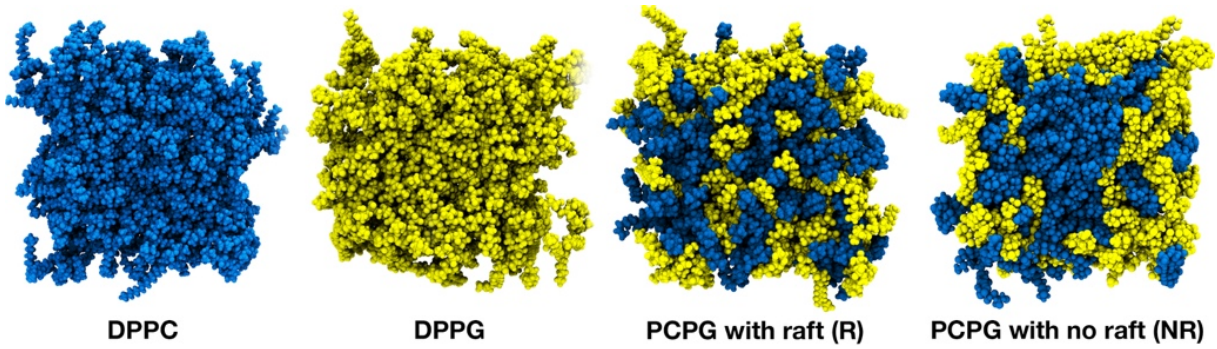


Figure 2. Initial membrane configurations membranes

TIP3P water molecules were used to solvate our systems, with an approximately 53 water/lipid ratio. $Na^+$ ions (Aqvist[21]) were included to counter-balance charges of membranes containing DPPG. All bilayer sets were minimized and equilibrated for 20 ps in a NVT ensemble and thereafter, in NPT conditions for 50 ns. After that, the bilayers were simulated for 860 ns (DPPC), 1100 ns (DPPG) and 1200 ns (for both PCPG-R and PCPG-NR). The area per lipid and membrane thickness were calculated for all membranes and then compared with experimental data and those obtained by Slipids authors (Tables S1 and S2). The last trajectory frames of the membrane simulations were used to build our peptide-lipid systems.

#### 2.3.2. Peptide-in-solution and peptide-lipid systems

Following a study by Beauchamp et al.[22], ff99sb-ildn-NMR force field was chosen to characterize BP100 in our modeling due to its good performance in simulating peptides and proteins structures in TIP3P water when compared with NMR measurements.

BP100 (H-Lys-Lys-Leu-Phe-Lys-Lys-Ile-Leu-Lys-Tyr-Leu-$NH_2$) has an amidated C-terminal and a +6 charge at physiological pH, with all its Lysines and N-terminal amine protonated.

To study secondary structure behavior of BP100 both in solution and in bilayers, two initial BP100 conformations were used: linear BP100 (**L**-BP100) and alpha-helical BP100 (**α**-BP100) (Fig. 1 a, b). In the peptide/water system, one peptide (**α**-BP100 or L-BP100 initial

conformation) were simulated in a cubic box with 3975 TIP3P water molecules for more than 1 microsecond with its +6 charges neutralized with 6 $Cl^-$ ions (Dang[23]). Simulations containing peptides with membranes had a peptide/lipid ratio of 1/128 and the peptide was initially positioned in parallel orientation with the membrane surface approximately 2 nm away. For the α-BP100, additionally, we tested two parallel orientations, where the polar amino acids were facing the membrane and a random orientation. For the perpendicular orientation we tested two ways with either the C-terminal or N-terminal facing the interface. For all these initial conditions, we obtained the same final location and orientation of the peptide that will be discussed in the results section.

To investigate the influence of small core alpha-helical sequences in BP100 to its stability when interacting with bilayers, constrained simulations of BP100 in DPPG membranes were performed. The alpha-helix dihedral angles ($\phi$ = -60°; $\psi$ = -40°) in 3 different regions were fixed: 1-5 (Lys-Lys-Leu-Phe-Lys), 4-8 (Phe-Lys-Lys-Ile-Leu) and 7-11 (Ile-Leu-Lys-Tyr-Leu) residues (Fig. 3). We maintained the constrained regions during the simulations.

Following the previous lipid membrane systems, energy-minimization, NVT, and NPT ensembles were used in the equilibration stage of the MD simulation.

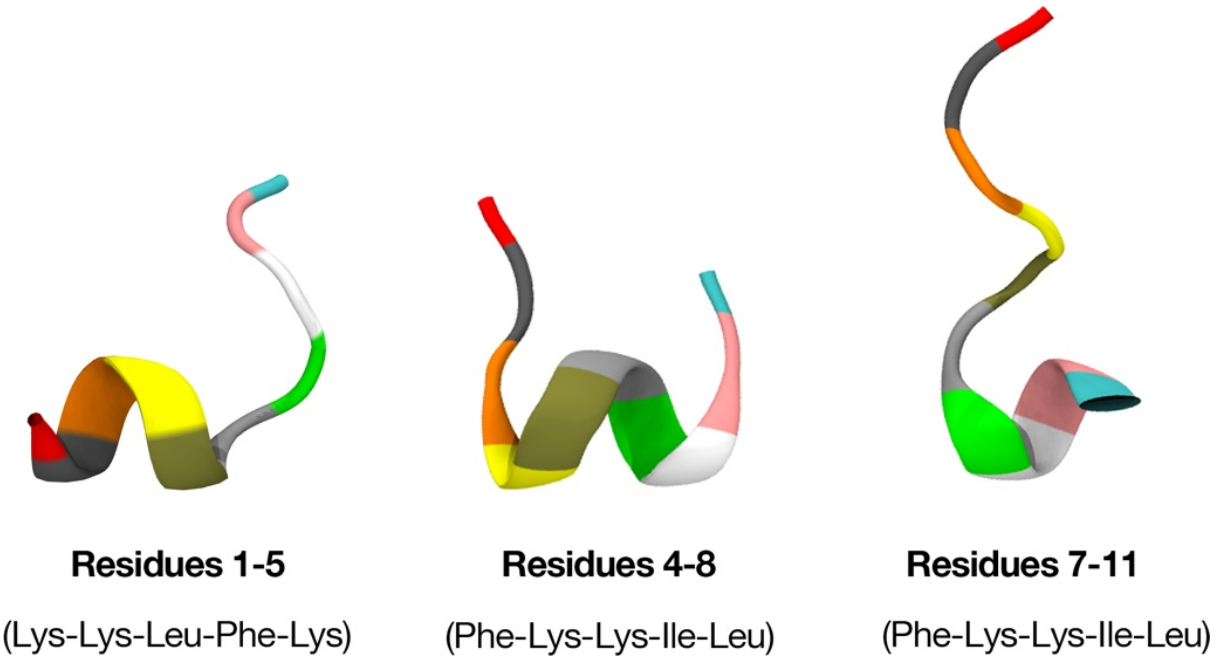


Figure 3. Starting structures for peptides with permanent constrained dihedral angles

### 2.3.3. Simulation details

MD simulations were carried out with a 2 fs time-step with a Leap-Frog integrator [24], in isobaric-isothermal (NPT) ensemble, at 323 K (50$^{o}$C) with temperature coupling treated separately for BP100, lipids, water and ions with the V-rescale thermostat[25]. Atmospheric pressure of 1 bar was kept with the Berendsen barostat[26] and semi-isotropic pressure coupling was used for all systems.

All bonds were constrained with LINCS[27] algorithm. Long-range electrostatic correction was treated by a Particle-mesh-Ewald method[28] with a real-space cut-off of 1.5 nm. van der Waals interactions were truncated at 1.5 nm distance with a switch function from 1.4 nm.

### 2.3.4. Simulation analyses

#### 2.3.4.1. Lipid/peptide contacts

For the computation of lipid contacts with BP100 and pair frequency, we labeled some lipid(s) and BP100 atoms as "polar" or "apolar", based on charges. Then, the radial distribution function (RDF) between each pair of apolar (or polar) atoms of the lipids/BP100 system were computed. The time window selected for computing these RDFs includes that of the membrane bound peptide 250 ns-before and 250 ns-after the peptide flip. The pairs with distinguishable RDF peaks and following minimum were used to analyze the number of polar and apolar contacts between lipids and peptide. A cutoff distance for each pair was defined from the position of the first minimum in the RDF curve, and a contact was defined as a pair of atoms at smaller distance than their corresponding cutoff distance. The simulations were analyzed and the total number of polar and apolar contacts as a function of time was obtained. Additionally, some polar and apolar pairs were analyzed individually.

#### 2.3.4.2. Peptide hydration

The time evolution of the solvent shell surrounding the peptide in its α and L conformations in all simulated membranes was analyzed using the minimum distance distribution function (MDDF, Fig. S5)[29] between the peptide and the water molecules, as well as the average number of water molecules N(r), within a distance r = 0.5 nm, named here as N(0.5). For comparison the MDDF of BP100 in water was used to define the bulk water hydration shell at the same distance (Fig. S5).

| | Simulations | Peptide/Lipid | Waters/Lipid | Time (ns) |
|---|---|---|---|---|
| Bilayers | DPPC | 0/128 | 54 | 860 |
| | DPPG | | 53 | 1100 |
| | PCPG-R | 0/[64/64] | 54 | 1200 |
| | PCPG-NR | | 52 | 1200 |
| Peptide in water | L-BP100 in water | 1/0 | - | 2000 |
| | α-BP100 in water | | - | 2850 |
| Peptide with bilayers | L-BP100 in DPPC | 1/128 | 54 | 1700 |
| | α-BP100 in DPPC | | 54 | 2000 |
| | L-BP100 in DPPG | 1/128 | 53 | 1700 |
| | α-BP100 in DPPG | | 53 | 2000 |
| | L-BP100 in PCPG-R | 1/[64/64] | 54 | 1600 |
| | α-BP100 in PCPG-R | | 54 | 2000 |
| | L-BP100 in PCPG-NR | 1/[64/64] | 52 | 1700 |
| | α-BP100 in PC/PG-NR | | 52 | 2000 |
| Partially constrained peptide in DPPG | α-BP100 (res1-5) in DPPG | 1/128 | 54 | 600 |
| | α-BP100 (res4-8) in DPPG | | 54 | 600 |
| | α-BP100 (res7-11) in DPPG | | 54 | 600 |

Table 1. Table containing all MD simulation sets carried out in this work. For bilayers, we used Slipids forcefield and ff99sb-ildn-NMR for BP100. All sets were simulated at 323 K (above DPPC and DPPG transition temperatures) and 1 bar. **L**-BP100 indicate constraint-free simulations using random coil BP100 as peptide starting configuration and **α**-BP100, as alpha helix. Res1-5, res4-8 and res7-11 indicate simulations with BP100 with permanent constraints on the referred residues.

# 2.4. Results

The 17 sets of simulations (Table 1) were run for more than 25 µs of simulation time, and each unconstrained peptide/membrane simulation had at least 1.6 µs of simulation. After comparing the simulated membrane properties with experimental and other computational studies (Table S1 and S2), we systematically analyzed the peptide conformation in solution and on bilayers, peptide trajectory, and dynamics on membranes and the effect of BP100 on model bilayers. In the following sections, we describe our results.

### 2.4.1 Secondary structure

#### 2.4.1.1. Peptide in solution

To study BP100 secondary structure in water, we did simulations for more than 2 µs with both α-BP100 and L-BP100 initial conformations. Figure 4 shows that BP100 conformation in solution was, predominantly, random coil. Starting with an alpha-helix conformation, the peptide lost the initial alpha helix conformation in approximately 40 ns and occasionally formed an alpha-helix turn in the 5-9 residue region (Fig. 4a). For L-BP100 in solution, we observed a similar pattern (Fig. 4b). Circular Dichroism (CD) shows that BP100 is random in solution[10,11,30] , and our simulations reproduced these data.

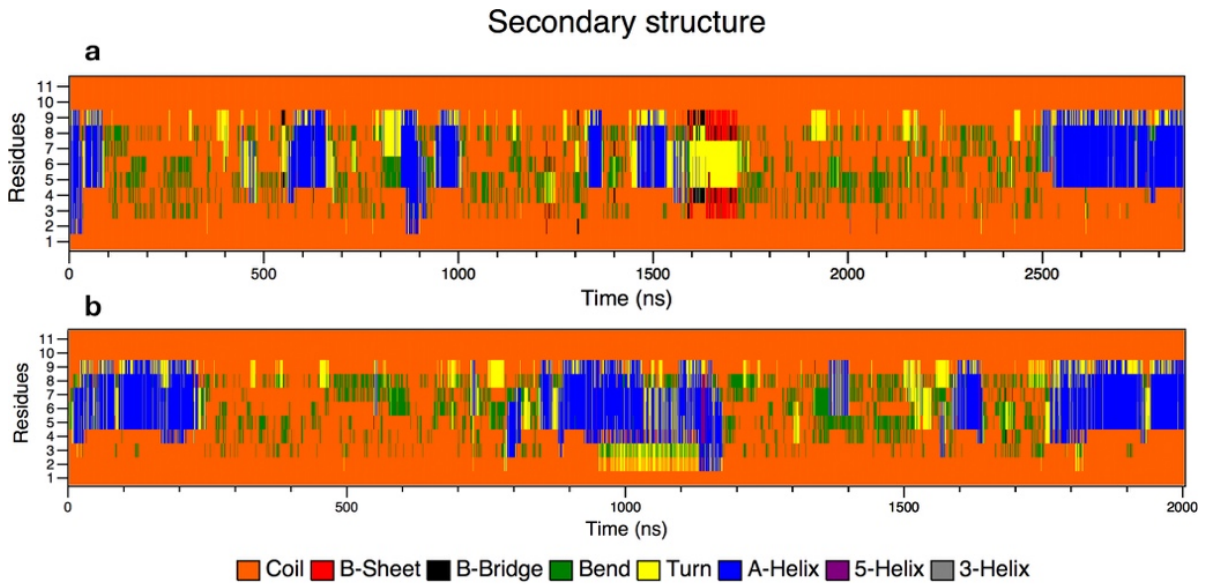


Figure 4. Secondary structure analyses graphs of α-BP100 (a) and L-BP100 (b) in solution. In both cases, the peptide shows predominance in random coil structure (orange) with occasional formation of 1 alpha helix turn (blue) in residues 5 to 9.

### 2.4.1.2. Peptide in bilayers

BP100 conformation, antimicrobial activity, and PG content are related[11]. We simulated α-BP100 and L-BP100 on DPPC, DPPG, PCPG-R, and PCPG-NR at 323 K, above DPPG and DPPC transition temperatures. In all cases, the peptide was rapidly adsorbed on the membranes and diffused laterally. Figure 5 shows that the BP100 alpha-helical conformation was proportional to PG content, as the alpha-helix percentage in DPPC is considerably smaller than that observed in DPPG-containing membranes. Alpha-helix formed in the 5 to 9 residues region (Lys-Lys-Ile-Leu-Lys) was highly stable in all simulations.

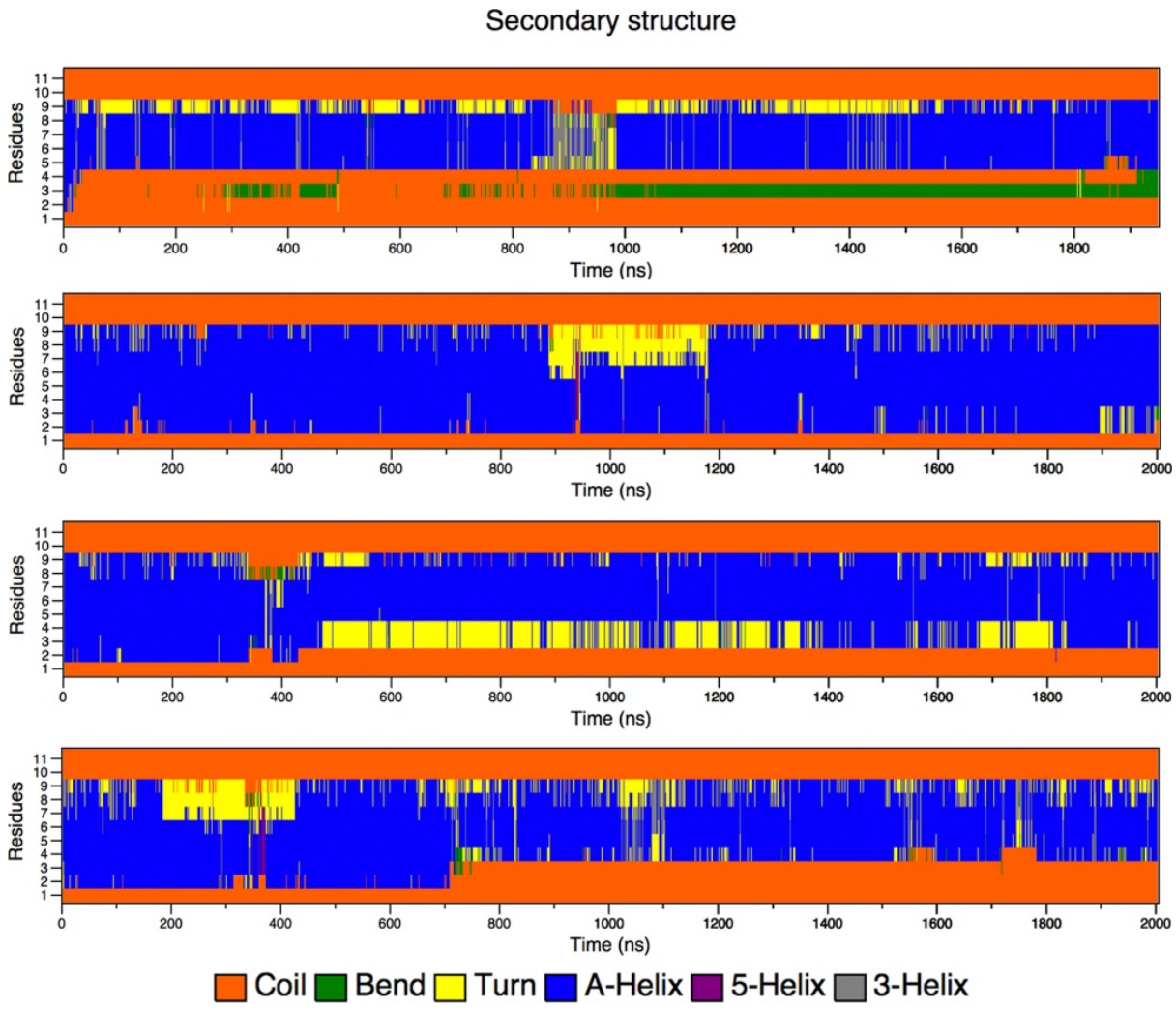


Figure 5. Secondary structure analyses of α-BP100 in DPPC (a), DPPG (b), PCPG-R (c) and PCPG-NR (d).

In DPPC, α-BP100 alpha-helix conformation reached a plateau at 38% helicity throughout the simulation, being relatively less stable than α-BP100 in bilayers containing DPPG, where a higher propensity of maintaining its conformation was observed. For pure DPPG (Fig. 5b) we found 73% (8 out of 11 residues) and for both PCPG (1:1) membranes we report 54% (6 out of 11) of helicity (Fig. 5c and 5d). No alpha-helix formation was detected in L-BP100 on bilayers simulations (Fig. S3). Therefore, the 1.8 μs simulation was not enough to present a spontaneous peptide folding.

The alpha-helix formed in the region of the residues 5 to 9 showed higher stability in all simulations with α-BP100 in bilayers (Fig. 5). This secondary structure pattern led us to suggest that the residues 5 to 9 are

related to helix nucleation, in which the formation of this helix core could be the first step in the AMP actions.

Following this assumption, we tested three conformations with α-BP100 torsionally constrained in three regions: res1-5, res4-8, res7-11 (Fig. 3) and simulated with pure DPPG membranes. Figure 6 shows the evolution of the secondary structure in each simulation.

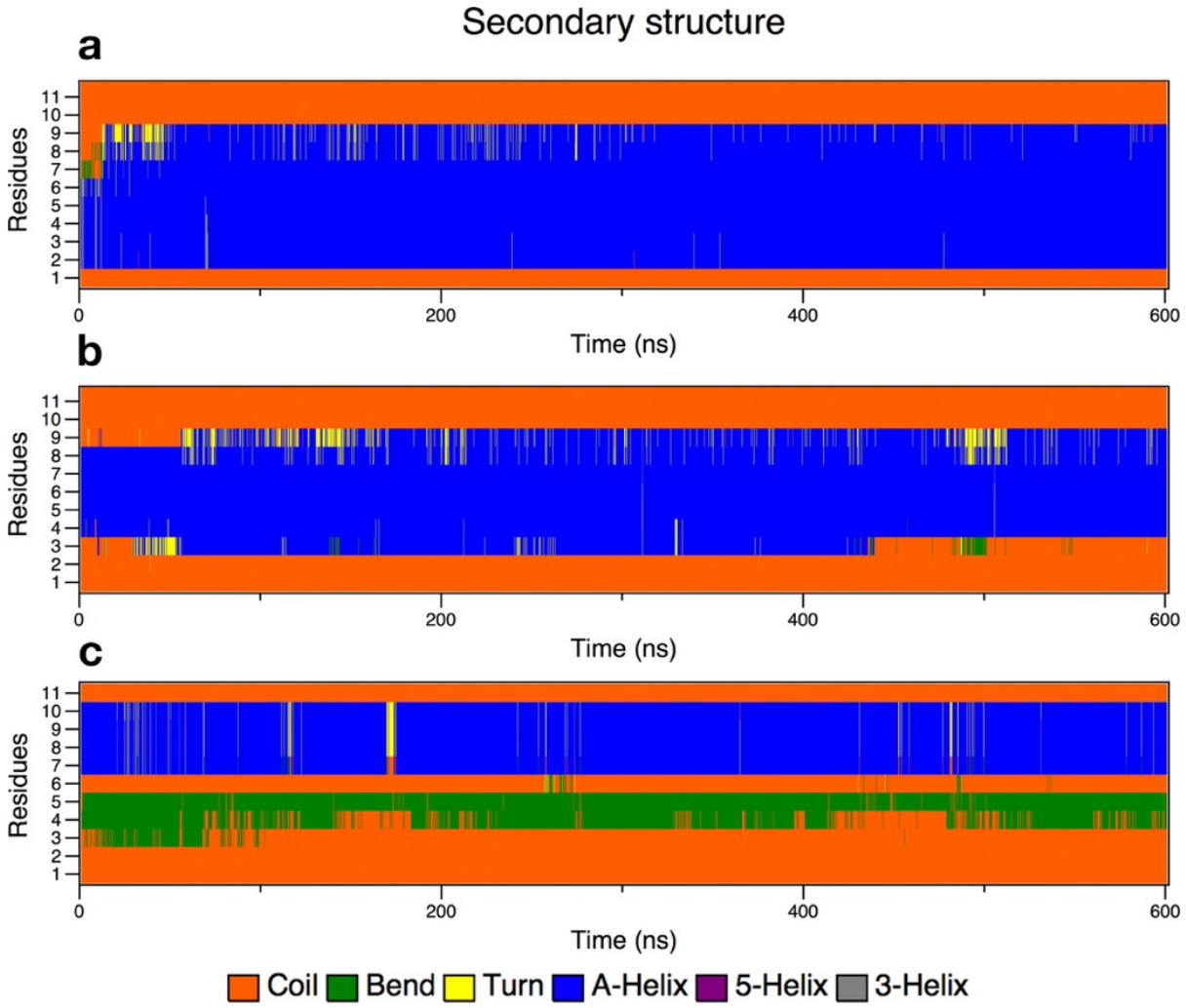


Figure 6. Secondary structure analyses graphs of BP100 in DPPG with one turn constraints on res1-5 (a), res 4-8 (b) and res7-11 (c).

α-BP100 with constraints on residues 1-5 (Lys-Lys-Leu-Phe-Lys) acquired identical helicity (73%) to α-BP100 with no constraints at the same conditions (Fig. 5b), after 50 ns of simulation (Fig. 6a), with a helix spanning from Lys2 to Lys9 (Fig. 6a). Constraints on residues 4-8 (Phe-Lys-Lys-Ile-Leu) showed overall 52% of helicity (Fig. 6b), with a helix

spanning from Phe4 to Lys9 (Fig. 6b). Constraints on residues 7-11 (Ile-Leu-Lys-Tyr-Leu) did not affect the rest of the peptide conformation (Fig. 6c) in 600 ns of simulation.

### 2.4.2. Peptide flip

Simulation trajectories analyses (Fig. 7) revealed that the peptide in alpha-helix conformation initially adsorbed at the DPPG-containing membranes interface with its hydrophilic facet in contact with the membrane, leaving the hydrophobic facet exposed to water. We observed that the alpha-helix rotated, inserting the hydrophobic facet into the hydrophobic region of the membrane. We define this dynamic phenomenon, observed in our simulations, as peptide flip. Although this final peptide orientation is known[31–34], no MD simulation on peptide flip has been reported.

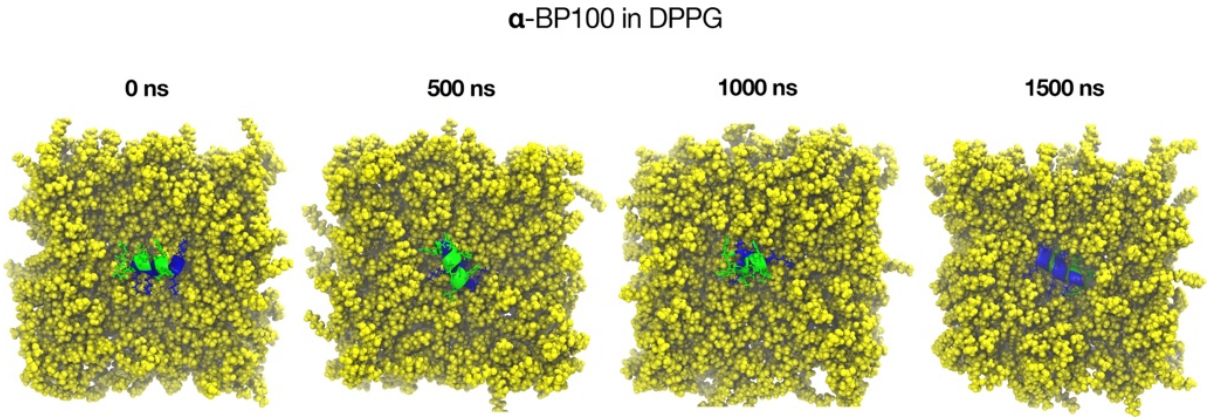


Figure 7. Peptide flip observed from above in α-BP100 in DPPG set after *circa* 1400 ns of simulation. In blue, polar facet and in green, the apolar facet. Peptide flip was also observed in α-BP100 in DPPC, α-BP100 in PCPG-R, and α-BP100 res(1-5) in DPPG simulations.

The peptide flip caused dehydration (Fig. 8). When in contact with membranes, depending on the secondary structure of the peptide and the lipid nature, the hydration of the peptide was slightly different. However, when the peptide flip took place, its hydration was drastically altered.

In the peptide/membrane simulations with L-BP100 as a starting configuration (Fig. 8a), no significant change in the number of water

molecules surrounding the peptide was observed in comparison the 150 obtained in the bulk aqueous solution. In the last 500 ns of simulation, N(0.5) was approximately 178 ± 11 in DPPC, 145 ± 7 in DPPG, 145 ± 13 in PCPG-NR, and 148 ± 3 in PCPG-R. No peptide flip was detected in the trajectories for those simulations. However, in the peptide/membrane simulations with α-BP100 as a starting configuration (Fig. 8b), N (0.5) lowered in DPPC (starting at ~700 ns), DPPG (~1500 ns) and PCPG-R (~390 ns). Alongside with dehydration, a peptide-flip was observed in DPPG and PCPG-R. For the α-BP100 in DPPC simulation, we observed a semi-flip, as the peptide alpha-helical conformation was only 38% (Fig. 5a), suggesting that the peptide overall polar/apolar segregation (Fig. 2c) was lost. The peptide flip transition time varied from 100 to 400 ns.

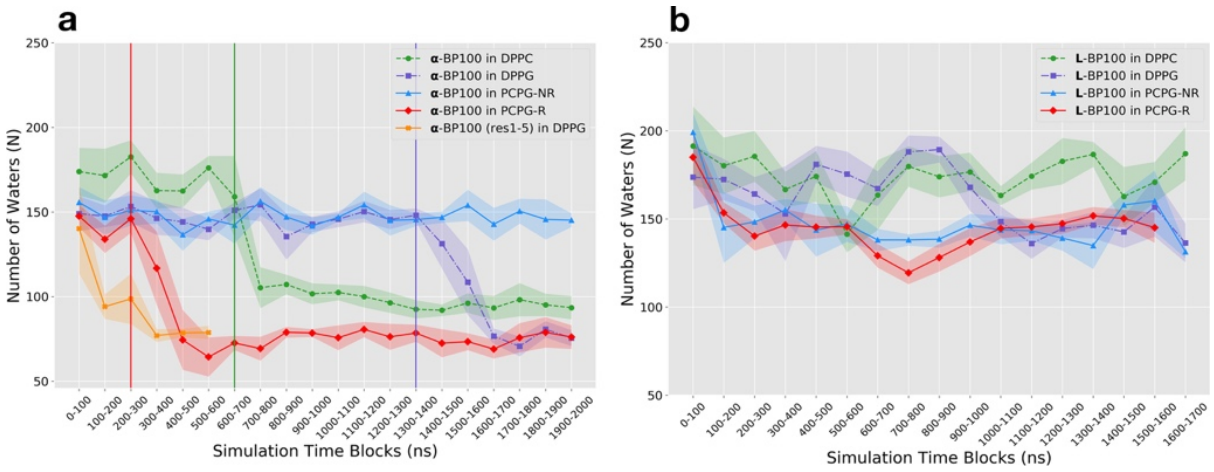


Figure 8. Average number of water molecules up to a distance of 0.5 nm, N(0.5), obtained from the minimum-distance distribution function (MDDF), between L-BP100 (a) and α-BP100 (b) and water molecules. Vertical lines indicate when peptide flip occurred.

During the peptide-flip, in the simulations of α-BP100 in DPPG and PCPG-R, the mean number N(0.5) was reduced from 147 ± 5 and 142 ± 7 to 76 ± 4 and 75 ± 4, respectively. These represent on average a reduction of approximately 48% in the number of water molecules in the hydration shell of α-BP100. In DPPC, we detected a smaller decrease in the hydration of α-BP100, around 45% (from 172 ± 8 to 94 ± 2), having around 20 water molecules more after the semi-flip. Figure 9 shows density

profile before and after peptide flip for α-BP100 in DPPG and in PCPG-R. We chose residues Lys5 and Ile7 to illustrate the changes in the mean position of hydrophobic and hydrophilic residues with respect to the membrane due to the peptide flip. These residues are polar and apolar, respectively, and located opposite to each other when in an alpha-helix conformation (Fig. 2c). Trajectory visualization and density profile (Figs. 7 and 9) clearly show the distinct orientation in BP100 hydrophobic facet before and after peptide flip. During the initial phase of approaching towards the membrane, BP100 polar side faces the membrane with its N-terminal residues (Lys1 and Lys2) interacting with the bilayer headgroups. After the flip, the apolar residues facet turns to the membrane, and simultaneously inserts into the bilayer, below the carbonyl carbons (C31) of the lipids (Fig. 9).

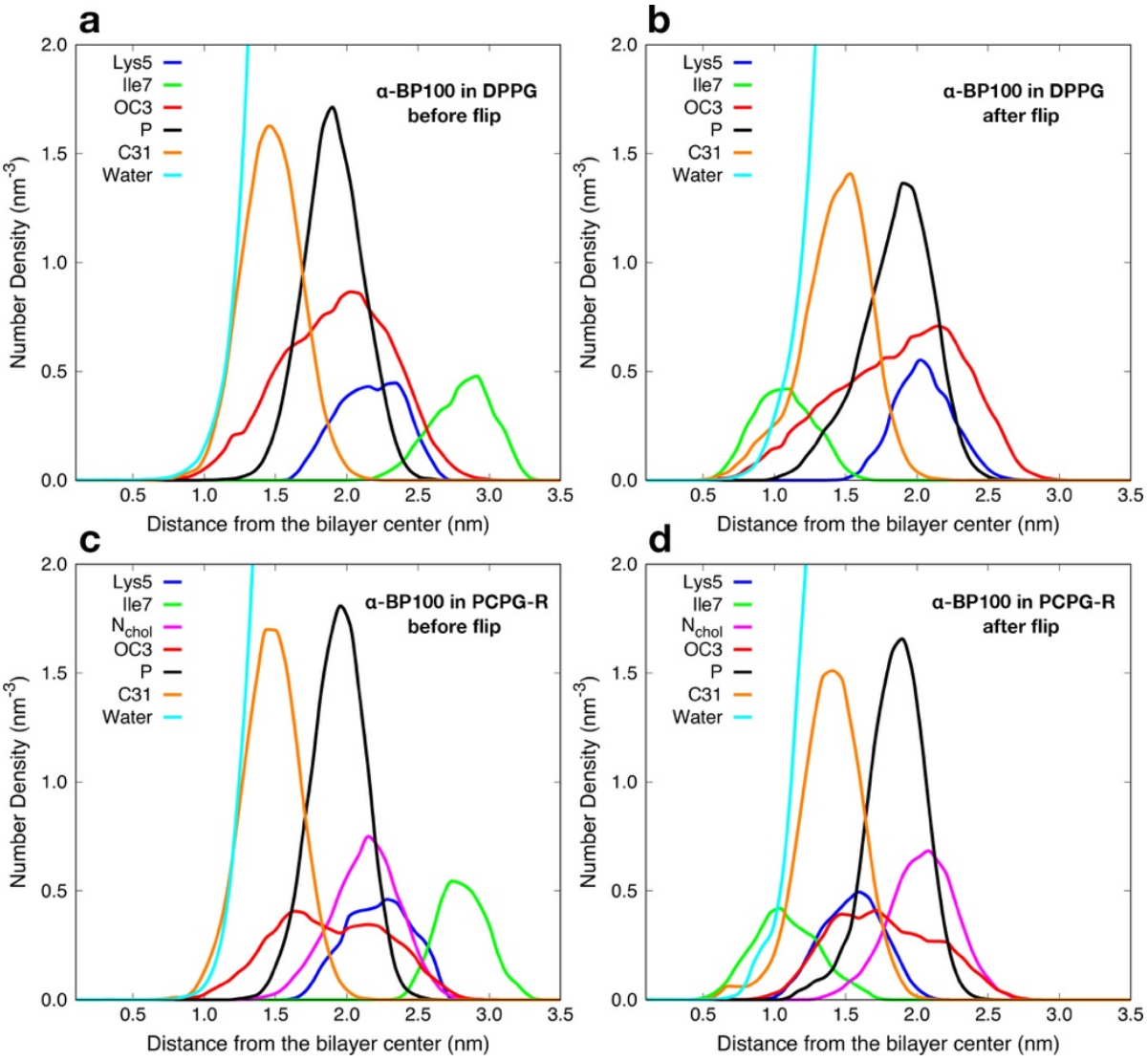


Figure 9. Peptide flip observed through number density analysis. a) and b) show respectively before and after the flip in α-BP100 in DPPG simulation; c) and d) demonstrate the flip for α-BP100 in PCPG-R simulation. Lys5 represents the polar side of BP100 and Ile7, the apolar facet (Fig. 2c). OC3 (DPPG head group further out glycerol Oxygen), $N_{chol}$ (DPPC head group choline Nitrogen), P (Phosphorus) and C31 (first carbon from sn-1 acyl chain) are shown to display BP100 insertion into the bilayer after the flip.

Peptide flip was not observed in α-BP100 in PCPG-NR, where DPPG lipids were initially scattered randomly. PG content might be related to the occurrence of the flip, but also, the PG content in the vicinity of BP100. Several studies suggest membrane active peptides cause anionic lipid clustering, or subdomain formation, upon binding to bilayers containing neutral and charged phospholipids[35–37]. The same mechanism could be involved in BP100/bilayers interactions.

### 2.4.3. Lipid clustering

The distribution of the lipids in the vicinity of BP100 was evaluated by computing the total number of lipids in contact with α-BP100 as a function of time (Fig. S5), the time-averaged values (Table 2, Fig. 10), and the lipid raft size distribution (Fig. S6).

| Average Number of Lipids in Contact with BP100 | | |
|---|---|---|
| Simulation | Lipid in Contact | Average |
| α-BP100 in DPPC | DPPC | 10.7 (± 2.6) |
| α-BP100 in DPPG | DPPG | 13.1 (± 1.4) |
| α-BP100 (1-5) in DPPG | DPPG | 13.5 (± 1.9) |
| α-BP100 in PCPG-R | Total | 12.3 (± 1.7) |
| | DPPC | 3.6 (± 1.5) |
| | DPPG | 8.7 (± 1.2) |
| α-BP100 in PCPG-NR | Total | 11.0 (± 1.7) |
| | DPPC | 2.7 (± 1.3) |
| | DPPG | 8.3 (± 1.6) |

Table 2. Average number of lipids in contact with BP100 in simulations using α-BP100 as the peptide starting configuration, except α-BP100 (1-5), which had permanent constraints on residues 1 to 5. Standard deviations are shown in parenthesis.

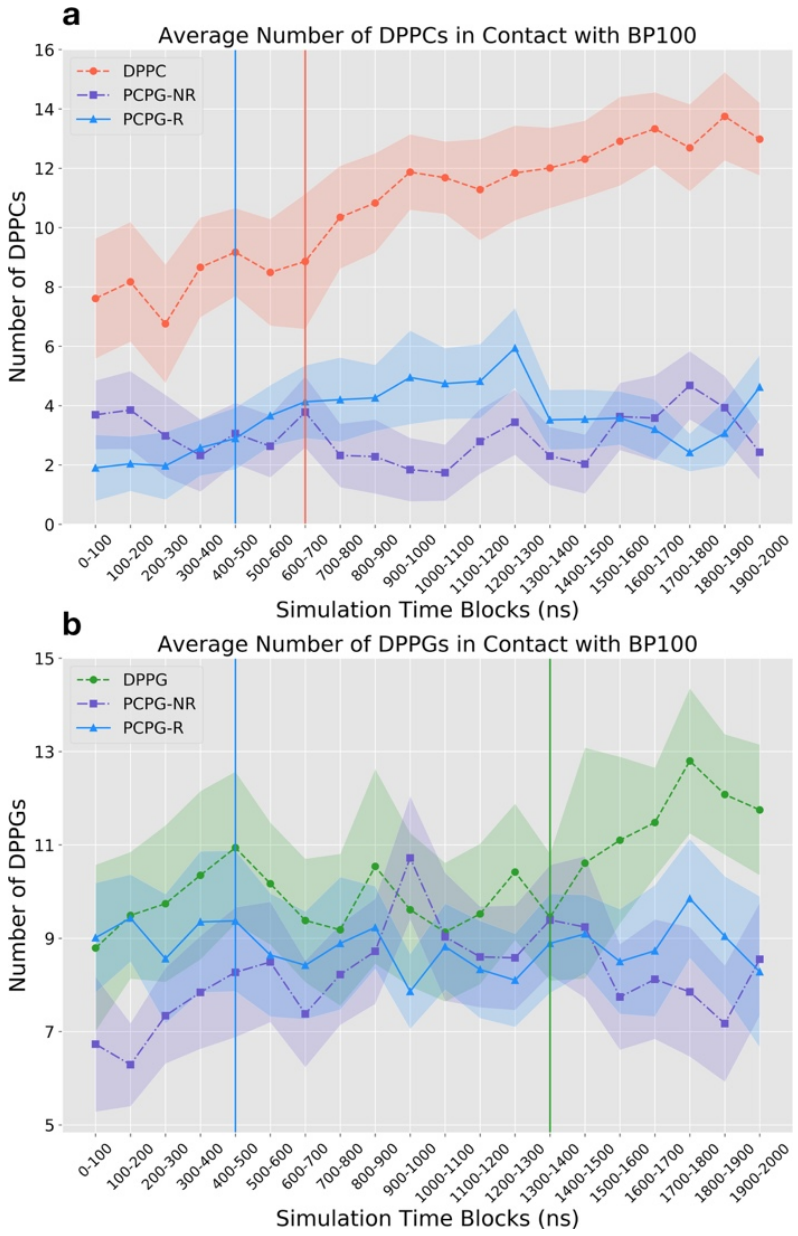


Figure 10: Average Number of DPPCs (a) and DPPGs (b) in contact with BP100 analyzed for all constraint-free simulations containing BP100 in an initially alpha helical conformation in DPPC, DPPG, PCPG-R and PCPG-NR membranes. Vertical lines represent the average time where peptide flip was observed. Standard deviation error bars are represented as fillings.

α-BP100 in DPPC simulation had on average 10.7 peptide/lipid contacts (Table 2) and had a steady increase in the number of contact lipids (Figs. 10b and S5a). This is due to the peptide losing its alpha-helical conformation (Fig. 5a), expanding the available peptide interaction area with the membrane. Lipid raft size distribution also shows a broader distribution of DPPC raft size, supporting this observation (Fig. S6a). A

semi-peptide flip was observed at ~700 ns of simulation and, concomitantly, while BP100 inserts into the bilayer as the density profile shows (Fig. S4a, b), the number of DPPCs in contact with BP100 increased (Fig. S5a).

α-BP100 in DPPG simulation shows on average 13.1 DPPGs in close contact with the peptide (Table 2). The number of DPPGs in contact rose after the flip, approximately in 1500 ns of simulation (Figs. 10a and S5b) and concurrently, BP100 inserted deeply into the membrane (Fig. 7a, b).

### 2.4.4. Polar and Apolar Interaction Analysis

Peptide contact analysis revealed the increase of lipid/peptide contacts after peptide flip and DPPG clustering on PCPG membranes. We analyzed the nature of the intermolecular interactions that determine peptide-membrane interactions throughout the simulations. We calculated the number of polar and apolar pair contacts between peptide atoms and membrane atoms (Figs. S7-S13). Using α-BP100 in PCPG-R system as an example, Figure 11 shows the sum of the 10 most frequent apolar/polar pairs between BP100 with DPPC and DPPG.

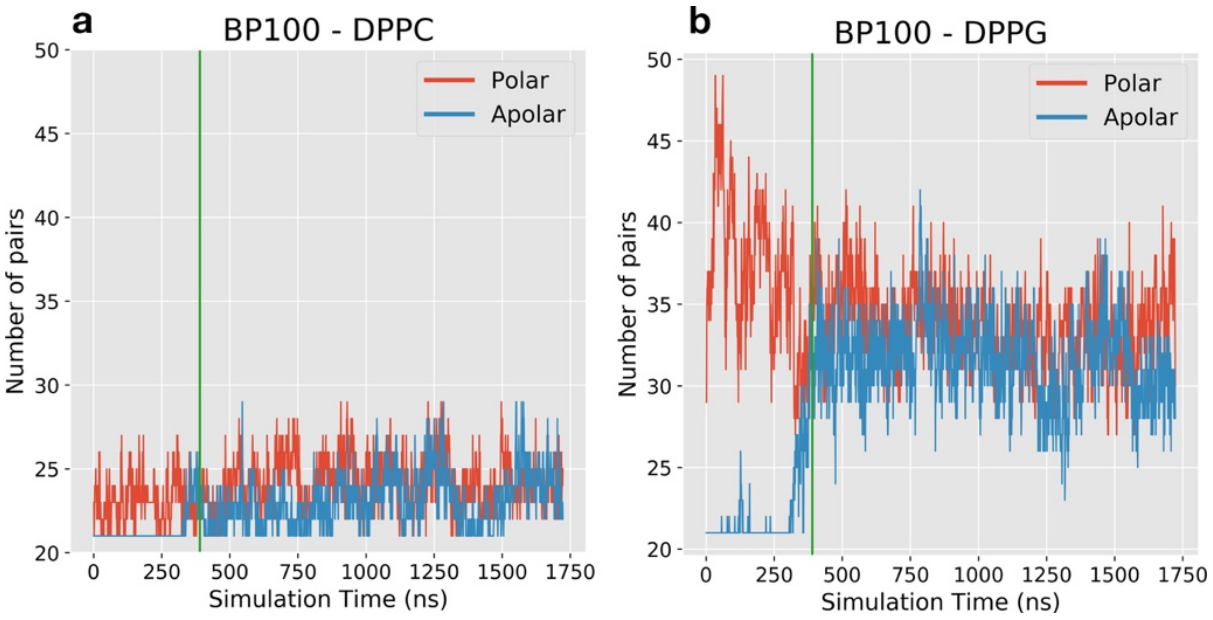


Figure 11: BP100 pair occurrence with DPPC (a) and DPPG (b) for α-BP100 in PCPG-R simulation. Graphs show the sum of the ten most frequent apolar/polar pairs during the simulation. Pairs were calculated using the monolayer facing the peptide. Green vertical lines indicate when peptide flip occurred (*circa* 390 ns).

The total number of pairs, regardless if it is polar or apolar, between BP100 and DPPG is clearly higher than that with DPPC (Fig. 11), which directly reflects on the number of lipids in contact with BP100 (Fig. 10). During the initial approach of the peptide towards the bilayer, polar interactions between charged Lysines and DPPG headgroup dominate the interaction (Figs. 11b, S9, S10, S12 and S13). The main interaction was between positively charged (+1) Lysine side chain amino group (NZ) and DPPG head phosphoglycerol group oxygens (OC2, OC3), even after peptide flip (Figs. S9, S10, S12, and S13).

Before the peptide flip, the number of polar contacts is greater than the apolar contacts for DPPG/BP100. As the peptide starts to flip, the number of apolar contacts increase, while the polar contacts decrease. After the peptide flip is completed, apolar contacts are as numerous as the polar contacts (Figs. 11 a,b and S7-10,13). Also, after the flip, apolar contacts between BP100 and DPPG were more frequent than with DPPC (Fig. 11b). The higher peptide/DPPG apolar contact frequency after the flip is also observed for other simulations with peptide flip (Figs. S7-10,13).

## 2.5. Discussion and conclusions

### 2.5.1. Peptide secondary structure

CD spectra of BP100 in solution and POPC LUVs show no secondary structure[10,11,30] Our simulations with BP100 in solution and DPPC membrane exhibited the same pattern. α-BP100 and L-BP100 in solution showed similar behavior, with a prevalence of random conformation (Fig. 4). In a related MD study of AMPs interacting with membranes,[17] an 8 µs-long all-atom MD simulation of BP100 in DMPC at 35℃ the authors reported a full helix length during 1.5 µs and a subsequent unfolding event of Lysines at positions 1 and 2, resulting in 81% of helicity on a pure zwitterionic bilayer. However, as reported for other simulated peptides in the same work, the forcefield used could result in an over-helical artifact[17]. A Brownian Dynamics simulation study of BP100 confined inside an

implicit POPC membrane reports a stable alpha-helix[18]. However, no experimental data confirms that BP100 diffuses freely in the membrane hydrophobic space and no secondary structure formation is reported for pure POPC vesicles[11].

In our simulations of α-BP100 and L-BP100 in DPPC membrane, the peptide quickly approached the membrane and remained on the surface during all simulation. Peptide-lipid pair analysis (Fig. S7) showed that cationic Lysine residues interacted mainly with phosphate groups of the DPPC bilayer, evidencing that electrostatic interactions were present.

In the case of L-BP100 in DPPC, no alpha-helical structure formation was observed (Fig. S3), and for α-BP100, the peptide alpha-helix conformation was mostly lost, although one helix turn from residues 5 to 9 remained (Fig. 5A). The minimum alpha-helix length detected by CD spectroscopy is proposed to encompass seven to eleven residues[38], hence the alpha-helix turn in residues 5-9 might not be detected by CD.

Alternatively, this could be an over-helical forcefield artifact,[22] but it also indicates the high stability of the alpha-helix formed by the (5 – 9) Lys-Lys-Ile-Leu-Lys sequence. This stability leads us to conjecture that BP100 alpha-helix formation could be initiated through a core sequence, a nascent helix[39]. The negatively charged membrane interface could promote the initial peptide folding. To support this, we performed three 600 ns-long simulations with constrained alpha helices of BP100 on three regions: residues 1 to 5 (Lys-Lys-Leu-Phe-Lys), 4 to 8 (Phe-Lys-Lys-Ile-Leu) and 7 to 11 (Ile-Leu-Lys-Tyr-Leu) in pure DPPG bilayers. The secondary structure analysis of the constrained BP100 simulations yielded different outcomes. Constraint on residues 1 to 5 rapidly induced almost full alpha-helix content from Lys2 to Lys9 (Fig. 6A), reaching 73% of helicity, similar to α-BP100 in DPPG without constraints (Fig. 5B). Constraint on residues 4 to 8 also showed a helix formation tendency (overall 63% helicity, 5 out of 11 residues, from Phe4 to Lys9). In sharp contrast, constraints on residues 7 to 11 (36% of helicity, 4 out of 11 residues, from Lys7 to Tyr10) had no effects on secondary structure

formation of BP100 during 600 ns simulation (Fig. 6C), indicating that this region has little influence on initial peptide folding.

Pace and Scholtz[40], based on experimental studies, proposed a helix propensity scale as $\Delta(\Delta G)$ values relative to Alanine set to zero. On the Pace and Scholtz scale, the 5-9 region has the highest helix promoting residues (overall helix propensity of 1.4 kcal/mol). We find 1.53 kcal/mol for residues 1 to 5 (Lys-Lys-Leu-Phe-Lys), 1.68 kcal/mol for residues 4 to 8 (Phe-Lys-Lys-Ile-Leu), and 1.62 kcal/mol for residues 7-11 (Ile-Leu-Lys-Tyr-Leu). Our secondary structure data indicates BP100 nascent helix could be formed either in the region between residues 1 to 5 or between residues 5 to 9. We favor the latter due to the presence of positively charged Lysine residues in the N-terminal side (Lys1 and Lys2) which could produce an energetically unfavorable barrier to initial peptide folding. The 5-9 region shows high stability in all constraint-free α-BP100/membranes simulations and has the overall lowest energy barrier in the helix propensity scale[40].

DPPG seems to have a helix-stabilizing effect on BP100. All the simulations with α-BP100 in DPPG-containing-membranes showed high alpha-helical content, including the region of residues 5 to 9. Our helicity results from the simulations with α-BP100 in pure DPPG (73%) and in PCPG (50:50) mixed bilayers (54%) are remarkably close with those reported in experimental studies: 54% in POPC:POPG (50:50)[11] and 61% in DMPC/DMPG (75:25) LUVs[10], and maximum observable alpha-helix spectrum for BP100 in pure POPG vesicles[11] proving that BP100 alpha-helical structure is dependent on PG content[11].

For L-BP100 simulations with DPPG, PCPG-R, and PCPG-NR, no secondary structure formation was detected (Fig. S3), with the peptide being in a random conformation. Non-biased random peptide simulations require much longer simulation time to sample the peptide conformational potential landscape or might dwell in several local minimum-energy states.

### 2.5.2. Peptide flip

BP100 is too short to span the bilayer thickness, especially in the alpha-helical conformation, and thus single molecule pore formation is an unlikely scenario. NMR data of BP100 in DMPC: DMPG (3:1)[10] shows that upon binding to negatively charged membranes, alpha-helical BP100 positions parallel to the membrane as in a surface-bound orientation, and has an azimuthal rotation angle close to 160°, with Lysine residues facing the solvent. Observed in our simulations, this arrangement is commonly observed with other CAMPs[30–33].

Peptide/membrane simulations with initially alpha-helical BP100 had its polar moiety facing the membrane, for being the most probable scenario in a physical environment. In the α-BP100 in DPPG (Fig. 7), α-BP100 in DPPC, α-BP100 in PCPG-R and α-BP100 (res1-5) in DPPG simulations trajectories, we observed the binding of BP100 from bulk solution to the membranes with its Lysines residues pointing towards the bilayer, and then, the peptide rotated, leaving its apolar facet facing the interior of the bilayer. We termed this transition peptide flip. Although BP100 surface-bound state is reported[12,17], no previous peptide/membrane MD simulation work has reported a peptide flip transition.

Peptide flip brings significant outcomes regarding BP100 localization in the membrane, in peptide/membrane interaction and the peptide hydration, possibly being a fundamental step of carpet mechanism for BP100 and other CAMPs. Through the density profile, we observed deep penetration of the peptide into the membrane through its apolar residues with larger side-chains, after the flip (Fig. 7). BP100 hydration analysis also shows a decrease in the overall peptide hydration after the flip (Fig. 8). Apolar/polar pair interaction analysis (Fig. 11) revealed that after the flip, the number of contacts between apolar residues from the lipids and the peptide increases significantly, while the number of contacts between polar groups of the lipids and the peptides slightly decreases. In other words, peptide flip intensifies peptide binding to membranes burying the apolar residues of the peptide deeper into the membrane core.

We investigated what factors could lead to the occurrence of BP100 peptide flip. Membrane composition appears to have a significant role. For BP100 alpha-helical structure formation is favored in negatively charged membranes[8]In our simulations, BP100 entirely flipped in DPPG enriched regions of the membrane. Peptide flip was detected in α-BP100 in DPPG, α-BP100 (res1-5) in DPPG and α-BP100 in PCPG-R systems.

No peptide flip was detected in the other constrained BP100 simulations (α-BP100 (res4-8) in DPPG and α-BP100 (res7-11) in DPPG). However, it is hasty to affirm that it is unlikely to expect peptide flip to happen in those systems with 600 ns of simulation time. For instance, peptide flip was observed after 1.4 μs of simulation in α-BP100 in DPPG.

Hydration analysis (Fig. 8b) and density profile (Fig. S4A, B) for α-BP100 in DPPC show also that BP100 flipped. However, alpha-helix secondary structure is mostly lost (Fig. 5a). For this reason, BP100 amphiphilic apolar-polar facet separation (Fig. 2c) is lost.

Additionally, the apolar moiety of the peptide could have a crucial role in peptide flip. Hydration analysis (Fig. 8) suggests peptide flip results in peptide dehydration and concomitantly enhances peptide/lipid interaction (Fig. 11), increasing specially apolar contacts (Fig 11). Similar behavior was observed in a study of the interaction of micelles with polyatomic counterions with apolar and polar moieties. Experimental results and MD simulations showed that counterions with the same apolar groups but different polar groups resulted in similar ionic affinities for dodecyltrimethylammonium micelles, and the simulations showed that counterion adsorption to the micelles was related with the dehydration of the apolar group of the counterions rather than by the polar group[41].

These factors could help to explain BP100 selectivity towards negatively charged bacterial membranes and low cytotoxicity. Results of leakage from inner compartment of LUVs upon addition of BP100 showed that BP100 leakage ability is proportional to PG content while the peptide has small effects on zwitterionic PC vesicles, observed through studies of zeta potential and vesicle leakage[11]. In a study of solid-state NMR of phospholipid bilayers, it was shown that BP100 did not perturb PC

bilayers even at high peptide/lipid ratio and caused membrane thinning on mixed DMPC/DMPG bilayers where a stronger effect was observed in anionic DMPG lipids compared to zwitterionic DMPC lipids[12].

In zwitterionic-lipid-enriched mammalian membranes, BP100 would bind to membranes through electrostatic interactions and the absence of a helix-promoting environment would prevent helix formation and even with peptide flip, as in our α-BP100 in DPPC simulation, it could lead to mild membrane thinning[11,12]. On the other hand, bacterial membranes with high content of anionic lipids on the outer part of the membrane, could promote peptide binding, alpha-helix nucleation, and propagation, leading to peptide flip and more pronounced membrane thinning, which is consistent with our observations from α-BP100 in DPPG, α-BP100 in PCPG-R and α-BP100 (res1-5) in DPPG sets. Although we could not detect membrane thinning in our simulations (Table S2), it should be noted that our simulations had only one peptide on 128-lipid-bilayers. A more pronounced effect on the membrane might be observed by increasing the number of peptides in the simulations.

### 2.5.3. DPPG subdomain formation

Lipid clustering, or subdomain formation, induced by CAMPs has been studied by several authors [5,14,35–37,42–45]. Through electrostatic interactions, CAMPs clusters anionic phosphatidylglycerol (PG) or cardiolipin (CL) lipids on the outer membrane of bacteria, inducing phase separation and phase boundary defects between lipid domains and the rest of the membrane, increasing membrane permeability[36]. It was first proposed by Epand et al.,[45] in a study with oligomers of lysine (OAK). Upon the addition of OAK in 1-palmitoyl-2-oleoyl phosphatidylethanolamine (POPE) and tetraoleoyl cardiolipin (TOCL) mixed vesicles, transition temperature shift was observed through differential scanning calorimetry, indicating lipid phase separation[45]. Lipid phase separation was later observed for other cAMPs and cell-penetrating-peptides[37,45,46]. Although

not so pronounced, BP100 ability to promote lipid phase separation was also detected by DSC on POPE/TOCL (75:25) vesicles[37].

Lipid phase separation promoted by CAMPs have also been observed in computational modeling studies. In a coarse-grained MD simulation study,[35] lipid cluster promotion was seen in POPE/POPG (70:30) membranes by Ltc1, a linear alpha-helical cAMP with overall +10 charge. Simulations showed Ltc1 induced POPG domains in small (256 lipids) and large membranes (512 or 2048 lipids). Also, due to peptide-POPG charge neutralization, Ltc1-induced anionic domains seem to facilitate peptide oligomerization, enhancing peptide activity on bacterial model membranes[35].

Likewise, our simulations suggest BP100 promotes PG aggregation. Two DPPC: DPPG (50:50) mixed bilayers were designed to explore lipid aggregation by the peptide. One membrane was composed of randomly mixed (PCPG-NR) and in the other, a 4 x 4 DPPG raft (PCPG-R) was positioned in the middle of both monolayers (see Methods 1 and Fig. 1). BP100 was able to cluster DPPGs in PCPG-NR, which can be observed by the amount of DPPG in contact with BP100 (Table 2). From a total of 11 lipids in the closer contact with BP100, 8.3 in average are DPPG corresponding to 75% of the lipid in the vicinity of the peptide. Additionally, this DPPG clustering can also be observed in lipid raft size distribution (Fig. S6E), reaching similar values of DPPG/peptide contact in α-BP100 in PCPG-R simulation (Fig. 10) and DPPG lipid raft size probability (Fig. S6D). These data suggest that even a short-lengthened CAMP as BP100 can promote anionic lipid clustering and also maintain it, supporting the experimental findings[37].

BP100 also adsorbs on pure zwitterionic PC membranes and promotes DPPC clustering as observed in Fig. S5A and S6A. However, possibly due to the presence of positively charged choline headgroups (Fig. 1d - left), secondary structure is lost (Fig. 5a) and the peptide turns into random coil, resulting in an increase of available interaction surface area with the DPPC headgroups, which is reflected in a broad distribution in lipid raft size distribution (Fig. S5A). Polar/Apolar pair analysis for α-BP100 in

PCPG-R (Fig. 11) helps to explain lipid aggregation. We computed the ten most frequent apolar and polar pairs between peptide and lipids. The number of polar pairs between the peptide and DPPG is higher than those with DPPC, and is maintained even after the flip (˜390 ns). As expected, +1 charged amino group (NZ) from Lysines side chains are the main participants in polar pairings (Figs. S7-S13), interacting with DPPG headgroup glycerol (OC2, OC3, Fig. 1d - right), phosphate group (P), and carbonyl groups (C21, C31, O21, O22, O31, O32) from chains sn1 and sn2 (Figs. S9, S10, S12, S13).

Peptide flip seems to contribute to lipid clustering. Polar/apolar pairs analysis (Fig. 11) and pair frequency (Fig. S8, S9) for the previous simulation, reveals that apolar pairs between BP100 and both lipids rise after peptide flip occurs ( ˜390 ns), intensifying peptide-membrane interaction. The same phenomena were observed for other simulations with peptide flip (Figs. S7, S10 and S13). As long as peptide flip had occurred, apolar residue side chains (from Leu3, Phe4, Ile7, Leu8 and Tyr10, and Leu11) were in close contact mainly with groups of the lipid tails (Fig. S7-S10, S13).

The mechanisms of bacterial toxicity via lipid clustering induced by CAMPs still have to be investigated. Moreover, possibly more than one mechanism could be involved in the process of bacterial killing. Evidence suggest lipid clustering by CAMPs could lead to negative charge concentration on membranes, promoting CAMPs attachment, leading to pore formation[5]. Anionic lipid clustering would have surrounding interfaces with the rest of the membrane which could lead to phase boundary defects, leading to slow leakage of inner cell content[32]. Also, CAMPs and cell-penetrating peptides could induce negative membrane curvature, enabling the internalization of peptides into cells, leading to intracellular killing mechanisms. The formation of lipid clusters patches would also lead to anomalies in membrane protein function, membrane fluidity, and membrane polarization. In a recent study[5] with cWFW, a cyclic antimicrobial peptide, it was shown *in vitro* and *in vivo* that cWFW promotes lipid phase separation, a sharp decrease in membrane fluidity.

The large phase separation appears to cause disorganization of membrane proteins, inhibiting cell wall synthesis and inducing autolysis.

BP100 mode of action on membranes is dependent on peptide/lipid ratio[11,47]. As our studies comprised of low peptide/lipid concentration (1/128), we suggest that at low peptide/lipid concentrations, BP100 causes lipid aggregation on negatively charged membranes, leading to phase boundary defects between negatively charged lipid rafts and the rest of the membrane. Through this, membrane permeability would increase, leading to slow leakage of the cell inner content.

# 2.6. References


1. Bahar, A. & Ren, D. Antimicrobial Peptides. *Pharmaceuticals* **6**, 1543–1575 (2013). doi:10.3390/ph6121543
2. Brogden, K. A. Antimicrobial peptides: Pore formers or metabolic inhibitors in bacteria? *Nature Reviews Microbiology* **3**, 238–250 (2005). doi:10.1038/nrmicro1098
3. Guilhelmelli, F. *et al.* Antibiotic development challenges: the various mechanisms of action of antimicrobial peptides and of bacterial resistance. *Front. Microbiol.* **4**, (2013). doi:10.3389/fmicb.2013.00353
4. Jenssen, H., Hamill, P. & Hancock, R. E. W. Peptide Antimicrobial Agents. *Clin. Microbiol. Rev.* **19**, 491–511 (2006). doi:10.1128/CMR.00056-05
5. Scheinpflug, K. *et al.* Antimicrobial peptide cWFW kills by combining lipid phase separation with autolysis. *Sci. Rep.* **7**, 1–15 (2017). doi:10.1038/srep44332
6. Li, J. *et al.* Membrane Active Antimicrobial Peptides: Translating Mechanistic Insights to Design. *Front. Neurosci.* **11**, 73 (2017). doi:10.3389/fnins.2017.00073
7. Li, Z. L., Ding, H. M. & Ma, Y. Q. Interaction of peptides with cell membranes: Insights from molecular modeling. *J. Phys. Condens. Matter* **28**, (2016). doi:10.1088/0953-8984/28/8/083001
8. Badosa, E. *et al.* A library of linear undecapeptides with bactericidal activity against phytopathogenic bacteria. *Peptides* **28**, 2276–2285 (2007). doi:10.1016/j.peptides.2007.09.010
9. Ferre, R. *et al.* Synergistic Effects of the Membrane Actions of Cecropin-Melittin Antimicrobial Hybrid Peptide BP100. *Biophys. J.* **96**, 1815–1827 (2009). doi:10.1016/j.bpj.2008.11.053
10. Wadhwani, P. *et al.* Dynamical structure of the short multifunctional peptide BP100 in membranes. *Biochim. Biophys. Acta - Biomembr.* **1838**, 940–949 (2014). doi:10.1016/j.bbamem.2013.11.001
11. Manzini, M. C. *et al.* Peptide:Lipid ratio and membrane surface charge determine the mechanism of action of the antimicrobial peptide BP100. Conformational and functional studies. *Biochim. Biophys. Acta - Biomembr.* **1838**, 1985–1999 (2014). doi:10.1016/j.bbamem.2014.04.004
12. Misiewicz, J. *et al.* Action of the multifunctional peptide BP100 on native biomembranes examined by solid-state NMR. *J. Biomol. NMR* **61**, 287–98 (2015). doi:10.1007/s10858-015-9897-8
13. Zamora-Carreras, H. *et al.* Alanine scan and 2H NMR analysis of the membrane-active peptide BP100 point to a distinct carpet mechanism of action. *Biochim. Biophys. Acta - Biomembr.* **1858**, 1328–1338 (2016). doi:10.1016/j.bbamem.2016.03.014
14. Epand, R. F., Savage, P. B. & Epand, R. M. Bacterial lipid composition and the antimicrobial efficacy of cationic steroid compounds (Ceragenins). (2007). doi:10.1016/j.bbamem.2007.05.023
15. J. Bond, P. & Khalid, S. Antimicrobial and Cell-Penetrating Peptides: Structure, Assembly and Mechanisms of Membrane Lysis via Atomistic and Coarse-Grained Molecular Dynamic Simulations. *Protein Pept. Lett.* **17**, 1313–1327 (2010). doi:10.2174/092986651100901131316. Ulmschneider, J. P. & Ulmschneider, M. B. Molecular Dynamics Simulations Are Redefining Our View of Peptides Interacting with Biological Membranes. *Acc. Chem. Res.* **51**, 1106–1116 (2018). doi:10.1021/acs.accounts.7b00613
17. Wang, Y. *et al.* How reliable are molecular dynamics simulations of membrane active antimicrobial peptides? *Biochim. Biophys. Acta - Biomembr.* **1838**, 2280–2288 (2014). doi:10.1016/j.bbamem.2014.04.009

18. Alves, C. S., Kairys, V., Castanho, M. A. R. B. & Fernandes, M. X. Interaction of antimicrobial peptides, BP100 and pepR, with model membrane systems as explored by Brownian dynamics simulations on a coarse-grained model. *Biopolymers* **98**, 294–312 (2012). doi:10.1002/bip.22075
19. Jämbeck, J. P. M. & Lyubartsev, A. P. Another Piece of the Membrane Puzzle: Extending Slipids Further. *J. Chem. Theory Comput.* **9**, 774–784 (2013). doi:10.1021/ct300777p
20. Martinez, L. *et al.* PACKMOL: A package for building initial configurations for molecular dynamics simulations. *J. Comput. Chem.* **30**, 2157–2164 (2009). doi:10.1002/jcc.21224
21. Åqvist, J. Ion-water interaction potentials derived from free energy perturbation simulations. *J. Phys. Chem.* **94**, 8021–8024 (1990). doi:10.1021/j100384a009
22. Beauchamp, K. A., Lin, Y. S., Das, R. & Pande, V. S. Are protein force fields getting better? A systematic benchmark on 524 diverse NMR measurements. *J. Chem. Theory Comput.* **8**, 1409–1414 (2012). doi:10.1021/ct2007814
23. Dang, L. X. Mechanism and Thermodynamics of Ion Selectivity in Aqueous Solutions of 18-Crown-6 Ether: A Molecular Dynamics Study. *J. Am. Chem. Soc.* **117**, 6954–6960 (1995). doi:10.1021/ja00131a018
24. Van Gunsteren, W. F. & Berendsen, H. J. C. A Leap-frog Algorithm for Stochastic Dynamics. *Mol. Simul.* **1**, 173–185 (1988). doi:10.1080/08927028808080941
25. Bussi, G., Donadio, D. & Parrinello, M. Canonical sampling through velocity rescaling. *J. Chem. Phys.* **126**, (2007). doi:10.1063/1.2408420
26. Berendsen, H. J. C., Postma, J. P. M., van Gunsteren, W. F., DiNola, A. & Haak, J. R. Molecular dynamics with coupling to an external bath. *J. Chem. Phys.* **81**, 3684 (1984). doi:10.1063/1.448118
27. Hess, B., Bekker, H., Berendsen, H. J. C. & Fraaije, J. G. E. M. LINCS: A Linear Constraint Solver for Molecular Simulations. *J Comput Chem* **18**, 1463–1472 (1997). https://doi.org/10.1002/(SICI)1096-987X(199709)18:12<1463::AID-JCC4>3.0.CO;2-H
28. Essmann, U. *et al.* A smooth particle mesh Ewald method. *J. Chem. Phys.* **103**, 8577 (1995). doi:10.1063/1.470117
29. Georg, H. C., Coutinho, K. & Canuto, S. Solvent effects on the UV-visible absorption spectrum of benzophenone in water: A combined Monte Carlo quantum mechanics study including solute polarization. *J. Chem. Phys.* **126**, 034507 (2007). doi:10.1063/1.2426346
30. Torcato, I. M. *et al.* Design and characterization of novel antimicrobial peptides, R-BP100 and RW-BP100, with activity against Gram-negative and Gram-positive bacteria. *Biochim. Biophys. Acta - Biomembr.* **1828**, 944–955 (2013). doi:10.1016/j.bbamem.2012.12.002
31. Tang, M., Waring, A. J. & Hong, M. Effects of arginine density on the membrane-bound structure of a cationic antimicrobial peptide from solid-state NMR. *Biochim. Biophys. Acta - Biomembr.* **1788**, 514–521 (2009). doi:10.1016/j.bbamem.2008.10.027
32. Ulmschneider, J. P. Charged Antimicrobial Peptides Can Translocate across Membranes without Forming Channel-like Pores. *Biophys. J.* **113**, 73–81 (2017). doi:10.1016/j.bpj.2017.04.056
33. Chen, C. H., Wiedman, G., Khan, A. & Ulmschneider, M. B. Absorption and folding of melittin onto lipid bilayer membranes via unbiased atomic detail microsecond molecular dynamics simulation. *Biochim. Biophys. Acta - Biomembr.* **1838**, 2243–2249 (2014). doi:10.1016/j.bbamem.2014.04.012
34. Glaser, R. W. *et al.* Concentration-dependent realignment of the antimicrobial peptide PGLa in lipid membranes observed by solid-state19F-NMR. *Biophys. J.* **88**, 3392–3397 (2005). doi:10.1529/biophysj.104.056424
35. Polyansky, A. A. *et al.* Antimicrobial Peptides Induce Growth of Phosphatidylglycerol Domains in a Model Bacterial Membrane. *J. Phys. Chem. Lett.* **1**, 3108–3111 (2010). doi:10.1021/jz101163e

36. Epand, R. M. & Epand, R. F. Domains in bacterial membranes and the action of antimicrobial agents. *Mol. Biosyst.* **5**, 580–587 (2009). doi:10.1039/b900278m
37. Wadhwani, P. *et al.* Membrane-Active Peptides and the Clustering of Anionic Lipids. *Biophys. J.* **103**, 265–274 (2012). doi:10.1016/j.bpj.2012.06.004
38. Manning, M. C., Illangasekare, M. & W. Woody, R. Circular dichroism studies of distorted α-helices, twisted β-sheets, and β-turns. *Biophys. Chem.* **31**, 77–86 (1988). https://doi.org/10.1016/0301-4622(88)80011-5
39. Dyson, H. J., Rance, M., Houghten, R. A., Wright, P. E. & Lerner, R. A. Folding Of Peptide Fragments Of Proteins In Water Solution 2. The Nascent Helix. *J. Mol. Biol.-In Press* 201–217 (1987). https://doi.org/10.1016/0022-2836(88)90447-0
40. Pace, C. N. & Scholtz, J. M. A helix propensity scale based on experimental studies of peptides and proteins. *Biophys. J.* **75**, 422–427 (1998). doi:10.1016/S0006-3495(98)77529-0
41. Lima, F. S. *et al.* Ion dehydration controls adsorption at the micellar interface: Hydrotropic ions. *Phys. Chem. Chem. Phys.* **19**, 30658–30666 (2017). doi:10.1039/c7cp05283a
42. Ladokhin, A. S. & White, S. H. 'Detergent-like' permeabilization of anionic lipid vesicles by melittin. *Biochim. Biophys. Acta - Biomembr.* **1514**, 253–260 (2001). doi:10.1016/S0005-2736(01)00382-0
43. Paterson, D. J., Tassieri, M., Reboud, J., Wilson, R. & Cooper, J. M. Lipid topology and electrostatic interactions underpin lytic activity of linear cationic antimicrobial peptides in membranes. *Proc. Natl. Acad. Sci.* 201704489 (2017). doi:10.1073/pnas.1704489114
44. Epand, R. M. & Epand, R. F. Bacterial membrane lipids in the action of antimicrobial agents. *J. Pept. Sci.* **17**, 298–305 (2011). doi:10.1002/psc.1319
45. Epand, R. M., Rotem, S., Mor, A., Berno, B. & Epand, R. F. Bacterial membranes as predictors of antimicrobial potency. *J. Am. Chem. Soc.* **130**, 14346–14352 (2008). doi:10.1021/ja8062327
46. Enoki, T. A. *et al.* Antimicrobial Peptide K0-W6-Hya1 Induces Stable Structurally Modified Lipid Domains in Anionic Membranes. *Langmuir* **34**, 2014–2025 (2018). doi:10.1021/acs.langmuir.7b03408
47. Carretero, G. P. B. *et al.* Synthesis, biophysical and functional studies of two BP100 analogues modified by a hydrophobic chain and a cyclic peptide. *Biochim. Biophys. Acta - Biomembr.* **1860**, 1502–1516 (2018). doi:10.1016/j.bbamem.2018.05.003

# 2.7. Supplementary Material

| **Area per Lipid (Å²/Lipid)** | | | | |
|---|---|---|---|---|
| | Ensemble | Our Simulation | Experimental | Other simulations |
| Pure Bilayers | DPPC | 61.7 (±1.0) | 63.3[1], 67.2[2], 71.2[3], 62 (±1.3)[4], 63.1 (±1.3)[5] | 62.6 (±0.5)[6], 61.8[7], 62.3 (±1.1)[8] |
| | DPPG | 63.2 (±1.3) | 67.0[9] | 64.5 (±0.4)[10] |
| | PCPG-R | 60.7 (±1.2) | - | - |
| | PCPG-NR | 60.6 (±1.2) | - | - |
| Bilayers + Peptide | L-BP100 in DPPC | 62.1 (±1.1) | | |
| | α-BP100 in DPPC | 62.3 (±1.2) | | |
| | L-BP100 in DPPG | 62.5 (±1.4) | | |
| | α-BP100 in DPPG | 62.3 (±1.3) | | |
| | L-BP100 in PCPG-R | 60.4 (±1.2) | | |
| | α-BP100 in PCPG-R | 60.8 (±1.3) | | |
| | L-BP100 in PCPG-NR | 60.7 (±1.2) | | |
| | α-BP100 in PCPG-NR | 60.1 (±1.2) | | |

Table S1: Comparison of area per lipid between experimental data and those obtained from our simulations. The average $A_L$ was obtained by dividing the average xy area of the simulation by the number of phospholipids in a monolayer (64). No area per lipid data was found for PCPG (50:50) membrane experimental data.

| Membrane Thickness (Å) | | | | |
|---|---|---|---|---|
| | Ensemble | Our simulation | Experimental | Other Simulations |
| Pure Bilayers | DPPC | 38.1 (± 0.6) | 34.2[3], 39.0[5], 38.0[11] | 37.7[6], 39.8[7] |
| | DPPG | 37.0 (± 0.9) | 35.5[9] | 34.9[10] |
| | PCPG-R | 38.3 (±0.6) | | |
| | PCPG-NR | 38.7 (± 0.8) | | |
| Bilayers + Peptide | L-BP100 in DPPC | 38.0 (±0.7) | | |
| | α-BP100 in DPPC | 38.1 (±0.6) | | |
| | L-BP100 in DPPG | 37.4 (±0.9) | | |
| | α-BP100 in DPPG | 37.7 (±0.8) | | |
| | L-BP100 in PCPG-R | 38.8 (±0.8) | | |
| | α-BP100 in PCPG-R | 39.1 (±0.9) | | |
| | L-BP100 in PCPG-NR | 38.6 (±0.8) | | |
| | α-BP100 in PCPG-NR | 39.1 (±0.9) | | |

Table S2: Comparison of membrane thickness between experimental data and those obtained from our simulations. Membrane thickness was calculated by averaging the distance between phosphorus atoms of each leaflet. No membrane thickness values for PCPG (50:50) membranes were found.

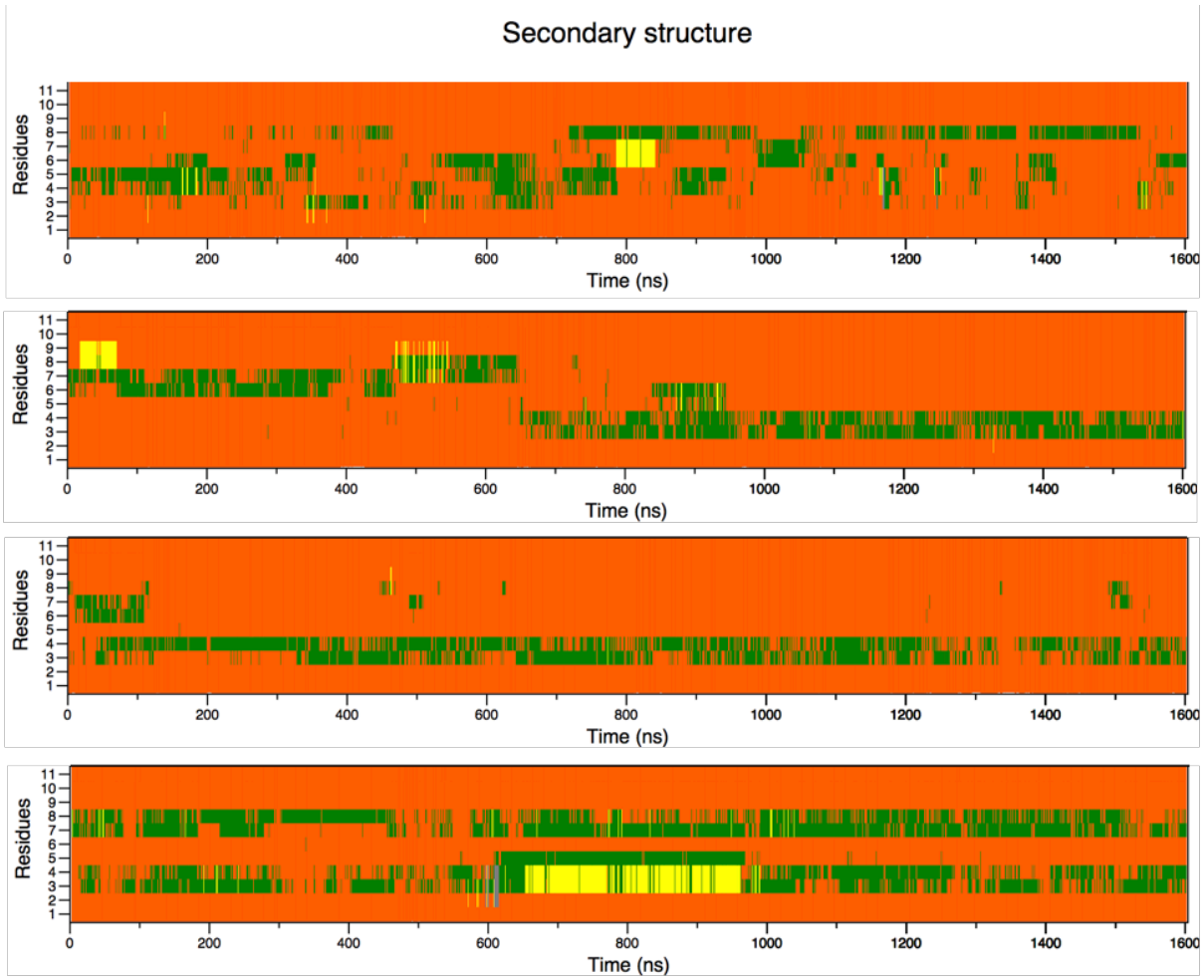


Figure S3: Secondary structure analyses graphs of **L**-BP100 in DPPC (a), DPPG (b), PCPG with raft (c) and PCPG without raft (d).

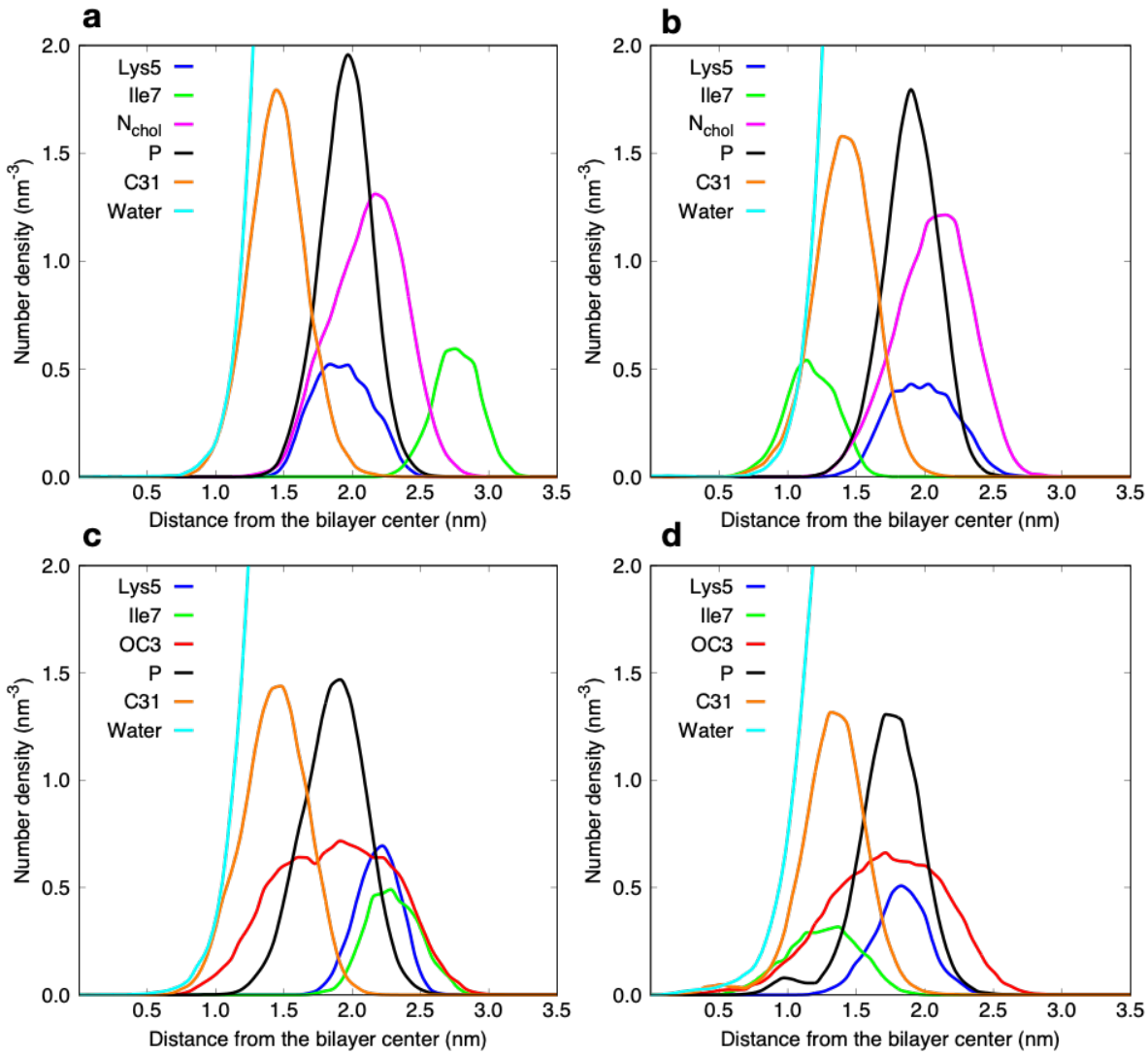


Figure S4: Peptide flip illustrated through number density graphs. a) and b) show respectively before and after peptide for α-BP100 in DPPC; c) and d) shows the peptide transition for α-BP100 (res1-5) in DPPG simulation. Deeper peptide insertion into the membrane happens after peptide flip. Concomitantly to peptide insertion, water infiltration was also noticeable.

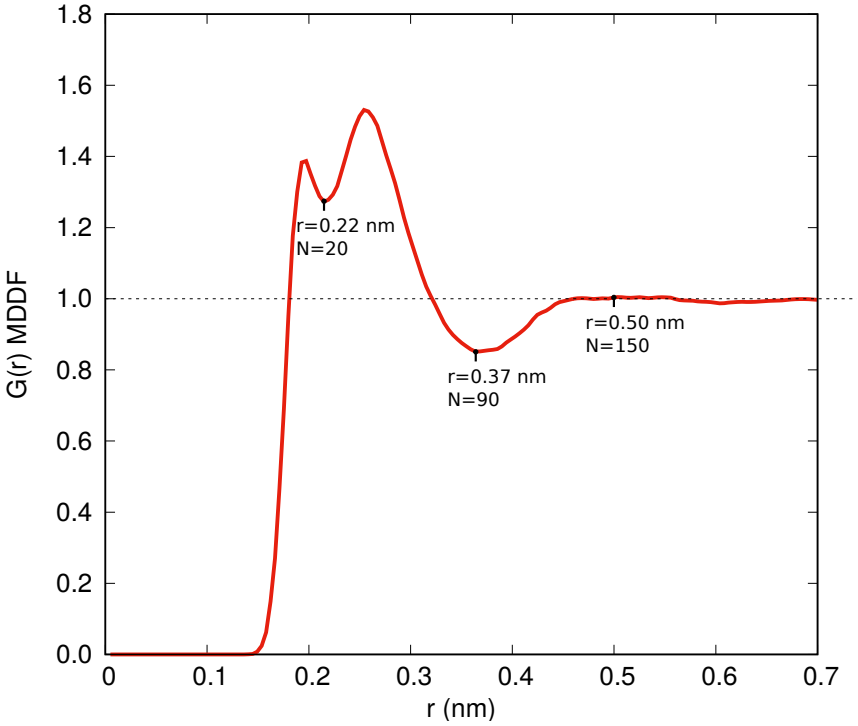


Figure S5: Minimum-distance distribution function (MDDF) between the peptide and the water molecules in the aqueous solution. For our comparative purposes, we first calculated the MDDF of BP100 in aqueous solution. In this distribution we obtained the first solvation shell up to 0.37 nm with 90 water molecules and beyond 0.5 nm no solvation shell could be identified anymore. The amount of water molecules obtained up to 0.5 nm was around 150 and this distance was used to perform further analyses for the comparative hydration of the peptide interacting with the membranes during the flip.

# 2.8. Supplementary Material references


1. Petrache, H. I. *et al.* Area per Lipid and Acyl Length Distributions in Fluid Phosphatidylcholines Determined by 2H NMR Spectroscopy. *Biophys. J.* **79,** 3172–3192 (2000).
2. Nagle, J. F. *et al.* X-ray structure determination of fully hydrated L alpha phase dipalmitoylphosphatidylcholine bilayers. *Biophys. J.* **70,** 1419–31 (1996).
3. Lis, L. J., McAlister, M., Fuller, N., Rand, R. P. & Parsegian, V. A. Interactions between neutral phospholipid bilayer membranes. *Biophys. J.* **37,** 657–65 (1982).
4. Nagle, J. F. Area/lipid of bilayers from NMR. *Biophys. J.* **64,** 1476–1481 (1993).
5. Kučerka, N., Nieh, M.-P. & Katsaras, J. Fluid phase lipid areas and bilayer thicknesses of commonly used phosphatidylcholines as a function of temperature. *Biochim. Biophys. Acta - Biomembr.* **1808,** 2761–2771 (2011).
6. Jämbeck, J. P. M. & Lyubartsev, A. P. Derivation and Systematic Validation of a Refined All-Atom Force Field for Phosphatidylcholine Lipids. *J. Phys. Chem. B* **116,** 3164–3179 (2012).
7. Tu, K., Tobias, D. J. & Klein, M. L. Constant pressure and temperature molecular dynamics simulation of a fully hydrated liquid crystal phase dipalmitoylphosphatidylcholine bilayer. *Biophys. J.* **69,** 2558–2562 (1995).
8. Kukol, A. Lipid Models for United-Atom Molecular Dynamics Simulations of Proteins. *J. Chem. Theory Comput.* **5,** 615–626 (2009).
9. Pan, J. *et al.* Molecular structures of fluid phase phosphatidylglycerol bilayers as determined by small angle neutron and X-ray scattering. *Biochim. Biophys. Acta - Biomembr.* **1818,** 2135–2148 (2012).
10. Jämbeck, J. P. M. & Lyubartsev, A. P. Another Piece of the Membrane Puzzle: Extending Slipids Further. *J. Chem. Theory Comput.* **9,** 774–784 (2013).
11. Kučerka, N. *et al.* Lipid Bilayer Structure Determined by the Simultaneous Analysis of Neutron and X-Ray Scattering Data. *Biophys. J.* **95,** 2356–2367 (2008).

# Chapter 3

# BP100 induces local membrane thinning and slows lipid dynamics

This chapter is a slightly modified version of a published article
https://doi.org/10.1039/D1RA06267K

## 3.1. Abstract

BP100, a short antimicrobial peptide, produces membrane perturbations that depend on lipid structure and charge, salts presence, and peptide/lipid molar ratios. As membrane perturbation mechanisms are not fully understood, the atomic scaled nature of peptide/membrane interactions requires a close-up view analysis. Molecular Dynamics (MD) simulations are valuable tools for describing molecular interactions at the atomic level. Here, we use MD simulations to investigate alterations in membrane properties consequent to BP100 binding to zwitterionic and anionic model membranes. We focused on membrane properties changes upon peptide binding, namely membrane thickness, order parameters, surface curvature, lipid lateral diffusion and membrane hydration. In agreement with experimental results, our simulations showed that, when buried into the membrane, BP100 caused a decrease in lipid lateral diffusion and lipid acyl-chain order parameters and sharp local membrane thinning. These effects were most pronounced on the closest lipids in direct contact with the membrane-bound peptide. In DPPG and anionic-aggregate-containing DPPC/DPPG membranes, peptide flip (rotation of its non-polar facet towards the membrane interior) induced marked negative membrane curvature and enhanced the water residence half-life time in the lipid hydrophobic core and transmembrane water transport in the direction of the peptide. These results further elucidate the consequences of the initial interaction of cationic alpha-helical antimicrobial peptides with membranes.

## 3.2. Introduction

According to the World Health Organization, "Antibiotic resistance is one of the biggest threats to global health, food security, and development today"[1]. Particularly, Gram-negative bacteria are more threatening, as they are naturally more resistant to antibiotics, mainly due to the extra protection provided by an outer-membrane formed mainly by negatively charged lipids and lipopolysaccharides[2,3]. Antimicrobial peptides (AMPs) are active against antibiotic-resistant bacteria, even in biofilms[4,5]. AMPs are a broad class of molecules that destroy or inhibit microbes' growth by different mechanisms, particularly disrupting the bacterial outer membrane[4,6,7]. This action mechanism is exciting and is effective against a large variety of Gram-negative bacteria[8–10]. Membrane disruption can occur by different pathways (barrel-stave, carpet, toroidal pore)[6], which may involve multiple peptides in cooperative processes[11]. Although AMPs have been widely studied, their therapeutic utilization is hindered by the lack of detailed understanding of their mechanism of action on membranes, a fundamental step in drug development[4]. FDA approved therapeutical use, mainly as topical medications, only a few of the more than three thousand known AMPs[12].

BP100 (H-KKLFKKILKYL-$NH_2$) is a short hybrid cationic alpha-helical AMP (CHAMP) designed by combining cecropin A and melittin, two antimicrobial peptides[13,14]. BP100 is highly selective towards Gram-negative bacteria, displays low minimal inhibitory concentrations and low cytotoxicity, making this peptide a potential candidate for drug development[13–15]. BP100 acts on the membrane, and its binding depends on the ratio of anion/zwitterionic lipid ratio of the membranes, being anionic lipid-rich membranes more prone to disruption than charge-neutral membranes[16]. Zeta potential measurements show that the increase of peptide/lipid ratio leads to the neutralization of the interfacial charge of large unilamellar vesicles and that the mechanism of membrane action also depends on the peptide/lipid ratio[16]. While BP100 is a random coil in bulk solution[17,18], it folds into an amphipathic alpha-helix when bound to

membranes, and the extent of alpha-helix formation when bound depends on the anionic lipid fraction in the vesicle[16–18]. Finally, BP100 can promote inner content leakage in unilamellar vesicles[16,18]. However, the peptide´s action mechanism on membranes seems to differ in low and high peptide-content or anionic lipid-content regimes: a gradual leakage is observed below a certain peptide/lipid ratio threshold, or below a certain anionic lipid content, and an instantaneous leakage above these ratios[16]. Atomistic molecular dynamics simulations (MD) in water and membranes show that this peptide is a random coil in an aqueous solution but maintains an alpha-helix conformation in membranes containing negatively charged lipids[19]. The hydrophobic facet of the alpha helix is buried inside the membrane hydrophobic core, while the hydrophilic facet of the helix is exposed to the bulk solution[19]. These findings correspond with the reported experimental results, even though such systems are heavily dependent on force field choices[20].

Simpler computational models can be used to evaluate the mechanism of membrane disruption by AMPs[21–24], due to its reduced computational cost[25]. For instance, Brownian dynamics simulations of coarse-grained peptides in implicit membrane models[21] suggest that BP100 disrupt membranes via the carpet model. Although these models can describe the membrane's effect on the structure and dynamics of the AMPs adsorbed at the interface, a few exceptions23 only captures the effect of AMPs on the membranes. However, due to the cooperative nature of the peptide action on membranes[11,26,27], it is essential to correctly depict a monomer's effect on the bilayer, as the binding of one peptide will disturb the membrane, altering the adsorption of subsequent peptides.

Thus, the understanding of isolated AMPs effects on membranes is necessary before describing its mechanisms of action at higher peptide concentrations correctly.

Here we present the findings from atomistic MD simulations of a single BP100 in membranes composed of anionic, zwitterionic, and mixtures of both lipids. We employed a distance-based scheme for a layered analysis of the outcomes of BP100 binding on bilayers. Membrane thickness, lateral

lipid diffusion, local membrane curvature, membrane hydration, and order parameters were investigated, and our results show more dramatic peptide effects on closer lipids from both monolayers. Also, these effects were dependent on the local composition of the membrane, i.e., more severe effects of BP100 on bilayers were observed when its local composition was richer in anionic lipids. This detailed description of BP100 effects in membranes of varied composition may provide the necessary information for future models to adequately describe the mechanism of action of BP100 on membranes at higher concentrations.

# 3.3. Methods

### 3.3.1. Simulation set-ups and details

We studied initially folded α-BP100 in lipid systems: in pure membranes (DPPC and DPPG), and mixed membranes DPPC:DPPG (50:50). All membranes contained 64 lipids on each leaflet. Two symmetrical mixed bilayers were studied: one with lipids randomly distributed in each monolayer (PCPG) and one with an initial aggregate of 16 DPPG lipids in the center of the monolayer with the remaining 16 DPPG and 32 DPPC lipids randomly distributed (PCPG*) (Table S1).

All-atom force fields Amberff99sb-ildn-NMR[28] and SLipids[29,30] were chosen for peptide and lipids were respectively after testing and validation[19]. Pure membranes topologies (DPPC and DPPG) were from the SLipids developer group website[31], and the mixed bilayers were assembled with PACKMOL[32] software. TIP3P water molecules solvated our systems reaching an approximately 53 water/lipid ratio. A single BP100 was initially positioned parallel to the membrane surface approximately 2 nm away. Aqvist[33] $Na^+$ ions and $Cl^-$ ions (Dang[34]) were introduced to counter-balance charges from BP100 and DPPG.

To integrate the equations of motion, we used a Leap-Frog integrator[35] with a 2 fs time-step. All simulations were performed in the NPT ensemble in which the temperature was kept constant at 323 K with the V-rescale thermostat[36] coupling separately peptide, lipids, water, and counter-ions with a  coupling constant of 0.1 ps. The Berendsen barostat[37] was used to keep the pressure constant with semi-isotropic pressure coupling at 1 bar with a coupling constant of 1 ps and compressibility of 4.5 x $10^{-5}$ bar. LINCS algorithm[38] was used to constrain all bonds. For long-range electrostatic correction Particle-mesh-Ewald method[39], with a real-space cut-off of 1.5 nm, was applied. Van der Waals interactions were truncated at a distance of 1.5 nm with a switch function from 1.4 nm. Each set-up was simulated for a total time of $\tau_{tot}$ = 2 μs, after an initial equilibration step.

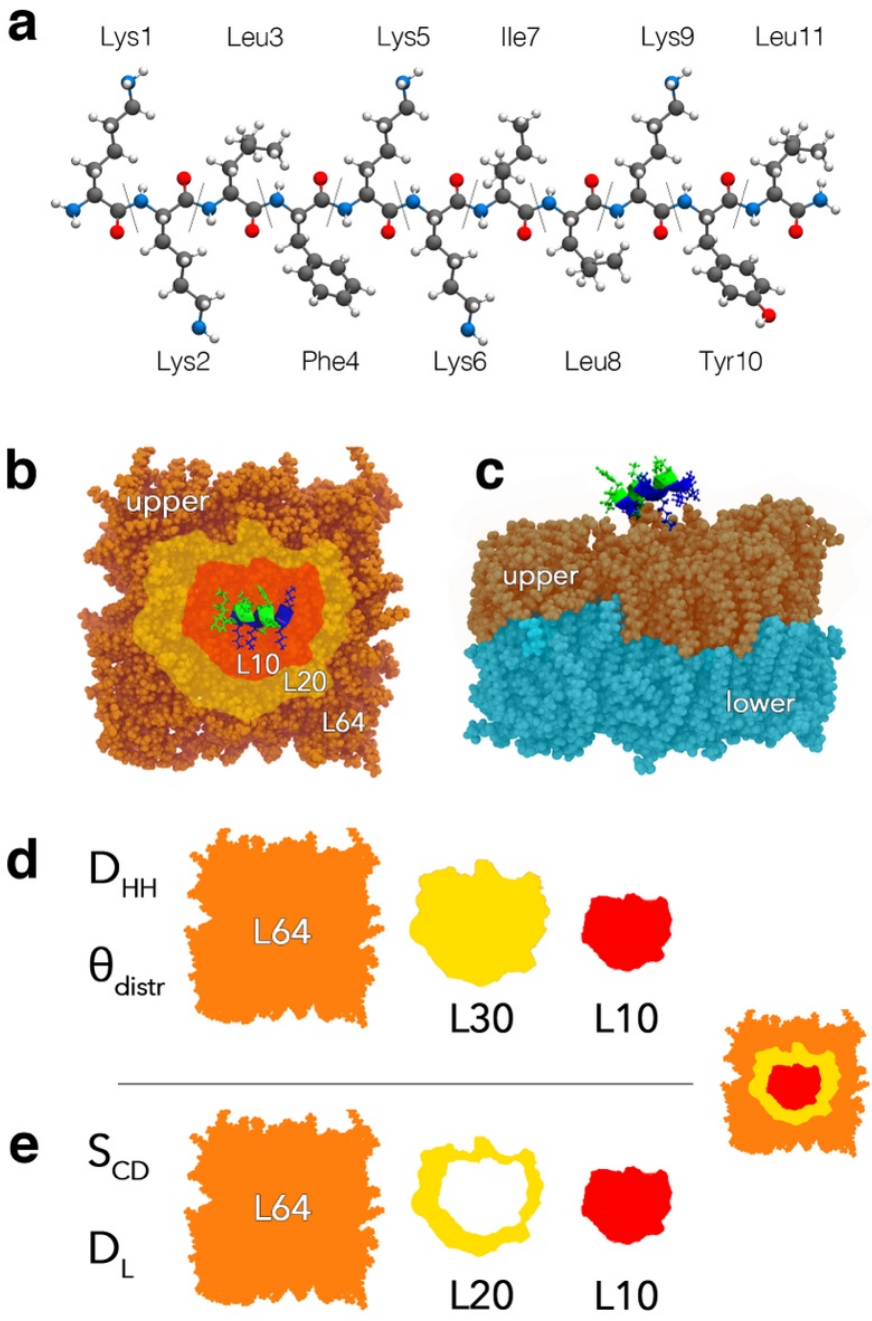


Figure 1: Lipid indexing for local and overall membrane analysis. (a) BP100 molecular structure. (b) Lipid indexing in relation to its phosphorus distance to BP100. Both monolayers were analyzed separately (c). For all analysis, L10 represents the first 10 closest lipids to BP100, and L64, the entire monolayer. For membrane-shape-dependent properties, such as membrane thickness and surface curvature angle distribution, SuAVE analysis package was utilized and L30 represents the first 30 closest lipids to BP100 (d). For deuterium order-parameters and lipid lateral diffusion coefficients, L20 groups the first 20 closest lipids to BP100 excluding the first 10 lipids (e).

To analyze the influence of BP100 on local membrane properties, we performed our lipid analysis in layers, taking into account the gradual distance to the peptide. Lipids were ranked according to the distance between their phosphorus atoms and the peptide atoms, using GROMACS *trjorder* command. For membrane thickness ($D_{HH}$) and surface curvature angle distribution ($\vartheta_{distr}$), the first 10, 30 lipids closest to BP100 and the entire monolayer were investigated (L10, L30, L64, Fig. 1C). For deuterium order parameters ($S_{CD}$) and lipid lateral diffusion coefficients ($D_L$) L10, L20, which excludes L10, and L64 were considered (Fig. 1D). Each monolayer was analyzed separately (Fig. 1), and for comparison, pure bilayer simulations were used as control. Due to peptide and lateral lipid movement during the simulation, lipid group indexing was updated every 10 ns (Fig. 2). This interval was chosen after simulation trajectories visual inspection.

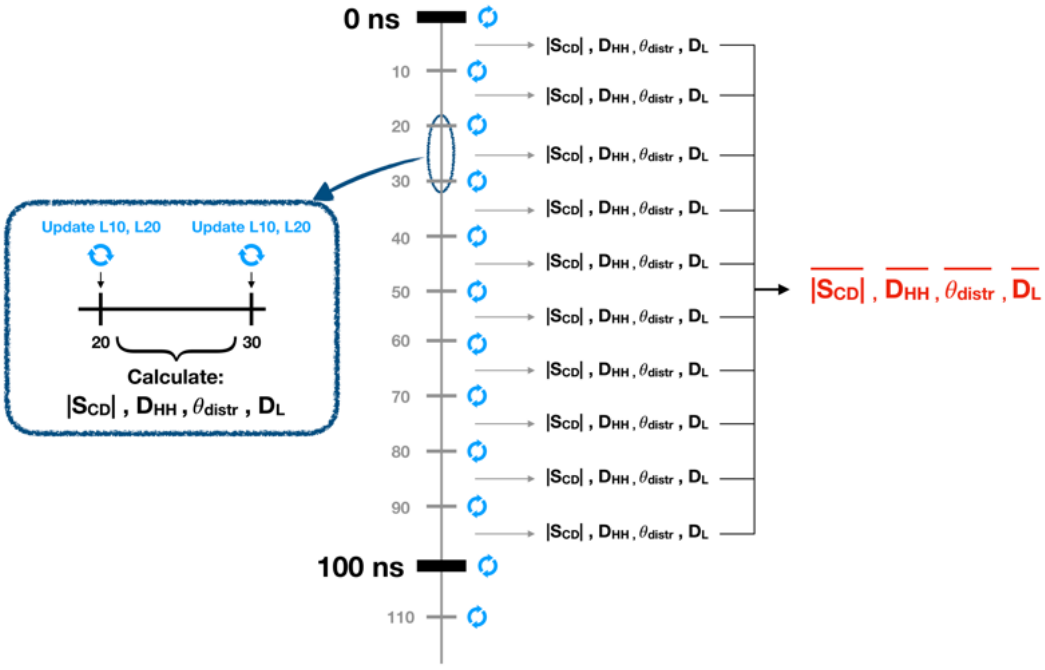


Figure 2: Lipid indexing update and calculation of membrane properties. Lipid indexing for lipid groups (L10, L20, and L30) were updated on every 10 ns to ensure accurate lipid selection. All membrane properties ($S_{CD}$, $D_{HH}$, $\vartheta_{distr}$, and $D_L$) were calculated in 10 ns windows. Then, 20 average and standard error values were obtained over blocs of 100 ns each.

Two hundred windows of 10 ns each was analyzed, considering the total simulation time $\tau_{tot}$ of 2000 ns. Then, they were averaged in blocks of 10 windows for all calculated lipid properties, resulting in 20 average values of 100 ns each with their respective standard error. This scheme is illustrated in Figure 2.

### 3.3.2. Membrane thickness ($D_{HH}$) and surface curvature angle distribution ($\vartheta_{distr}$)

Accurate calculation of membrane thickness ($D_{HH}$) and surface curvature ($\vartheta_{distr}$) requires proper consideration of the bilayer shape. This calculation was achieved by using SuAVE software package[40], which fits a rectangular grid mesh (Fig. 3) based on the location of a selection of atoms (i.e., phosphorus from the lipids phosphate group) and then calculates the average distance between the upper and lower grids for $D_{HH}$ (Fig. 3A) and the distribution of the angles ($\vartheta_{distr}$, Fig. 3B) between the z-axis and the normal vector of each rectangular grid for surface curvature analysis. Higher angles indicate the membrane is curved.

Using SuAVE[40], membrane surface grids for L10, L30, and L64 were obtained using phosphorus atoms positions at every 10 ns, and their respective $D_{HH}$ and $\vartheta_{distr}$ values were computed.

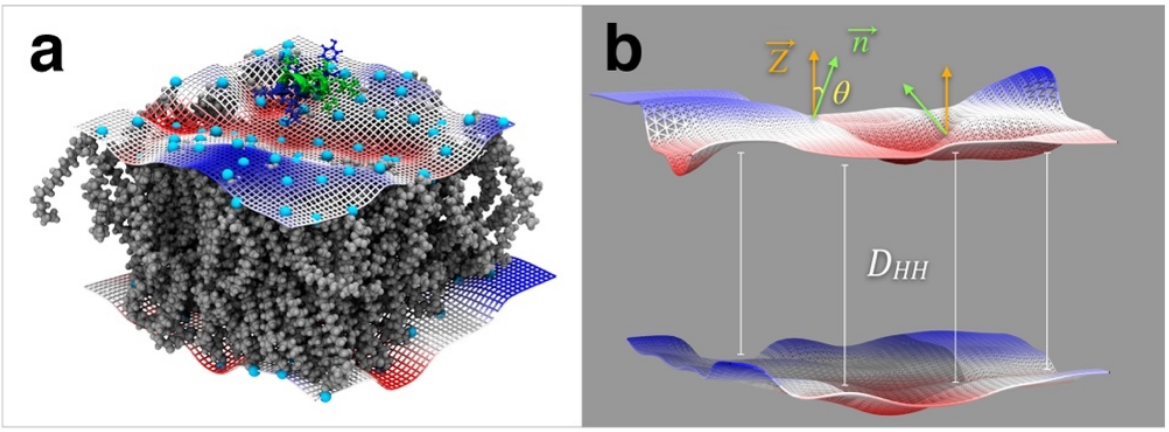


Figure 3: Membrane thickness and surface curvature angle distribution analysis using SuAVE. SuAVE software generates a grid (a) onto the position of selected atoms of the membrane (in our case, phosphorus atoms, in cyan) considering a specific number of rectangular partition bins along the x and y axes, chosen by the user. Surface curvature is analyzed by measuring the angle between the z-axis and the normal vector of each surface rectangular grid (b) and an angle distribution is generated. Higher angles indicate membrane curvature. Membrane thickness (b) was obtained by calculating the average distance between both upper and lower grids.

### 3.3.3. Deuterium order parameters ($S_{CD}$) and lipid lateral diffusion coefficient ($D_L$)

Deuterium order-parameters ($S_{CD}$) and lipid lateral diffusion coefficients ($D_L$) were obtained using GROMACS 5.0.2[41–43]. The local order of a lipid bilayer can be described by $^2$H-NMR deuterium order parameters ($S_{CD}$) as $S_{CD} = (1/2)\langle 3cos^2\theta - 1\rangle$, where $\theta$ is the angle between vector Carbon-Deuterium (actually C-H bond vectors in our simulations) and the membrane normal, whereas the brackets indicate the average during the simulation.

$|S_{CD}|$ values for the sn1 acyl chain were calculated for all simulations and lipid groups (L10, L20, L64) in both leaflets. The sn1 acyl chain was selected as a representative sample of lipid order parameters.

The lipid lateral diffusion coefficient ($D_L$) can be obtained from MSD $= 4D_Lt$, where MSD is the mean square displacement of an atom as a function of time, $t$. MSD of the phosphorus atoms from each lipid group were calculated at every 10 ns. Then, $D_L$ was obtained from the slope of the least square fitting between 2 to 5 ns of each 10-ns-time-window.

## 3.4. Results

We analyzed four simulation sets that run for $\tau_{tot}$ = 2 µs each. BP100 was initially folded as an alpha-helix and positioned approximately 2 nm away from the membranes (DPPC, DPPG, PCPG and PCPG*). Control simulations of pure membranes gave the expected area per lipid and membrane thickness[44–48]. Peptide secondary structure analysis and the average number of lipids in contact with BP100 were investigated previously[19]. Moreover, in the peptide/membrane simulations, BP100 approached the membrane with its positively charged facet and rotated, facing its non-polar residues to the membrane core, while maintaining its alpha-helical structure (Fig. S2B). This motion, which we previously defined as peptide flip (Fig. S3), is accompanied by peptide dehydration and an increase in non-polar contacts between peptide and membrane[19]. However, in DPPC, although the peptide flipped, its alpha-helical structure was lost (Table S4), and therefore we will refer to it as a semi peptide-flip. The following sections present our focus on the peptide effects on the membrane.

### 3.4.1. Membrane thickness

All trajectories showed BP100 adsorbed onto the membranes and continued embedded throughout the simulations. We observed peptide flip in the BP100 on DPPC (˜700 ns), DPPG (˜1500 ns), and PCPG* (˜390 ns) simulations[19]. Table 1 presents the values of membrane thickness averaged over the entire simulation, and control shows $D_{HH}$ values for membrane-only simulations. In all simulations, compared to the overall membrane thickness (L64), L10 shows lower values, indicating bilayer thinning where BP100 was bound. The overall membrane thickness values (L64) take into account all monolayer lipids; thus, the actual thickness difference between L10 and the rest of the membrane was higher in all cases. L10 thickness reduction was detected for all simulations, and it was significantly higher in membranes with an anionic lipid aggregate (Table

1 and Fig. S5). L30, L64, and control membranes shared similar thicknesses, indicating BP100 thinning activity was limited to the first near lipids, close to the peptide.

Simulations with peptide flip and anionic membranes, namely BP100 in DPPG and PCPG*, showed the lowest membrane thicknesses in L10, with averaged values of 3.50 ± 0.12 and 3.57 ± 0.10, respectively (Table 1). In the BP100 in DPPC simulation, despite peptide flip, the peptide lost some of the alpha-helical conformation (45% of helicity, Table S4).

| Membrane thickness (nm) | | | | |
|---|---|---|---|---|
| | L10 | L30 | L64 | Pure Membrane |
| BP100 in DPPC | 3.71 ± 0.08 | 3.75 ± 0.04 | 3.77 ± 0.03 | 3.79 ± 0.03 |
| BP100 in DPPG | 3.50 ± 0.12 | 3.67 ± 0.05 | 3.72 ± 0.03 | 3.70 ± 0.05 |
| BP100 in PCPG* | 3.57 ± 0.10 | 3.77 ± 0.05 | 3.83 ± 0.04 | 3.82 ± 0.04 |
| BP100 in PCPG | 3.72 ± 0.10 | 3.82 ± 0.05 | 3.84 ± 0.02 | 3.83 ± 0.04 |

Table 1: BP100 induces membrane thinning in anionic bilayers. Average membrane thickness ($D_{HH}$) and standard deviation obtained for all simulations.

An anionic lipid aggregate, either as a membrane patch (PCPG*) or in the whole membrane (DPPG), seemed essential for the peptide-induced membrane thinning (Table 1). This can also be visualized by comparing the obtained thicknesses in L10 for BP100 in PCPG and PCPG*. While both simulations share the same membrane composition and only differ in their lipid distribution, PCPG shows an average thickness of 3.57 ± 0.10 nm in L10 and PCPG*, 3.72 ± 0.10 nm (Table 1).

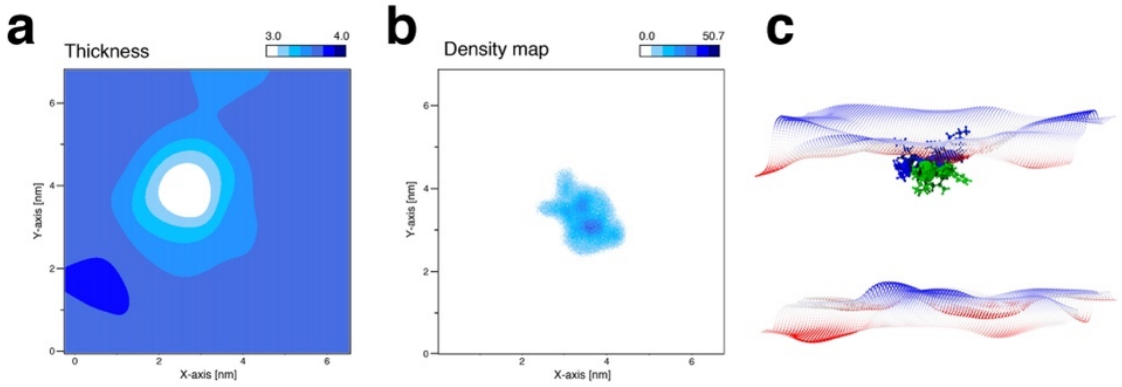


Figure 4: BP100 induces membrane thinning in anionic bilayers. Membrane thickness map for BP100 in DPPG (a) and peptide density map (b), averaged from 1600 to 1700 ns of simulation, after peptide flip. BP100 induced membrane thinning is clearly visible by the superposition of both maps. In (c), a snapshot at 1600 ns; BP100 positively charged residues are colored in blue and the non-polar residues in green. The upper and lower grids were generated by SuAVE taking into account the positions of the DPPG phosphorus atoms. BP100 thinning activity is stronger on anionic-lipid-aggregate-containing membranes (PCPG* and DPPG).

According to the peptide distance, the gradual membrane thinning can be visualized through number density graphs (Figs. S6 and S7). Number density graphs of before and after peptide flip revealed the distance shortening between upper-L10 and lower-L10, particularly in BP100 in DPPG (Fig. S6B) and BP100 in PCPG* (Fig. S7A) simulations. Although the upper-L10 position was affected by BP100 the most, shown by the curve broadening of upper-L10 signal, lower-L10 is also pulled towards the peptide (Figs. S6B and S7A), demonstrating that BP100 binding effect has an impact on the opposite bilayer leaflet. Figure 4 shows membrane thickness and peptide density in 2D mapping obtained from the BP100 in DPPG simulation, where membrane thinning was the most significant (Table 1). A simulation snapshot at 1600 ns is shown in Figure 4C. A negative curvature was visible by overlaying the BP100 position with SuAVE grids generated based on the DPPG phosphorus atoms positions (Fig. 4C). The overlay of 2D membrane thickness and peptide density mappings gives information on the peptide position and its outcomes on membrane thickness. In DPPC, semi peptide flip showed mild effect (Fig.

S6A) on membrane thickness, while in BP100 in DPPG and PCPG* simulations, a valley on the membrane matching the peptide position is evident (Figs. 4 and S8C). We confirmed that peptide flip increased membrane thinning by analyzing the data before and after the flip in DPPG (Fig. S8B). The membrane was affected by peptide adsorption (Fig. S8B - before), but peptide flip made the membrane thinner, decreasing the membrane thickness of the first surrounding lipids from 3.2 nm to 3.0 nm, on average (Fig. S8B - after). In PCPG*, we observed similar results (Fig. S8C) as in DPPG, with membrane thickness decrease after the flip. In PCPG (Fig. S8D), where no flip occurred, no change was detected, comparing the simulation beginning and end.

### 3.4.2. Surface curvature

2D membrane thickness mappings indicated that the membrane surface was altered by BP100 binding and flip. To investigate these effects quantitatively, we calculated the distribution of the surface curvature angle $\vartheta$, defined as the angle between the normal vector of the surface rectangular grid partitions and the z-axis. Larger $\vartheta$ values indicate greater membrane surface curvature. Figure 5 shows the distribution of $\vartheta$ in different upper monolayer regions for BP100 in PCPG* simulation.

Comparison of the $\vartheta$ distribution for all upper lipid groups (L10, L30, L64) against control showed an increase in the percentage of lipids populating higher $\vartheta$ (20°-50°) (Fig. 5). These data show that the binding of a single peptide changed the overall membrane topology. The depression shown in 2D membrane thickness mappings (Fig. S8) indicated BP100 caused negative curvature on anionic bilayers.

For BP100 in DPPG and PCPG* simulations, the surface angle distribution for upper-L10 and upper-L30 showed a most significant portion of $\vartheta$ populating lower values before the flip (Figs. 5A, S9B and S10A). After peptide flip, the surface of upper-L10 showed a broader and flattened distribution curve, with an increase in the population of higher angle values (30°-50°), compared to the overall upper monolayer (upper-

L64), and lower monolayer (lower-L64), demonstrating peptide flip caused local membrane curvature (Fig. 5B, S9A and S10B).

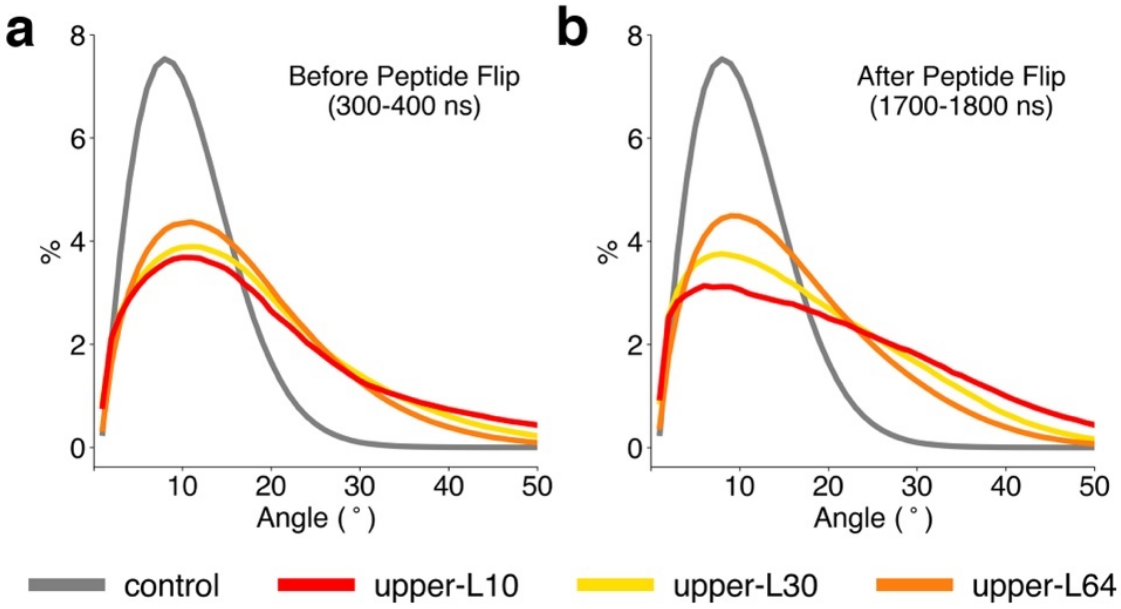


Figure 5: Peptide flip induces negative membrane curvature. Membrane surface curvature angle ($\vartheta_{distr}$) distribution before (a) and after (b) the flip in the BP100 in PCPG* simulation. Higher angles indicate increased membrane curvature. Control curves represent $\vartheta_{distr}$ from pure membrane simulations.

In the BP100 in DPPC (Fig. S9A) and BP100 in PCPG (Fig. S10B), no remarkable shifts in angle distribution were detected. Semi-peptide flip was insufficient to alter upper-L10 surface angle distribution in the BP100 in DPPC simulation (Fig. S9A). These data substantiate our findings in that not only anionic lipid content is essential for peptide activity on membranes, but its distribution is crucial as well[19].

### 3.4.3. Lipid order parameters

Lipid chain order parameters were evaluated to investigate whether BP100 binding influenced lipid hydrophobic chain ordering and dynamics. Sn1 carbon chain of lipids (Fig. S11) was taken as a representative of the overall lipid acyl chains. Figure 6 shows lipid sn1 acyl chain order

parameters of distinct membrane regions from BP100 in DPPG simulations before and after the simulation.

Even in earlier stages of peptide binding to the membrane (Fig. 6A), upper-L10 and lower-L10 lipids showed more disordered chains than control and other membrane regions. Nevertheless, with peptide flip, a sharp decrease in $S_{CD}$ was observed for upper-L10, showing the BP100 effect on its immediate neighboring lipids after flipping (Fig. 6B).

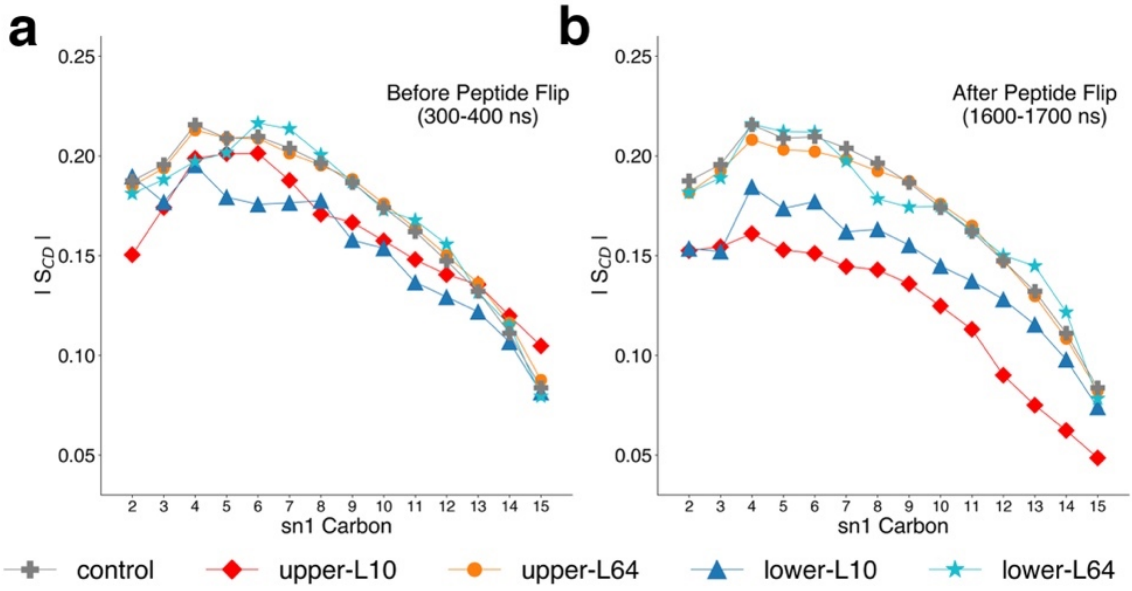


Figure 6: BP100 decreases local lipid chain order parameter. Order parameters of sn1 DPPG acyl chain in the BP100 in DPPG simulation before (a) and after (b) the flip. The sn1 lipid chains were used for calculating lipid order parameters of the 10 and 20 closest lipids to BP100 the entire monolayer on both monolayers. Control sn1 $S_{CD}$ data was taken averaging over an entire peptide-free membrane simulation.

In all simulations, the $S_{CD}$ profiles of the upper-L10 and lower-L10 acyl chains were significantly lower compared to other regions of the upper monolayer (Figs. 6 and S12). This behavior was observed in simulations with negatively charged bilayers (Figs. 6 and S12), with both upper-L10 and lower-L10 having higher conformational freedom due to BP100 binding.

In simulations where peptide flip was observed, the decrease in upper-L10 order before and after the flip was apparent for all acyl chain carbons

(Figs. 6 and S12), even for BP100 in DPPC with a semi-flip (Fig. S12A). Table 2 shows the averaged order parameters of all sn1 chain carbons in upper-L10. In simulations where peptide flip occurred, namely DPPC, DPPG, and PCPG*, a decrease of 9%, 23%, and 17% in $\langle|S_{CD}|\rangle$ is observed after the flip, compared to control. In contrast, in PCPG albeit the presence of anionic lipids, we found a reduction of 5% in $\langle|S_{CD}|\rangle$ compared to control (Table 2). The decrease in overall lipid acyl chain order parameters in upper-L10 can be explained by the insertion of BP100 hydrophobic residues into the bilayer core, increasing the acyl chain(s) freedom.

| Lipid Lateral Diffusion ($10^{-7}$ $cm^2s^{-1}$) | | | | | |
|---|---|---|---|---|---|
| | Upper-L10 | Upper-L20 | Upper-L64 | Pure Membrane | Literature |
| BP100 in DPPC | 0.9 ± 0.2 | 1.3 ± 0.2 | 1.6 ± 0.2 | 1.6 ± 0.3 | 1.8[44],1.78[47], ~1.5[45] |
| BP100 in DPPG | 0.6 ± 0.2 | 1.1 ± 0.2 | 1.2 ± 0.2 | 1.3 ± 0.2 | 0.9[48] |
| BP100 in PCPG* | 0.6 ± 0.2 | 1.0 ± 0.2 | 1.2 ± 0.2 | 1.2 ± 0.2 | - |
| BP100 in PCPG | 0.7 ± 0.3 | 1.1 ± 0.3 | 1.2 ± 0.2 | 1.3 ± 0.2 | - |

Table 2: Averaged lipid sn1-chain order parameter, $\langle|S_{CD}|\rangle$, for lipids in upper-L10, obtained from the initial and last 300 ns of simulation. Peptide flip was observed in DPPC, DPPG and PCPG* simulations, thus their $\langle|S_{CD}|\rangle$ values from the last 300 ns of simulation are post-peptide flip. Control values are presented for comparison.

In the BP100/DPPC simulations, semi peptide flip lowered the order parameters of the closest lipids in contact (upper-L10, Fig. S12A and Table 2). However, the loss of the alpha-helical conformation led to less peptide penetration (Fig. S6A) and limited insertion of hydrophobic residues into the bilayer. Lower peptide penetration explains the discrepancy between $S_{CD}$ profiles of other lipid groups and upper-L10 after the flip (Fig. S12A). The BP100/PCPG order parameter profile (Fig. S12B) showed upper-L10 and lower-L10 decrease in chain order late in the simulation. Presumably, the binding of BP100 produced a weak effect on

the acyl-chain order parameters, as evidenced by the higher $|S_{CD}|$ values (Table 2) for all carbons of the acyl chain compared to simulations where peptide flip took place (DPPC, DPPG, and PCPG*). These data highlight the importance of anionic lipid aggregates for the peptide to maintain a helix conformation and, later, a full flip.

### 3.4.4. Lipid lateral diffusion

We investigated alterations in lipid dynamics upon peptide binding in the near and far vicinity of BP100. Lipid lateral diffusion coefficients for L10, L20, and L64 in both leaflets were calculated from the slopes of the mean-square displacements (MSD) in the xy-plane (Table 3).

| Lipid Lateral Diffusion ($10^{-7}$ $cm^2s^{-1}$) | | | | | |
|---|---|---|---|---|---|
| | Upper-L10 | Upper-L20 | Upper-L64 | Pure Membrane | Literature |
| BP100 in DPPC | 0.9 ± 0.2 | 1.3 ± 0.2 | 1.6 ± 0.2 | 1.6 ± 0.3 | 1.8[44],1.78[47], ~1.5[45] |
| BP100 in DPPG | 0.6 ± 0.2 | 1.1 ± 0.2 | 1.2 ± 0.2 | 1.3 ± 0.2 | 0.9[48] |
| BP100 in PCPG* | 0.6 ± 0.2 | 1.0 ± 0.2 | 1.2 ± 0.2 | 1.2 ± 0.2 | - |
| BP100 in PCPG | 0.7 ± 0.3 | 1.1 ± 0.3 | 1.2 ± 0.2 | 1.3 ± 0.2 | - |

Table 3: Lipid lateral diffusion values of different lipid regions for all simulations (Figure 1) and available experimental and theoretical data are also presented for comparison. Our simulation data reveal lipid lateral mobility is approximately 50% lower in the first surrounding of BP100 (upper-L10) compared to a peptide absence scenario (lower-L64) and membranes with higher anionic lipid content are more affected due to stronger electrostatic interactions and flip.

The calculated lateral diffusion coefficients in upper-64 for DPPC and DPPG were 1.6 ± 0.2 and 1.2 ± 0.2, respectively. These values were well within experimental results and similar to our controls (Table 3). Systematic analysis of lipid dynamics considering the proximity to BP100

reveals an approximately 50% decrease of lipid lateral diffusion in upper-L10 compared to pure membrane systems, for all simulations (Table 3).

Similar to changes in membrane thickness, order parameters, and membrane curvature, BP100 effect on lipid lateral diffusion is more substantial on upper-L10, while upper-L20 and lower-L64 show similar values (Table 3). We also calculated the diffusion for the 5 closest lipids to BP100 and the results found are similar to upper-L10, showing that 1:10 peptide/lipid ratio is where BP100 shows the most capacity for membrane disturbing effects (Table S13).

## 3.5. Discussion

In our simulations, BP100 promoted membrane thinning, depending on the membrane's composition (Table 1, Figs. 4 and S8). While marginal thinning was observed in membranes without PG agglomerates, more severe effects were observed in simulations where the peptide was in close contact with PG-enriched regions. Furthermore, our layered analysis showed that the peptide effect was more substantial to lipids closer to the peptide and that the effect vanished after a couple of lipid layers (after L20). These results show, simultaneously, the effect of BP100 on membranes and its dependence on membrane composition. Peptide-induced membrane thinning has been observed both experimentally in microscopy experiments[49], X-ray difraction[50], circular dichroism[51,52], and NMR[53–55]. Molecular simulations of membrane/CHAMPs systems[56–58] also support the experimental observations.

Additionally, BP100 is known for its activity-dependence on membrane charge, and its disrupting effect increases with negatively charged membranes[16], due to the electrostatic interactions with negatively charged groups of the membrane[19]. Finally, the considerable observed difference between the PC/PG mixture membranes with and without PG agglomerate points to the fundamental importance of lipid organization close to the BP100, i.e., the effect of the peptide on the membrane does

not solely depend on the amount of PG content in the membrane, but also the local distribution of PG in the BP100 vicinities. We emphasize here that lipid clustering is reported in some CHAMPs/membrane systems[8,59,60].

Using SuAVE analysis software[40], which fits a surface at the membrane interface, a local and negative Gaussian membrane curvature was observed, induced by BP100 (Fig. 5). Once more, the lipids closer to the peptide were more disturbed by the peptide, as the angle distribution function for the L10 group is skewed towards higher angles, compared with other lipids in the membrane. Also, the peptide effect increased when peptide flip occurred. The L20 was also disturbed but not to the same extent observed for the L10 group. Similar to the thinning effect, no significant peptide effect was observed in DPPC membrane (Fig. S9A) or PC/PG membrane without PG agglomerate (Fig. S10B), highlighting the importance of electrostatic interactions between the positively charged groups of BP100 and the negatively charged groups of PG. CHAMPs-induced membrane curvature is already reported, both by experimental[61–63] and computational methods[64–66], and it seems to be a necessary condition for membrane pore formation[61,67,68], usually a collective process that involves several peptides. Our simulations show that a single BP100 can induce high local negative curvature, changing the local lipid packing and, consequently, the binding of additional peptides in this peptide-perturbed region of the membrane.

Along with membrane thinning and local negative curvature, BP100 promoted a significant decrease in the calculated order parameter, $S_{CD}$ (Fig. 6), throughout the lipids acyl chain (sn1), which corresponds to an increase in conformational freedom of the hydrophobic chains upon BP100 binding. In line with previous properties, this $S_{CD}$ decrease depended on the proximity between the lipid and the peptide, having closer lipids to BP100 (L10 group) higher conformational freedom than the other lipids in the membrane. Local lipid distribution modulated the effect of BP100 on the $S_{CD}$ of the lipids, as the observed reduction was greater in the simulation with (than without) the PG agglomerate. These findings

corroborate the trends observed in experimental measurements of $S_{CD}$ of BP100-containing systems[53,55]. Our results showed that the orientation of the peptide with respect to the membrane changes the computed $S_{CD}$ values, as in DPPG and PCPG*, where a full flip took place, $S_{CD}$ profiles of upper-L10 and lower-L10 (Fig. S12 and Table 2) were significantly lower than other lipid groups, their respective controls, and other simulations (Table 2).

Lateral diffusion of lipids was analyzed from our simulations, as it constitutes an essential component of the membrane dynamics and cell functions. Lipid lateral diffusion alteration upon peptide binding has been studied by several peptides experimentally[69–73] and theoretically[74,75]. For example, the neurotoxic Alzheimer's disease peptide amyloid-beta increases lipid diffusion as shown by neutron scattering experiments[71,73]. Alpha helical and/or cationic peptides such as gramicidin, mellitin, and cWFW slow down lipids[69,70,76]. In our simulations, BP100 decreased the upper-L10 lipid lateral diffusion coefficients ($D_L$) by up to 50% (Table 3) compared with the lipid diffusions in membranes without the peptide, regardless of the composition of the membrane. We note that we also computed the $D_L$ of upper L5 (Table S13), and the results were similar to those of upper L10, suggesting that the ca. 10 lipids closest to BP100[19] are more affected than non-neighboring lipids. No significant effects of peptide flip on $D_L$ were found in our simulations. Similarly, to previous computed lipid/membrane properties, this decrease was most significant in upper-L10 than in other lipid groups, highlighting BP100 capacity of disturbing nearby lipids in the membrane. Although lateral diffusion of lipids in membranes is a more complex process than a simple 2D motion of lipids[77], our results showed that BP100 reduces local lipid mobility. This reduction is compatible with recent reports on both *in vivo* and *in vitro* effect of a CHAMP on membrane fluidity[76].

## 3.6. Conclusion

Our results demonstrated that a single BP100 peptide can largely affect anionic or zwitterionic/anionic lipid membrane local properties. Membrane thinning was observed, while membranes acquired a curved conformation, concomitant with increased lipids chain conformational freedom, reduced lipid lateral diffusion and favored the water residence half-life time in the membrane hydrophobic core, and transmembrane water transport into the peptide direction. These effects depended upon the lipids neighboring BP100: a minimum amount of anionic lipid is necessary for BP100 to disturb the membrane. Thus, our results confirmed the need for correct representation of single peptide-membrane interaction, as several membrane properties can be (locally) affected.

Experimental results (circular dichroism, NMR, dynamic light scattering, zeta potential, electrophoretic mobility and leakage of dyes with fluorescence) of BP100 action upon membranes of various anionic lipid content suggest that the clustering of negatively charged lipids was required for membrane disruption[16]. Taken together with previous reports that alpha-helical BP100 inserts its hydrophobic residues inside membrane hydrophobic region while maintaining the electrostatic interactions of charged residues with lipid headgroups[19], the present results provide a more clear picture of the early stages of BP100-anionic membrane interaction while providing insights on BP100 mechanism of action for membrane disruption.

The electrostatic long-range peptide-lipids interaction must drive BP100 towards the membrane when adsorption occurs. The highly positively charged peptide may promote anionic lipid clustering, locally disturbing membrane while acquiring an alpha-helix conformation. Such events would trigger a cooperative process, with anionic lipid clustering increasing the probability of subsequent BP100 binding, in line with the mechanism of action of CHAMPs upon membranes proposed by Epand and Epand[78,79].

# 3.6. References


1. Antibiotic resistance. https://www.who.int/news-room/fact-sheets/detail/antibiotic-resistance.
2. Silhavy, T. J., Kahne, D. & Walker, S. The bacterial cell envelope. *Cold Spring Harb. Perspect. Biol.* **2**, 1–16 (2010) doi: 10.1101/cshperspect.a000414.
3. Jubeh, B., Breijyeh, Z. & Karaman, R. Resistance of gram-positive bacteria to current antibacterial agents and overcoming approaches. *Molecules* **25**, (2020) doi: 10.3390/molecules25122888.
4. Li, J. *et al.* Membrane Active Antimicrobial Peptides: Translating Mechanistic Insights to Design. *Front. Neurosci.* **11**, 73 (2017) doi: 10.3389/fnins.2017.00073.
5. Pletzer, D., Coleman, S. R. & Hancock, R. E. W. Anti-biofilm peptides as a new weapon in antimicrobial warfare. *Curr. Opin. Microbiol.* **33**, 35–40 (2016) doi: 10.1016/j.mib.2016.05.016.
6. Brogden, K. A. Antimicrobial peptides: Pore formers or metabolic inhibitors in bacteria? *Nature Reviews Microbiology* vol. 3 238–250 (2005) doi: 10.1038/nrmicro1098.
7. Nguyen, L. T., Haney, E. F. & Vogel, H. J. The expanding scope of antimicrobial peptide structures and their modes of action. *Trends Biotechnol.* **29**, 464–472 (2011) doi: 10.1016/j.tibtech.2011.05.001.
8. Epand, R. M., Rotem, S., Mor, A., Berno, B. & Epand, R. F. Bacterial membranes as predictors of antimicrobial potency. *J. Am. Chem. Soc.* **130**, 14346–14352 (2008) doi: 10.1021/ja8062327.
9. Paterson, D. J., Tassieri, M., Reboud, J., Wilson, R. & Cooper, J. M. Lipid topology and electrostatic interactions underpin lytic activity of linear cationic antimicrobial peptides in membranes. *Proc. Natl. Acad. Sci.* 201704489 (2017) doi:10.1073/pnas.1704489114 doi: 10.1073/pnas.1704489114.
10. Bahar, A. & Ren, D. Antimicrobial Peptides. *Pharmaceuticals* **6**, 1543–1575 (2013) doi: 10.3390/ph6121543.
11. Wang, J. *et al.* The cooperative behaviour of antimicrobial peptides in model membranes. *Biochim. Biophys. Acta - Biomembr.* **1838**, 2870–2881 (2014) doi: 10.1016/j.bbamem.2014.07.002.
12. Chen, C. H. & Lu, T. K. Development and challenges of antimicrobial peptides for therapeutic applications. *Antibiotics* **9**, (2020) doi: 10.3390/antibiotics9010024.
13. Badosa, E. *et al.* A library of linear undecapeptides with bactericidal activity against phytopathogenic bacteria. *Peptides* **28**, 2276–2285 (2007) doi: 10.1016/j.peptides.2007.09.010.
14. Ferre, R. *et al.* Synergistic Effects of the Membrane Actions of Cecropin-Melittin Antimicrobial Hybrid Peptide BP100. *Biophys. J.* **96**, 1815–1827 (2009) doi: 10.1016/j.bpj.2008.11.053.
15. Guell, I. *et al.* Improvement of the Efficacy of Linear Undecapeptides against Plant-Pathogenic Bacteria by Incorporation of D-Amino Acids. *Appl. Environ. Microbiol.* **77**, 2667–2675 (2011) doi: 10.1128/aem.02759-10.
16. Manzini, M. C. *et al.* Peptide:Lipid ratio and membrane surface charge determine the mechanism of action of the antimicrobial peptide BP100. Conformational and functional studies. *Biochim. Biophys. Acta - Biomembr.* **1838**, 1985–1999 (2014) doi: 10.1016/j.bbamem.2014.04.004.
17. Wadhwani, P. *et al.* Dynamical structure of the short multifunctional peptide BP100 in

membranes. *Biochim. Biophys. Acta - Biomembr.* **1838**, 940–949 (2014) doi: 10.1016/j.bbamem.2013.11.001.

18. Carretero, G. P. B. *et al.* Synthesis, biophysical and functional studies of two BP100 analogues modified by a hydrophobic chain and a cyclic peptide. *Biochim. Biophys. Acta - Biomembr.* **1860**, 1502–1516 (2018) doi: 10.1016/j.bbamem.2018.05.003.
19. Park, P. *et al.* Binding and Flip as Initial Steps for BP-100 Antimicrobial Actions. *Sci. Rep.* **9**, 8622 (2019) doi: 10.1038/s41598-019-45075-5.
20. Wang, Y. *et al.* How reliable are molecular dynamics simulations of membrane active antimicrobial peptides? *Biochim. Biophys. Acta - Biomembr.* **1838**, 2280–2288 (2014) doi: 10.1016/j.bbamem.2014.04.009.
21. Alves, C. S., Kairys, V., Castanho, M. A. R. B. & Fernandes, M. X. Interaction of antimicrobial peptides, BP100 and pepR, with model membrane systems as explored by Brownian dynamics simulations on a coarse-grained model. *Biopolymers* **98**, 294–312 (2012) doi: 10.1002/bip.22075.
22. Su, J., Marrink, S. J. & Melo, M. N. Localization Preference of Antimicrobial Peptides on Liquid-Disordered Membrane Domains. *Front. Cell Dev. Biol.* **8**, 1–11 (2020) doi: 10.3389/fcell.2020.00350.
23. Panahi, A. & Feig, M. Dynamic heterogeneous dielectric generalized Born (DHDGB): An implicit membrane model with a dynamically varying bilayer thickness. *J. Chem. Theory Comput.* **9**, 1709–1719 (2013) doi: 10.1021/ct300975k.
24. Thøgersen, L., Schiøtt, B., Vosegaard, T., Nielsen, N. C. & Tajkhorshid, E. Peptide aggregation and pore formation in a lipid bilayer: A combined coarse-grained and all atom molecular dynamics study. *Biophys. J.* **95**, 4337–4347 (2008) doi: 10.1529/biophysj.108.133330.
25. Lipkin, R. & Lazaridis, T. Computational studies of peptide-induced membrane pore formation. *Philos. Trans. R. Soc. B Biol. Sci.* **372**, (2017) doi: 10.1098/rstb.2016.0219.
26. Huang, H. W. Molecular mechanism of antimicrobial peptides: The origin of cooperativity. *Biochim. Biophys. Acta - Biomembr.* **1758**, 1292–1302 (2006) doi: 10.1016/j.bbamem.2006.02.001.
27. J. Bond, P. & Khalid, S. Antimicrobial and Cell-Penetrating Peptides: Structure, Assembly and Mechanisms of Membrane Lysis via Atomistic and Coarse-Grained Molecular Dynamic Simulations. *Protein Pept. Lett.* **17**, 1313–1327 (2010) doi: 10.2174/0929866511009011313.
28. Beauchamp, K. A., Lin, Y. S., Das, R. & Pande, V. S. Are protein force fields getting better? A systematic benchmark on 524 diverse NMR measurements. *J. Chem. Theory Comput.* **8**, 1409–1414 (2012) doi: 10.1021/ct2007814.
29. Jämbeck, J. P. M. & Lyubartsev, A. P. Derivation and Systematic Validation of a Refined All-Atom Force Field for Phosphatidylcholine Lipids. *J. Phys. Chem. B* **116**, 3164–3179 (2012) doi: 10.1021/jp212503e.
30. Jämbeck, J. P. M. & Lyubartsev, A. P. Another Piece of the Membrane Puzzle: Extending Slipids Further. *J. Chem. Theory Comput.* **9**, 774–784 (2013) doi: 10.1021/ct300777p.
31. Slipids Force Field Downloads. http://www.fos.su.se/~sasha/SLipids/Downloads.html.
32. Martinez, L. *et al.* PACKMOL: A package for building initial configurations for molecular dynamics simulations. *J. Comput. Chem.* **30**, 2157–2164 (2009) doi: 10.1002/jcc.21224.
33. Åqvist, J. Ion-water interaction potentials derived from free energy perturbation simulations. *J. Phys. Chem.* **94**, 8021–8024 (1990) doi: 10.1021/j100384a009.

34. Dang, L. X. Mechanism and Thermodynamics of Ion Selectivity in Aqueous Solutions of 18-Crown-6 Ether: A Molecular Dynamics Study. *J. Am. Chem. Soc.* **117**, 6954–6960 (1995) doi: 10.1021/ja00131a018.
35. Van Gunsteren, W. F. & Berendsen, H. J. C. A Leap-frog Algorithm for Stochastic Dynamics. *Mol. Simul.* **1**, 173–185 (1988) doi: 10.1080/08927028808080941.
36. Bussi, G., Donadio, D. & Parrinello, M. Canonical sampling through velocity rescaling. *J. Chem. Phys.* **126**, (2007) doi: 10.1063/1.2408420.
37. Berendsen, H. J. C., Postma, J. P. M., van Gunsteren, W. F., DiNola, A. & Haak, J. R. Molecular dynamics with coupling to an external bath. *J. Chem. Phys.* **81**, 3684 (1984) doi: 10.1063/1.448118.
38. Hess, B., Bekker, H., Berendsen, H. J. C. & Fraaije, J. G. E. M. LINCS: A Linear Constraint Solver for Molecular Simulations. *J Comput Chem* **18**, 1463–1472 (1997).
39. Essmann, U. *et al.* A smooth particle mesh Ewald method. *J. Chem. Phys.* **103**, 8577 (1995) doi: 10.1063/1.470117.
40. Santos, D. E. S., Pontes, F. J. S., Lins, R. D., Coutinho, K. & Soares, T. A. SuAVE: A Tool for Analyzing Curvature-Dependent Properties in Chemical Interfaces. *J. Chem. Inf. Model.* **60**, 473-484 (2019) doi: 10.1021/acs.jcim.9b00569.
41. Van Der Spoel, D. *et al.* GROMACS: Fast, flexible, and free. *J. Comput. Chem.* **26**, 1701–1718 (2005) doi: 10.1002/jcc.20291.
42. Hess, B., Kutzner, C., van der Spoel, D. & Lindahl, E. GROMACS 4: Algorithms for Highly Efficient, Load-Balanced, and Scalable Molecular Simulation. *J. Chem. Theory Comput.* **4**, 435–447 (2008) doi: 10.1021/ct700301q.
43. Abraham, M. J. *et al.* GROMACS: High performance molecular simulations through multi-level parallelism from laptops to supercomputers. *SoftwareX* **1**, 19–25 (2015) doi: 10.1016/j.softx.2015.06.001.
44. Pfeiffer, W., Henkel, T. H., Sackmann, E., Knoll, W. & Knoll, W. Local dynamics of lipid bilayers studied by incoherent quasi-elastic neutron scattering. *Epl* **8**, 201–206 (1989) doi: 10.1209/0295-5075/8/2/016.
45. Filippov, A. V., Rudakova, M. A., Oradd, G. & Lindblom, G. Lateral diffusion of saturated phosphatidylcholines in cholesterol- containing bilayers. *Biophysics (Oxf).* **52**, 307–314 (2007) doi: 10.1134/S0006350907030098.
46. Filippov, A., Orädd, G. & Lindblom, G. The effect of cholesterol on the lateral diffusion of phospholipids in oriented bilayers. *Biophys. J.* **84**, 3079–3086 (2003) doi: 10.1016/S0006-3495(03)70033-2.
47. Lindblom, G. & Orädd, G. Lipid lateral diffusion and membrane heterogeneity. *Biochim. Biophys. Acta - Biomembr.* **1788**, 234–244 (2009) doi: 10.1016/j.bbamem.2008.08.016.
48. Korchowiec, B., Stachowicz-Kuśnierz, A. & Korchowiec, J. The role of DPPG in lung surfactant exposed to benzo[a] pyrene. *Environ. Sci. Process. Impacts* **21**, 438–445 (2019) doi: 10.1039/c8em00497h.
49. Dawson, C. R., Drake, A. F., Helliwell, J. & Hider, R. C. The interaction of bee melittin with lipid bilayer membranes. *BBA - Biomembr.* **510**, 75–86 (1978) doi: 10.1016/0005-2736(78)90131-1.
50. Wu, Y., He, K., Ludtke, S. J. & Huang, H. W. X-ray diffraction study of lipid bilayer membranes interacting with amphiphilic helical peptides: diphytanoyl phosphatidylcholine with alamethicin at low concentrations. *Biophys. J.* **68**, 2361–2369 (1995) doi: 10.1016/S0006-3495(95)80418-2.
51. Chen, F. Y., Lee, M. T. & Huang, H. W. Evidence for membrane thinning effect as the mechanism for peptide-induced pore formation. *Biophys. J.* **84**, 3751–3758 (2003) doi:

10.1016/S0006-3495(03)75103-0.

52. Chen, F. Y., Lee, M. T. & Huang, H. W. Sigmoidal concentration dependence of antimicrobial peptide activities: A case study on alamethicin. *Biophys. J.* **82**, 908–914 (2002) doi: 10.1016/S0006-3495(02)75452-0.
53. Misiewicz, J. *et al.* Action of the multifunctional peptide BP100 on native biomembranes examined by solid-state NMR. *J. Biomol. NMR* **61**, 287–98 (2015) doi: 10.1007/s10858-015-9897-8.
54. Mecke, A., Lee, D. K., Ramamoorthy, A., Orr, B. G. & Banaszak Holl, M. M. Membrane thinning due to antimicrobial peptide binding: An atomic force microscopy study of MSI-78 in lipid bilayers. *Biophys. J.* **89**, 4043–4050 (2005) doi: 10.1529/biophysj.105.062596.
55. Grage, S. L., Afonin, S., Kara, S., Buth, G. & Ulrich, A. S. Membrane thinning and thickening induced by membrane-active amphipathic peptides. *Front. Cell Dev. Biol.* **4**, (2016) doi: 10.3389/fcell.2016.00065.
56. Neale, C., Hsu, J. C. Y., Yip, C. M. & Pomès, R. Indolicidin binding induces thinning of a lipid bilayer. *Biophys. J.* **106**, 29–31 (2014) doi: 10.1016/j.bpj.2014.02.031.
57. Velasco-Bolom, J. L., Corzo, G. & Garduño-Juárez, R. Molecular dynamics simulation of the membrane binding and disruption mechanisms by antimicrobial scorpion venom-derived peptides. *J. Biomol. Struct. Dyn.* **36**, 2070–2084 (2018) doi: 10.1080/07391102.2017.1341340.
58. Duay, S. S., Sharma, G., Prabhakar, R., Angeles-Boza, A. M. & May, E. R. Molecular Dynamics Investigation into the Effect of Zinc(II) on the Structure and Membrane Interactions of the Antimicrobial Peptide Clavanin A. *J. Phys. Chem. B* **123**, 3163–3176 (2019) doi: 10.1021/acs.jpcb.8b11496.
59. Wadhwani, P. *et al.* Membrane-Active Peptides and the Clustering of Anionic Lipids. *Biophys. J.* **103**, 265–274 (2012) doi: 10.1016/j.bpj.2012.06.004.
60. Epand, R. F., Wang, G., Berno, B. & Epand, R. M. Lipid segregation explains selective toxicity of a series of fragments derived from the human cathelicidin LL-37. *Antimicrob. Agents Chemother.* **53**, 3705–3714 (2009) doi: 10.1128/AAC.00321-09.
61. Schmidt, N. W. & Wong, G. C. L. Antimicrobial peptides and induced membrane curvature: Geometry, coordination chemistry, and molecular engineering. *Current Opinion in Solid State and Materials Science* vol. 17 151–163 (2013) doi: 10.1016/j.cossms.2013.09.004.
62. Drin, G. & Antonny, B. Amphipathic helices and membrane curvature. *FEBS Lett.* **584**, 1840–1847 (2010) doi: 10.1016/j.febslet.2009.10.022.
63. Matsuzaki, K. *et al.* Relationship of membrane curvature to the formation of pores by magainin 2. *Biochemistry* **37**, 11856–11863 (1998) doi: 10.1021/bi980539y.
64. Ramakrishnan, N., Sunil Kumar, P. B. & Radhakrishnan, R. Mesoscale computational studies of membrane bilayer remodeling by curvature-inducing proteins. *Phys. Rep.* **543**, 1–60 (2014) doi: 10.1016/j.physrep.2014.05.001.
65. Chen, R. & Mark, A. E. The effect of membrane curvature on the conformation of antimicrobial peptides: Implications for binding and the mechanism of action. *Eur. Biophys. J.* **40**, 545–553 (2011) doi: 10.1007/s00249-011-0677-4.
66. Kumar, T. V. V. & Sanil, G. A Review of the Mechanism of Action of Amphibian Antimicrobial Peptides Focusing on Peptide-Membrane Interaction and Membrane Curvature. *Curr. Protein Pept. Sci.* **18**, 1263–1272 (2017) doi: 10.2174/1389203718666170710114932.
67. Schmidt, N., Mishra, A., Lai, G. H. & Wong, G. C. L. Arginine-rich cell-penetrating

peptides. *FEBS Lett.* **584**, 1806–1813 (2010) doi: 10.1016/j.febslet.2009.11.046.

68. Schmidt, N. W. *et al.* Criterion for amino acid composition of defensins and antimicrobial peptides based on geometry of membrane destabilization. *J. Am. Chem. Soc.* **133**, 6720–6727 (2011) doi: 10.1021/ja200079a.
69. Buck, Z. N. *et al.* Effect of melittin on water diffusion and membrane structure in DMPC lipid bilayers. *Epl* **123**, (2018) doi: 10.1209/0295-5075/123/18002.
70. Orädd, G. & Lindblom, G. NMR studies of lipid lateral diffusion in the DMPC/gramicidin D/water system: Peptide aggregation and obstruction effects. *Biophys. J.* **87**, 980–987 (2004) doi: 10.1529/biophysj.103.038828.
71. Buchsteiner, A., Hauß, T., Dante, S. & Dencher, N. A. Alzheimer's disease amyloid-B peptide analogue alters the ps-dynamics of phospholipid membranes. *Biochim. Biophys. Acta - Biomembr.* **1798**, 1969–1976 (2010) doi: 10.1016/j.bbamem.2010.06.024.
72. Rai, D. K. *et al.* Neutron scattering studies of the interplay of amyloid β peptide(1-40) and an anionic lipid 1,2-dimyristoyl-sn-glycero-3-phosphoglycerol. *Sci. Rep.* **6**, 1–11 (2016) doi: 10.1038/srep30983.
73. Buchsteiner, A., Hauß, T. & Dencher, N. A. Influence of amyloid-β peptides with different lengths and amino acid sequences on the lateral diffusion of lipids in model membranes. *Soft Matter* **8**, 424–429 (2012) doi: 10.1039/c1sm06823g.
74. Goose, J. E. & Sansom, M. S. P. Reduced Lateral Mobility of Lipids and Proteins in Crowded Membranes. *PLoS Comput. Biol.* **9**, (2013) doi: 10.1371/journal.pcbi.1003033.
75. Ebersberger, L. *et al.* Lipid Dynamics in Membranes Slowed Down by Transmembrane Proteins. *Front. Cell Dev. Biol.* **8**, 1–14 (2020) doi: 10.3389/fcell.2020.579388.
76. Scheinpflug, K. *et al.* Antimicrobial peptide cWFW kills by combining lipid phase separation with autolysis. *Sci. Rep.* **7**, 1–15 (2017) doi: 10.1038/srep44332.
77. Apajalahti, T. *et al.* Concerted diffusion of lipids in raft-like membranes. *Faraday Discuss.* **144**, 411–430 (2009) doi: 10.1039/b901487j.
78. Epand, R. M. & Epand, R. F. Domains in bacterial membranes and the action of antimicrobial agents. *Mol. Biosyst.* **5**, 580–587 (2009) doi: 10.1039/b900278m.
79. Epand, R. M. & Epand, R. F. Bacterial membrane lipids in the action of antimicrobial agents. *J. Pept. Sci.* **17**, 298–305 (2011) doi: 10.1002/psc.1319.

## 3.7. Supplementary Material

| | Simulated Systems | Peptide/Lipid | Water | Time (ns) |
|---|---|---|---|---|
| Bilayers | DPPC | 0/128 | 54/Lipid | 860 |
| | DPPG | | 53/Lipid | 1100 |
| | PCPG | 0/[64/64] | 54/Lipid | 1200 |
| | PCPG* | | 52/Lipid | 1200 |
| Peptide with Bilayers | BP100 in DPPC | 1/128 | 54/Lipid | 2000 |
| | BP100 in DPPG | | 53/Lipid | 2000 |
| | BP100 in PCPG | | 54/Lipid | 2000 |
| | BP100 in PCPG* | | 52/Lipid | 2000 |

Table S1: All MD simulated systems carried out in this work at 1 bar and 323 K (above DPPC and DPPG transition temperatures). We used Slipids forcefield[1] for the lipids, ff99sb-ildn-NMR[2] for BP100 and TIP3P for the water. L-BP100 and α-BP100 indicate constraint-free simulations using linear and alpha helix initial conformations respectively. Images below: (a) shows the simulated membranes seen from above and in (b) an example of a peptide-membrane initial simulation set-up (water and ions are not shown for clarity).

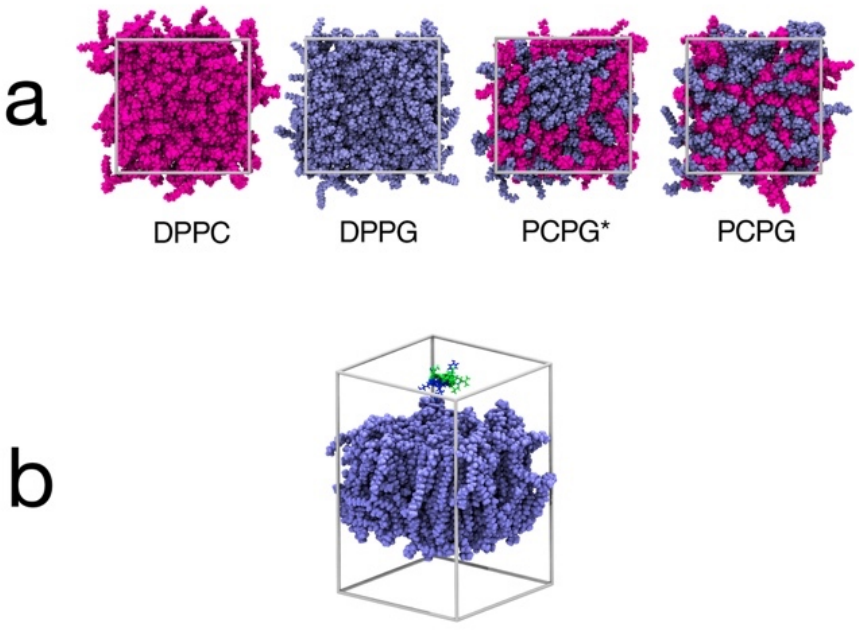

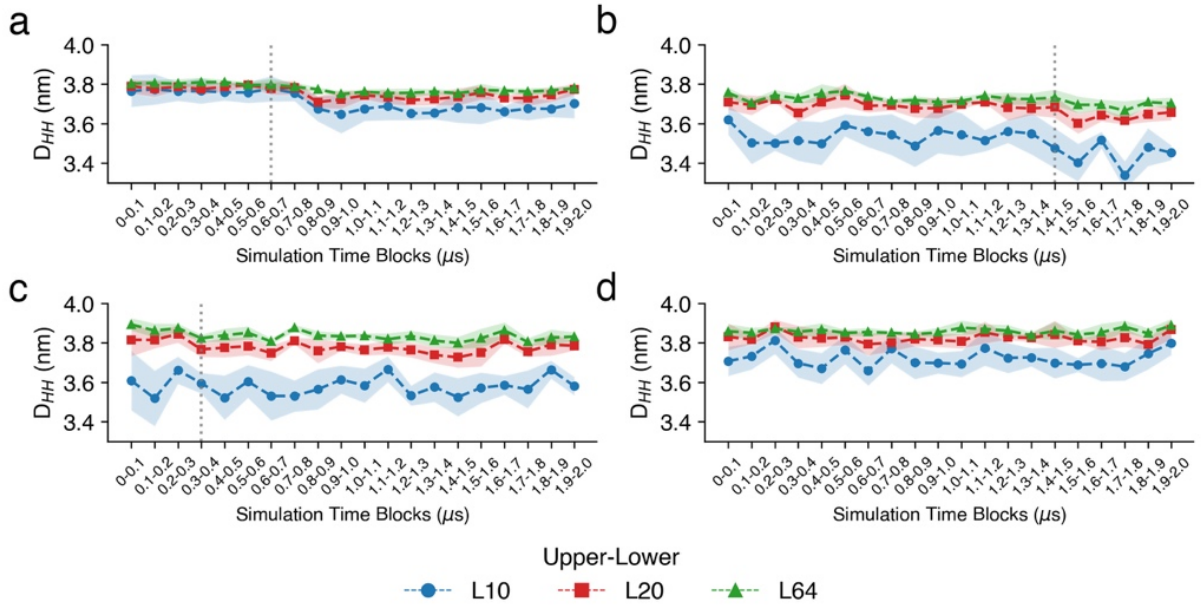


Figure S1: BP100 causes local membrane thinning. Graphs show membrane thickness throughout simulation time for simulations of α-BP100 in DPPC (a), DPPG (b), PCPG* (c), and PCPG (d). Bilayer thickness was obtained using SuAve software, measuring the average distance between the upper and lower leaflets surface grids, generated by SuAve. Each point represent data averaged over 100 ns of simulation. Standard deviations are represented as fillings and red dotted lines indicate when peptide flip took place.

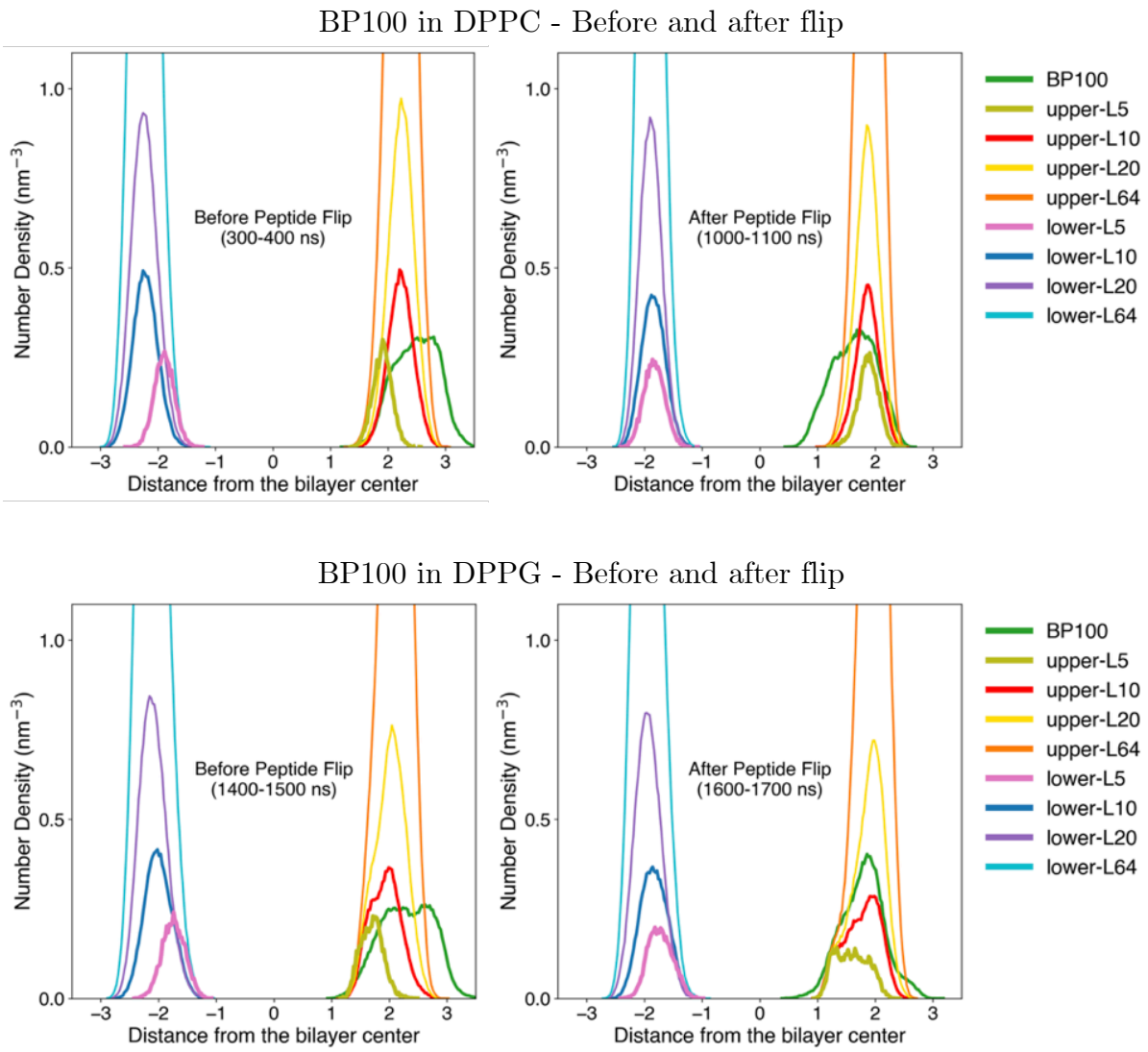


Figure S2: Membrane curvature induced by peptide flip observed through number density analysis. Number density graphs showing 100-ns-averaged positions of the peptide and lipids before and after peptide flip. In simulations with anionic lipids, membrane thinning is observed by the distance shortening between upper-L10 and lower L10.

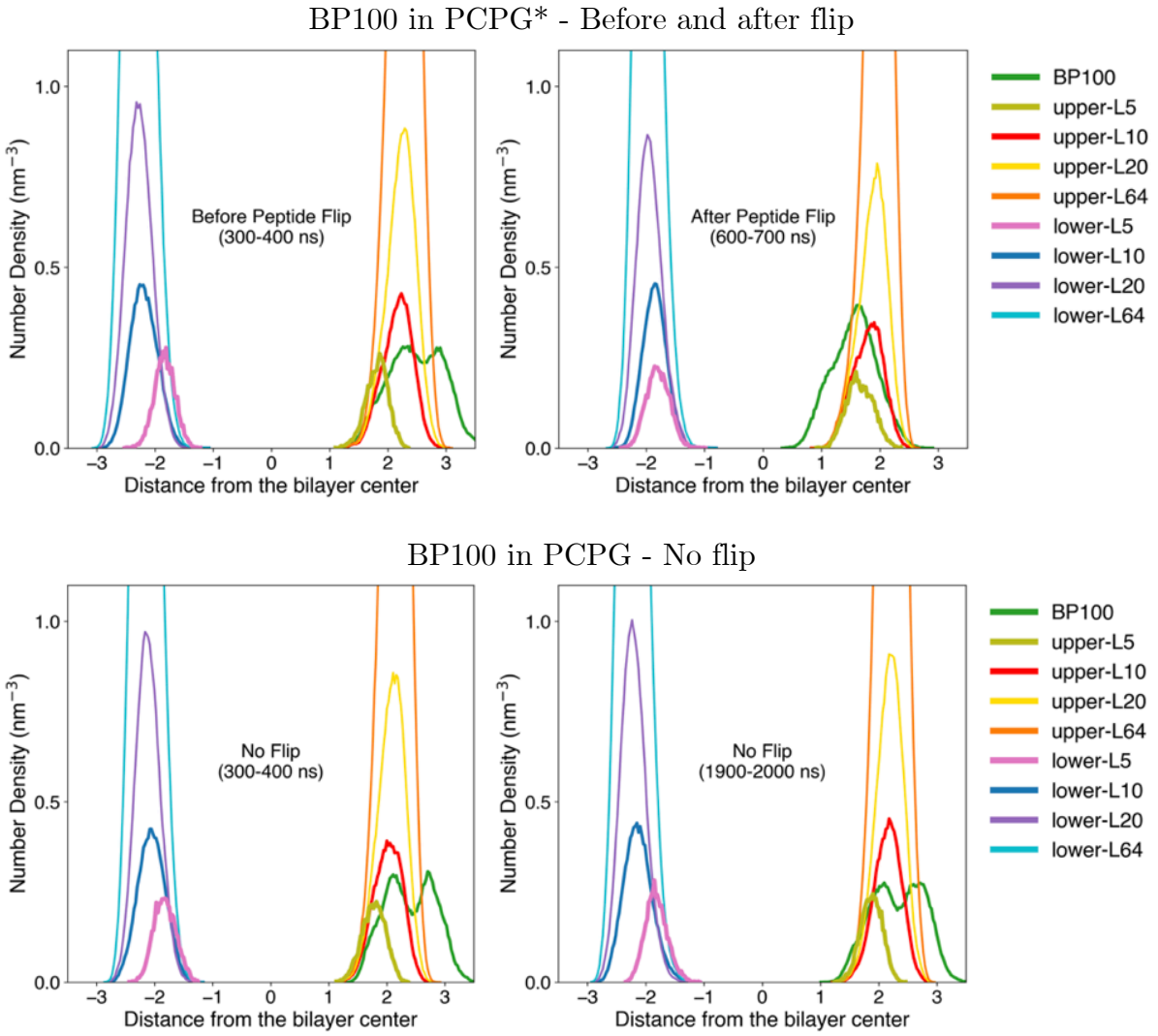


Figure S3: Membrane curvature induced by peptide flip observed through number density analysis. Number density graphs showing 100-ns-averaged positions of the peptide and lipids before and after peptide flip. In simulations with anionic lipids, membrane thinning is observed by the distance shortening between upper-L10 and lower L10.

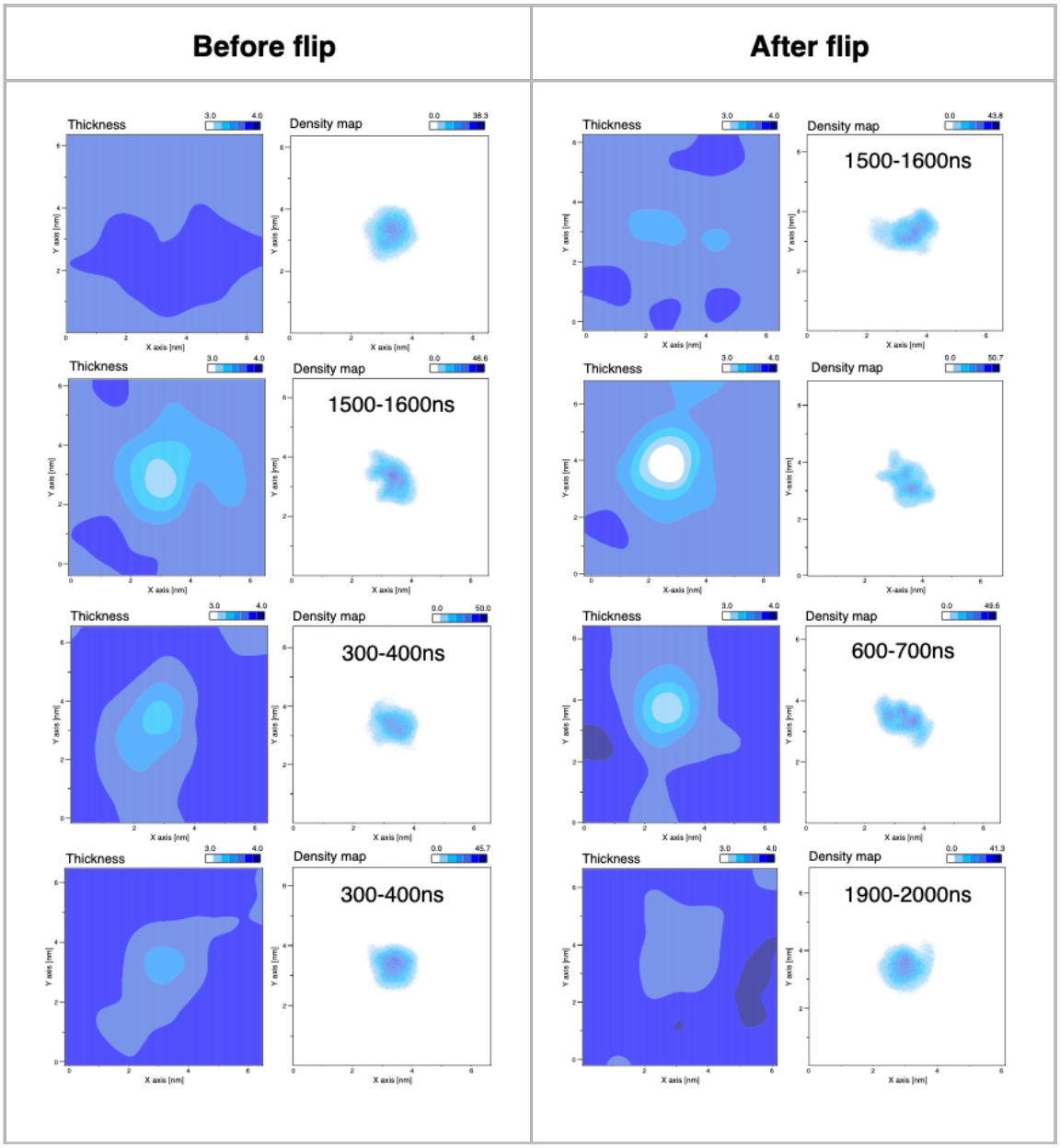


Figure S4: Membrane thickness and peptide density in 2D mappings are shown in pairs (before and after) for each simulation set: BP100 in DPPC (a), in DPPG (b), in PCPG* (c), and in PCPG (d). Note that peptide flip was found in all simulations except BP100 in PCPG (d). Thicknesses are scaled in nm and density maps in $nm^3$.

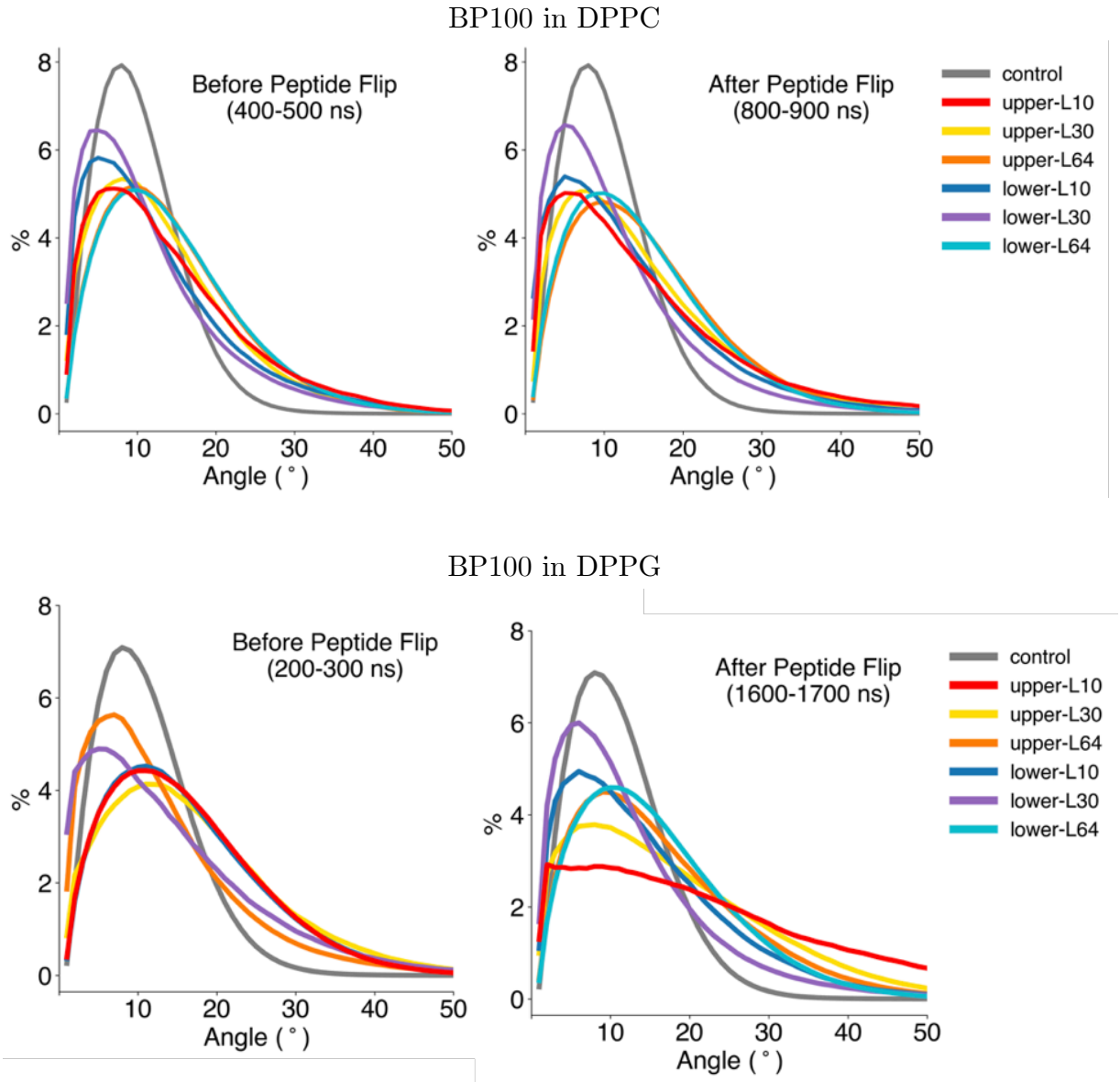


Figure S5: **Peptide flip induces negative membrane curvature.** Membrane surface curvature angle distribution for lipid groups in BP100 in DPPC (a) and in PCPG (b) simulations. The angle distribution was calculated using the SuAve analysis software[3], measuring the angle between the normal vector of the surface rectangular grid partition and the z-axis. Higher angles indicate membrane curvature. To assess peptide flip influence on membrane curvature, membrane surface curvature angle distribution was calculated before and after peptide flip. It should be noted that in the BP100 in DPPC, a semi-flip was observed, due to the partial unfolding of BP100 (see reference 4 for details).

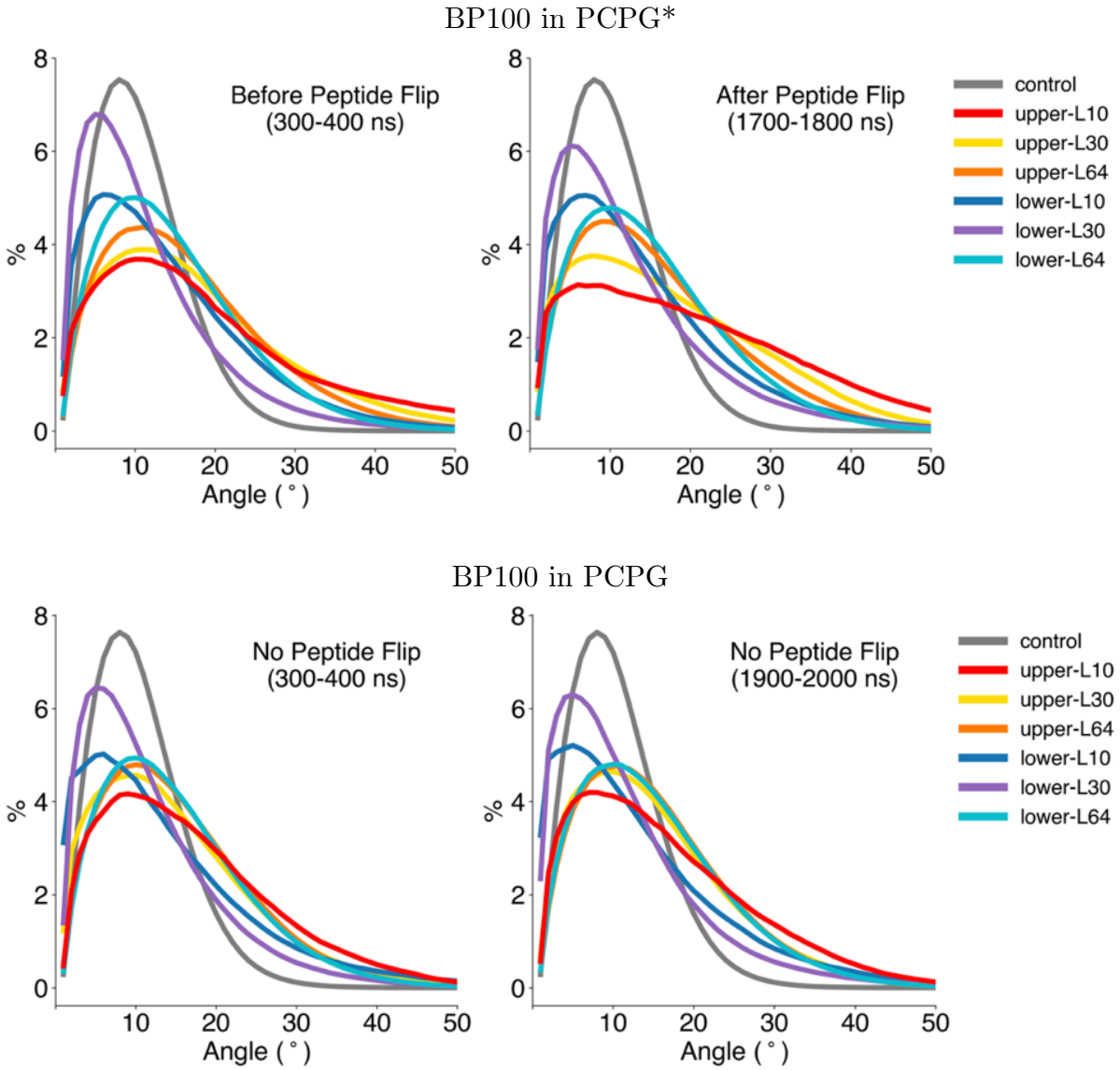


FIGURE S6: **Peptide flip induces negative membrane curvature.** Membrane surface curvature angle distribution for BP100 in PCPG* (a) and in PCPG (b). In BP100 in PCPG*, flip occurred at ~1500 ns and no flip was observed in the PCPG simulation.

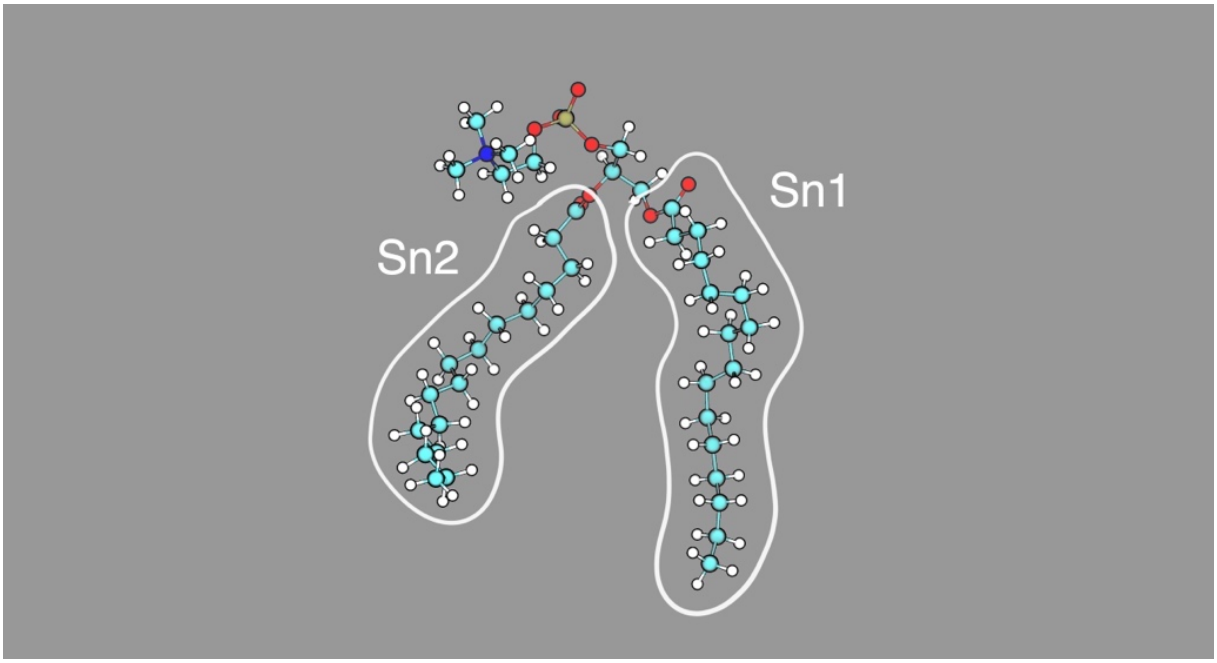


Figure S7: Stereospecific numbering of phospholipids (Sn1 and Sn2) in DPPC. For deuterium order parameter analysis, only sn1 acyl chain $S_{CD}$ was computed. Carbon atoms are colored in cyan, Hydrogens in white, Oxygens in red, Nitrogen in blue, and Phosphorus in beige.

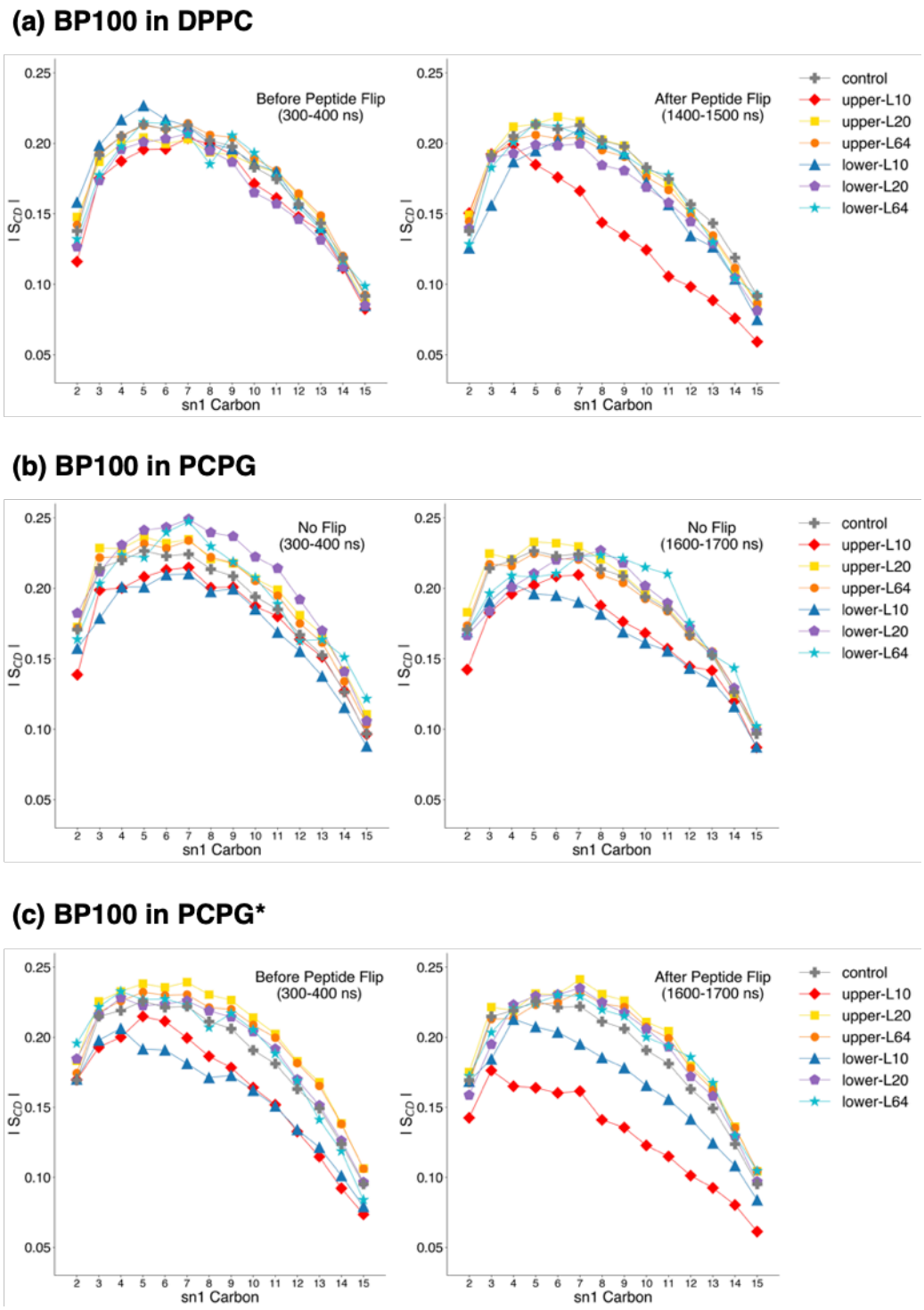


Figure S8: **Peptide flip decreases lipid order parameter.** Order parameters before and after flip for BP100 in DPPC (a) and PCPG* (c), and beginning and end of the simulation for BP100 in PCPG (b). Sn1 chain of lipids was used as representative for calculating lipid order parameters for L10, L20, and L64 for both monolayers. Order parameters were calculated in 100 ns time windows. Control data were obtained from pure membrane simulations, averaging order parameters from the last 800 ns of simulation. Semi-flip occurred at ~700ns for BP100 in DPPC and full peptide flip at ~400ns for PCPG*.

| Lipid Lateral Diffusion ($10^{-7}$ $cm^2s^{-1}$) | | | | | | |
|---|---|---|---|---|---|---|
| | upper-L5 | upper-L10 | upper-L20 | lower-L64 | Control | Literature |
| DPPC | 0.8 (± 0.3) | 0.9 (± 0.2) | 1.3 (± 0.2) | 1.6 (± 0.2) | 1.6 (± 0.2) | 1.8[5],1.78[6], ~1.5[7], 1.5[8] |
| DPPG | 0.5 (± 0.2) | 0.6 (± 0.2) | 1.1 (± 0.2) | 1.2 (± 0.2) | 1.3 (± 0.2) | 0.9[9] |
| PCPG* | 0.5 (± 0.2) | 0.6 (± 0.2) | 1.0 (± 0.2) | 1.2 (± 0.2) | 1.2 (± 0.2) | |
| PCPG | 0.6 (± 0.2) | 0.7 (± 0.3) | 1.1 (± 0.3) | 1.2 (± 0.2) | 1.3 (± 0.2) | |

Table S9: **BP100 binding leads to local lipid slow down.** Lipid lateral diffusion coefficients were calculated from the slopes of the mean-square displacements (MSD) in the xy-plane of selected lipids. Lateral diffusion coefficients for pure membranes were used as control and values found in the literature are shown for comparison.

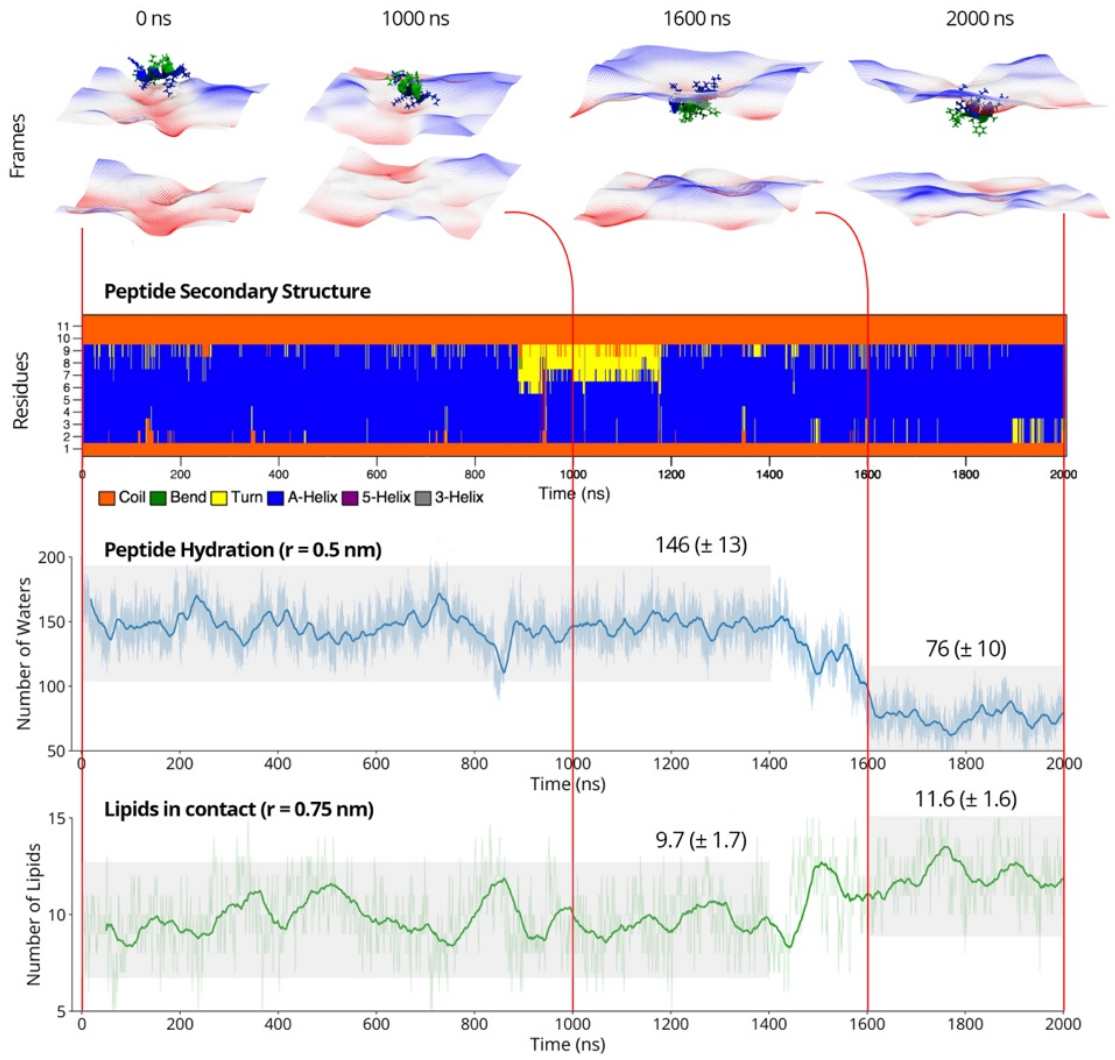


Figure S10: **Peptide flip. (A)** Snapshots from BP100 in DPPG simulation; positively charged residues are colored in blue and non-polar residues in green. Upper and lower grids were generated by averaging the positions of DPPG phosphorus atoms. **(B)** BP100 secondary structure along the simulation. **(C)** Peptide hydration analysis, calculating the number of waters around the peptide using a cut-off = 0.5 nm. **(D)** Number of DPPG lipids in close contact with BP100 using a cut-off = 0.75 nm.
Initially, the peptide binds to the membrane with its positively charged facet facing the membrane, driven by electrostatic interactions. At approximately 1400 ns, BP100 flips turning its non-polar facet to the membrane hydrophobic core, burying the peptide inside the membrane, below the bilayer phosphates (in (A), see frames 1600 ns and 2000 ns). To this dynamic phenomenon, we designated as **peptide flip**. Alpha-helical structure preservation seems to be crucial for peptide flip (B), and the flip is accompanied by drastic peptide dehydration (C). We calculated 146 (±13) (0-1400 ns) waters before peptide flip and 76 (±10) (1600-2000 ns) waters after the flip. A slight increase in the average number of lipids in close contact with BP100 was detected. We obtained 9.7 ±1.7 (0-1400 ns) lipids before the flip and 11.6 ±1.6 (1600-2000 ns) lipids after the flip. Peptide flip occurred also in DPPC and PCPG* simulations. For more information, see ref 6.

| Helicity (%) - Last 100 ns | |
|---|---|
| BP100 in DPPC | 45 |
| BP100 in DPPG | 72 |
| BP100 in PCPG* | 72 |
| BP100 in PCPG | 54 |

Table S11: Helicity percentage averaged over the last 100 ns of each simulation.

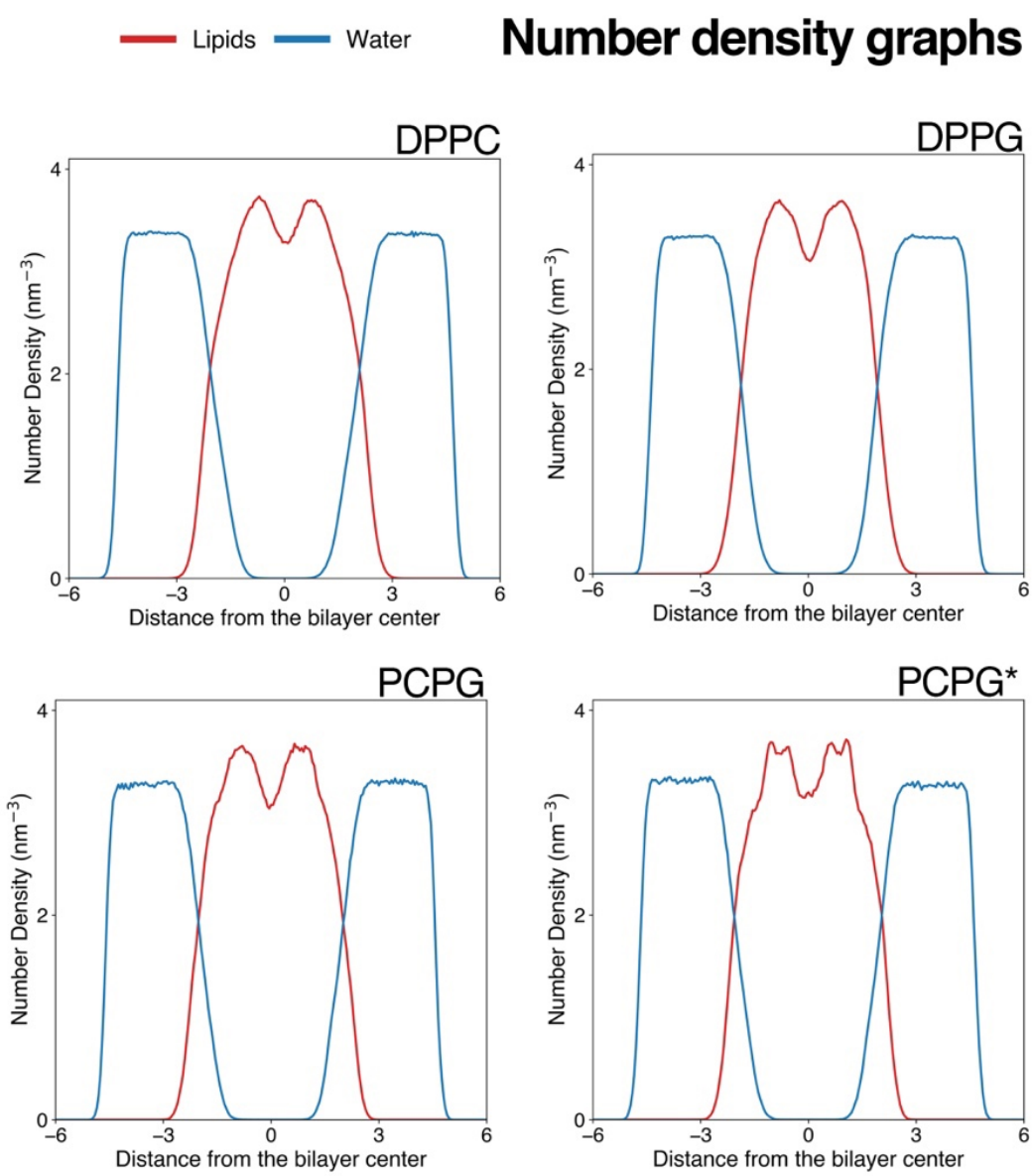


Figure S11: Number density profile of water and lipids for pure membrane systems over the last 100 ns of simulations.

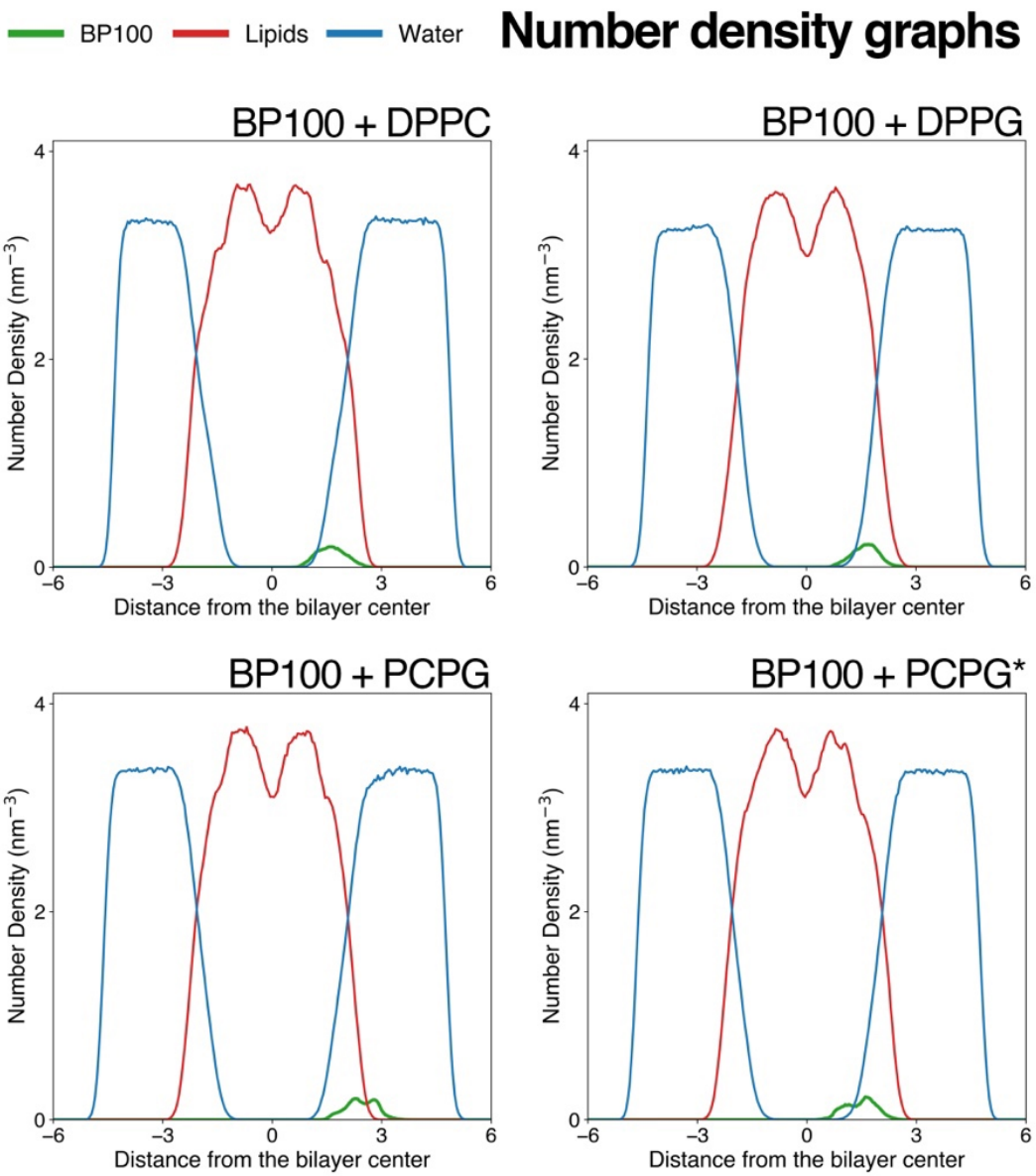


Figure S12: Number density profile of waters, lipids and peptide in peptide/membranes systems over the last 100 ns of simulations. Peptide flip was observed in DPPC, DPPG, and PCPG* simulations.

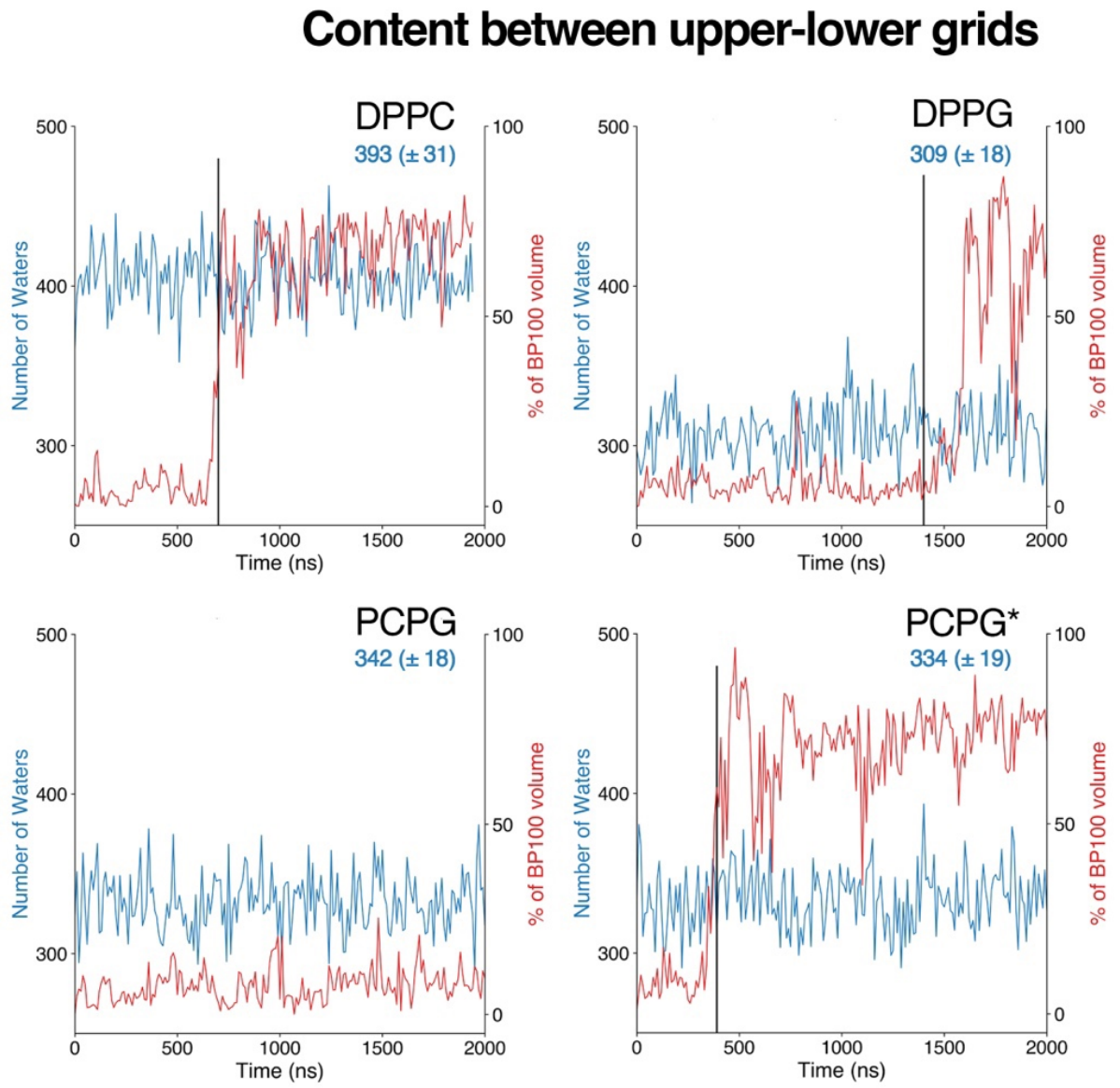


Figure S13: Membrane hydration in peptide/membrane simulations. The number of water molecules accounted between the upper and lower surface grids (R3 region) is shown for all peptide/membrane simulations, as well as the percentage of peptide volume insertion into the R3 region. Vertical lines indicate when peptide flip was observed and the average number of waters are shown on the top right corner in blue. For control systems, we computed an average of 390 (± 28), 307 (± 18), 341 (± 20), and 336 (± 17) waters for DPPC, DPPG, PCPG and PCPG* simulations, respectively.

# 3.8. Supplementary Material references

1. Pfeiffer, W.; Henkel, T. H.; Sackmann, E.; Knoll, W.; Knoll, W. Local Dynamics of Lipid Bilayers Studied by Incoherent Quasi-Elastic Neutron Scattering. *Epl* **1989**, *8* (2), 201–206. https://doi.org/10.1209/0295-5075/8/2/016.

2. Lindblom, G.; Orädd, G. Lipid Lateral Diffusion and Membrane Heterogeneity. *Biochim. Biophys. Acta - Biomembr.* **2009**, *1788* (1), 234–244. https://doi.org/10.1016/j.bbamem.2008.08.016.

3. Filippov, A. V.; Rudakova, M. A.; Oradd, G.; Lindblom, G. Lateral Diffusion of Saturated Phosphatidylcholines in Cholesterol- Containing Bilayers. *Biophysics (Oxf).* **2007**, *52* (3), 307–314. https://doi.org/10.1134/S0006350907030098.

4. Lindblom, G.; Orädd, G.; Filippov, A. Lipid Lateral Diffusion in Bilayers with Phosphatidylcholine, Sphingomyelin and Cholesterol. An NMR Study of Dynamics and Lateral Phase Separation. *Chem. Phys. Lipids* **2006**, *141* (1–2), 179–184. https://doi.org/10.1016/j.chemphyslip.2006.02.011.

5. Korchowiec, B.; Stachowicz-Kuśnierz, A.; Korchowiec, J. The Role of DPPG in Lung Surfactant Exposed to Benzo[a] Pyrene. *Environ. Sci. Process. Impacts* **2019**, *21* (3), 438–445. https://doi.org/10.1039/c8em00497h.

6. Park, P. *et al.* Binding and Flip as Initial Steps for BP-100 Antimicrobial Actions. *Sci. Rep.* **9**, 8622 (2019) doi: 10.1038/s41598-019-45075-5.

# Chapter 4

# Vesicle protrusion induced by antimicrobial peptides suggests common carpet mechanism for short antimicrobial peptides

## 4.1. Abstract

Short cationic alpha-helical antimicrobial peptides (SCHAMPs) are promising candidates to combat the growing global threat of antimicrobial resistance. They are short-sequenced, selective against bacteria and have rapid action by destroying membranes. The full understanding of their mechanism of action will provide key information to design more potent and selective SCHAMPs. Molecular Dynamics (MD) simulations are invaluable tools that provide detailed insights of the peptide:membrane interaction at the atomic- and meso-scale level. Here we use atomistic and coarse-grained MD to investigate the detailed steps in the interaction of four promising SCHAMPs with membranes, namely BP100, Decoralin, Neurokinin-1, and Temporin L. Following experimental set-ups, we explored the effects of SCHAMPs on anionic membranes and vesicles at multiple peptide concentrations. Our results showed all four peptides shared similar initial binding steps in anionic membranes, by binding initially to the membrane through electrostatic interactions and then flipping on their axis, dehydrating and inserting its hydrophobic moieties into the membrane core. At higher concentrations, fully alpha-helical peptides induced membrane budding and protrusions on anionic vesicles. Our results suggest the carpet mode of action is fit for the description of SCHAMPs lysis activity and we discuss the importance of large hydrophobic residues in SCHAMPs design and activity.

# 4.2. Introduction

In recent years antimicrobial resistance (AMR) has become a growing global health concern[1–3]. A 2022 systematic global analysis revealed 4.95 million deaths were associated with bacterial antibiotic resistance[4]. And it has been estimated that antibiotic-resistant diseases will kill as many as 10 million per year by 2050, which is more than the number of people who die from cancer worldwide[5].
The strategies to combat AMR can be categorized in two fronts, prevention and treatment. Some of the strategies in the prevention category are public awareness, access to sanitation, increase vaccine coverage, reduction in the misuse of antibiotics in agriculture[5,6] and clinical practices[7], and rapid diagnostics[3]. In the treatment front, the development of novel antibiotics and improvement of currently used drugs are the main challenges[2–4].

One category of antimicrobials that have shown promising results are antimicrobial peptides (AMPs)[8]. These are found in several different organisms across all kingdoms of life as part of their innate defense system and mainly kill bacteria by disrupting its cell membrane[2,6,8]. Short cationic alpha-helical antimicrobial peptides (SCHAMPs) are short sequenced AMPs rich in basic and hydrophobic aminoacids, which characteristically adopt an unordered conformation in water and an amphipathic alpha-helical structure in nonpolar solvents, and negatively charged bilayers and micelles[8,9].

SCHAMPs display selectivity towards bacterial membranes compared to mammalian cells due to their higher content of negatively charged lipids[8,10] and absence of sterols[11,12] and are also effective against fungi[8,13], biofilms[14] and even cancer cells, as demonstrated by Decoralin[15]. Their shorter size offer several advantages such as lesser cost of production in bulk, and its composition can be easily tunable in case of requirements regarding toxicity, stability or half-life[16].

Despite SCHAMPs promising attributes their use has been limited due to the lack of detailed understanding of their mechanism of action on membranes. Current models that can explain membrane disruption by AMPs suggest either pore-formation or the carpet mechanism[9]. However, due to their shorter length, the formation of pores by SCHAMPs is inviable[17–20] and increasing evidence favors the carpet mechanism at a peptide to lipid ratio (P/L) threshold[21–25]. In a study using KIAGKIA (Lys-Ile-Ala-Gly-Lys-Ile-Ala) motifs of varied lengths, it was shown that the formation of transmembrane pores by AMPs are only possible when AMPs are long enough to span the hydrophobic bilayer core[20].

A detailed molecular description of SCHAMPs carpet mechanism is still to be investigated as such understanding is a fundamental step to design more efficient and selective AMPs. Molecular Dynamics (MD) simulations are invaluable computational tools to study molecular systems in atomistic detail and have been widely used to investigate the interaction between AMPs and membranes at the molecular level[26].

Successful descriptions of AMPs binding and pore formation via atomistic simulations show that these phenomena are in the microsecond scale[27,28] and thus, the faster Martini forcefield was widely used to describe the pore forming action of various AMPs, such as maculatin 1.1[29], alamethicin[30], magainin-2[27,31–33], and melittin[32] . The majority of the studied AMPs are long ( $>$ 17 residues), being capable of spanning as transmembrane peptides through the hydrophobic thickness of synthetic lipid bilayers[20] and therefore, one has to be careful when grouping SCHAMPs in the same category of mode of action of larger AMPs.

Our previous atomistic MD simulation studies of SCHAMP BP100 (KKLFKKILKYL), a hybrid of AMPs cecropin A and melittin[34], show that the alpha-helical structure on negatively charged membranes favors the dehydration of BP100 hydrophobic moiety via peptide rotation and insertion into the membrane core[35]. We coined the term "peptide flip" to such dynamical behavior. In addition, single BP100 causes local membrane thinning, negative curvature and slows lipid lateral diffusion[36]. In coarse-grained MD simulations of BP100 on a phase-separated membrane, it was

shown the peptide preferentially binds at the liquid-disordered phase over the liquid-ordered one, and has low oligomerization propensity, even at high concentrations[33].

In order to investigate the occurrence of a common mechanism of action for SCHAMPs, we selected BP100 and three other peptides. The criteria for selection were the similarity in the number of aminoacids and folding behavior in solution (unordered) and in negatively charged membranes (alpha-helical). We chose Neurokinin-1 (RPKPQQFFGLM)[37,38] (also known as Substance P), a human neurotransmissor with AMP properties, Decoralin (SLLSLIRKLIT)[39], a SCHAMP isolated from the venom of *Oreumenes decorates* wasps, and Temporin-L[40], from the skin of the frog *Rana temporaria* which displayed the highest activity among temporins. The folding in solution and in anionic membranes for all four peptides have been extensively studied through experimental[21,34,38,39,41,42] and/or theoretical approaches[35,43].

In this present study, we performed atomistic MD simulations of BP100, Decoralin, NK-1, and Temporin-L on membrane models to explore the occurrence of a common initial binding step and its effect on local membrane properties. We further explored and described in details the effect of peptide concentration on vesicles using coarse-grained MD, analyzing vesicle structural alterations. This detailed description and comparison of SCHAMPs effect in membranes at the low and high peptide concentration may be expanded for the wide-range of available SCHAMPs and provide key information for designing more efficient, selective and less cytotoxic antibiotics.

# 4.3. Methods

### 4.3.1. Peptides

Three SCHAMPs (Figure 1B-D) were selected from the Antimicrobial Peptide Database[44] (APD3, https://aps.unmc.edu) based on their similarity with a previously studied SCHAMP, BP100[35,36]. They are short peptides (11 to 13 aminoacids), amphiphilic in alpha-helix conformation, which is their predominant secondary structure when in contact with negatively charged membranes [21,34,38,39,41,42]. And in solution, as BP100, they have no secondary structure. We also used BP100 (Fig. 1A) to compare with the other 3 peptides in similar conditions.

### 4.3.2. Molecular Dynamics

All simulations were run with GROMACS 5.1.4[45–47] version and analyzed with GROMACS 2020.6.

#### 4.3.2.1. All-atom simulations set-ups and analysis

For all-atom simulations, *ff99sb-ildn-NMR*[48] force field was used for the peptides and the SLipids[49–51] forcefield for the lipids. SLipids forcefield was previously validated[35] and for the *ff99sb-ildn-NMR* forcefield, we validated it by simulating all 4 peptides in water and in membranes and comparing their secondary structure profile with structural experimental data[38,42,52,53] (Fig. S1; Fig. 2, column 3). Although the peptides showed an over-helical behavior in water (Fig. S1), this is expected[48] and the forcefield was capable of reproducing experimental structural properties in membranes (Fig. 2, column 3).

Peptides were initially folded as alpha-helices without constraints and positioned approximately 2 nm away from the membrane (Figure 1E). Previous data suggest negatively charged membranes favor the occurrence of peptide flip[35], in which the amphiphilic peptide approaches the membrane with its polar facet and then it turns, facing the membrane

with its non-polar facet and burying the peptide into the membrane core. In order to compare with previous results obtained with BP100[35,36] we simulated peptides on mixed bilayer of palmitoyloleoylphosphatidylcholine (POPC) and POPG (palmitoyloleoylphosphatidylglycerol) in a 1:1 ratio. Membranes containing 64 lipids on each leaflet were assembled using PACKMOL[54] and were solvated with TIP3P water model, with an average of 55 water molecules per lipid. After counter-ions were added to neutralize the systems, all set-ups were equilibrated. Membrane-only systems were also simulated and used as controls.

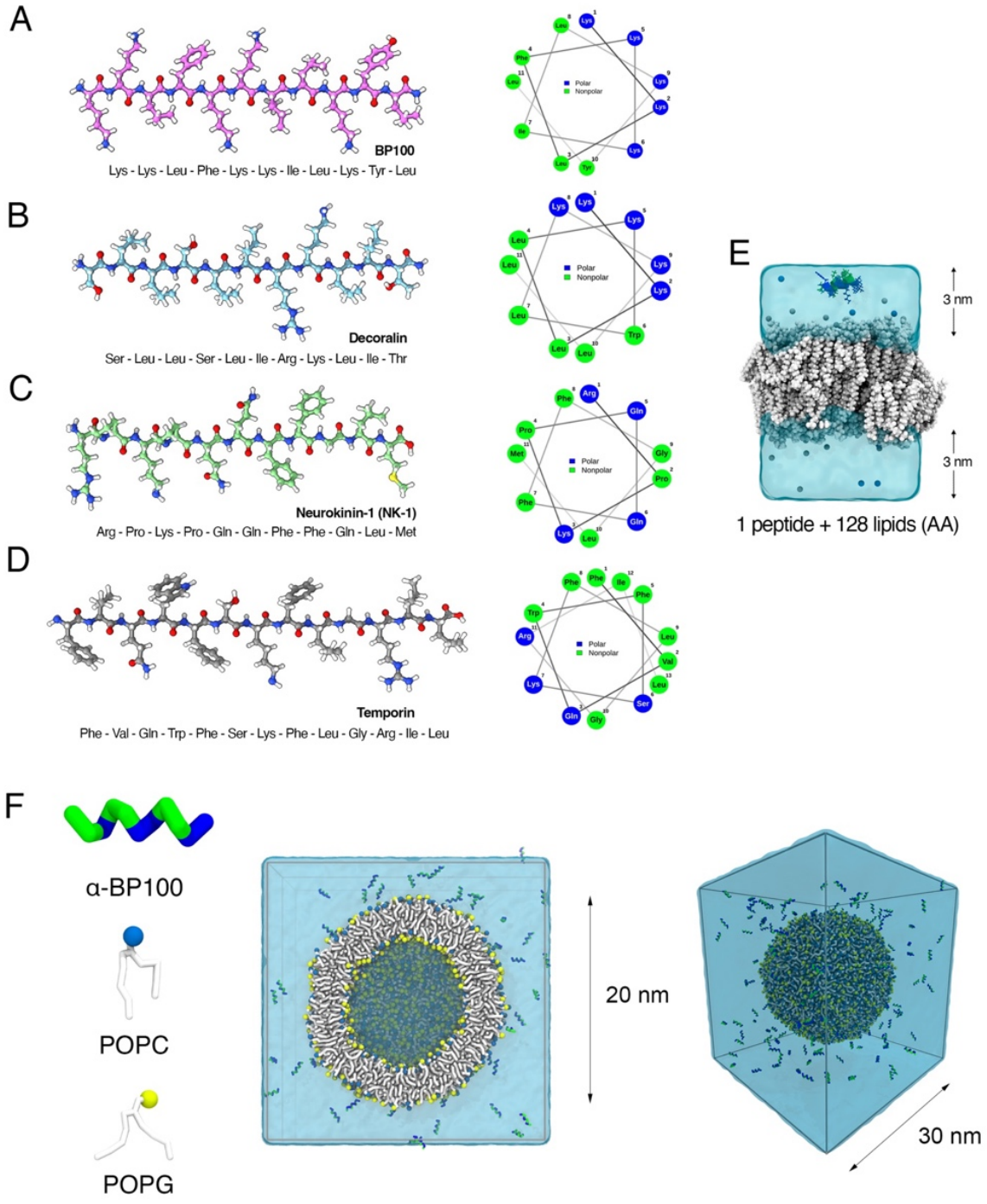


**Figure 1 - Antimicrobial peptides and set-ups used in this study.** BP100 (A), Decoralin (B), NK-1 (C), and Temporin-L (D) atomic structures and their respective helical wheel projections. All-atom peptide:lipid systems in (E). Peptides were pre-folded as alpha-helices without the use of constraints. Coarse-grained vesicle were generated using CHARMM-GUI's *Vesicle Builder*[63,64] and peptides were inserted in the extra-vesicular solution (F). Images rendered in VMD 1.9.4[82] and USCF ChimeraX[83].

Simulations were run with a time-step of 2 ps and all bonds were constrained using the LINCS[55] algorithm. Neighbor-searching was accomplished using the Verlet cut-off algorithm at every 50 fs. Short-range electrostatic and van der Waals interactions were computed using a 1.5 nm cut-off, using a potential-switch function from a 1.4 nm cut-off. Long-range electrostatic interactions were treated using the Particle Mesh Ewald[56] method. Temperature was set to 323K, above the lipid transition temperature, and coupled using the V-rescale[57] thermostat with a coupling constant of 0.1 ps. Semiisotropic pressure was coupled using the Parrinello-Rahman barostat at 1 bar with a coupling constant of 1.0 ps. Periodic boundary conditions were applied in all three dimensions. Energy minimization step was performed using the steepest descent method, followed by NVT and NPT steps. Each production run was carried out for 2 μs for each peptide, resulting in a total of 8 μs.

Peptide hydration and lipid clustering analysis were calculated using the *gmx trjorder,* computing the number of waters and lipids surrounding the peptides along the simulation, using a 0.5 and 0.75 nm cut-off, respectively. The secondary structure of peptides was analyzed using the DSSP program. Following a previous protocol of analyzing lipids in layers, we calculated the lateral diffusion coefficient ($D_L$) for the first 10, 20 (excluding the first 10 lipids) and 64 lipids closest to the peptide in the monolayer in which the peptide was bound. The coefficient $D_L$ can be obtained from MSD = 4 $D_L t$, where MSD is the mean square displacement of an atom as a function of time (t). We calculated the MSD of the phosphorus atoms from each lipid group at every 10 ns using the *gmx msd* command. Then, $D_L$ was obtained from the slope of the least square fitting between 2 to 5 ns of each 10 ns-time-window. 2D membrane thickness was obtained using the SuAVE analysis package[58], which fits a rectangular grid mesh based on the location of membrane atoms (i.e. phosphorus atoms) and then calculates the average thickness by computing the distance between the upper and lower grids. Peptide density and the percentage of peptide volume inserted ($V_{pept}$) was calculated using the *s_ dens* command from SuAVE.

#### 4.3.2.2. Coarse-graining simulations and analysis

For coarse-graining simulations, we used the Martini3[59–61] force field. All peptide atomistic structures were converted to coarse-grained structure with the *Martinize2* script[62], including the -scfix flag and assigning alpha-helical secondary structure for BP100, Decoralin, and Temporin-L. For NK-1, the first four residues (Arg-Pro-Lys-Pro) were assigned as random coil due to the presence of proline residues and the remaining aminoacids as alpha helical. Elastic network models and virtual G$\bar{o}$ sites were not applied.

With the goal of a more direct comparison between experimental and theoretical data and obtaining mechanistic insights at a molecular level, peptide/vesicle systems were also prepared.

The initial vesicle structures were obtained from the CHARMM-GUI webserver[63], using *Vesicle Builder* in *Martini Marker*[64]. Although experimental LUVs are close to 100 nm in diameter, we chose to simulate vesicles of approximately 20 nm diameter-size which retains structural similarity of larger LUVs while reducing computational cost and allows proper sampling time. In order to compare directly with LUV leakage experiments, we used mixed vesicles of POPC and POPG at equal proportion (1:1), with symmetrical composition between leaflets (1772 and 1106 lipids in the outer and inner leaflet, respectively), and pure POPC vesicles (1701 and 1057 lipids in the outer and inner leaflet, respectively).

Vesicles were hydrated with CG water in a 30 x 30 x 30 nm simulation box and neutralized with counter-ions (Fig. 1F).

The vesicles obtained from CHARMM-GUI contained six water pores with a radius of 20 Å, allowing for lipid flip-flop and free movement of water molecules to equilibrate the interior and exterior compartments. Equilibration runs of vesicle-only systems were performed in 5 steps, with decreasing water pore diameter and increasing simulation time-step (see Table S2 for detailed information). After equilibration steps, production runs were performed for 10 µs and used as controls.

In order to explore peptide effects on vesicles at low, medium and high peptide concentration, we built 5 systems by adding peptides into pre-equilibrated vesicle-only systems, reaching a peptide:lipid (P/L) ratio of 0.01 (low), 0.05 (low), 0.10 (medium), 0.20 (high), and 0.30 (high). Table 1 shows all the simulation set-ups used in this work.

For peptide-vesicle CG simulations, energy minimization was performed using the steepest descent method for 10,000 steps. Systems were then equilibrated for 10 ns with a 10 fs timestep. For production runs we used a 20 fs time step and ran each system for 10 µs. Simulations were extended to 50 µs when needed. Pressure coupling was achieved using the Berendsen barostat in the equilibration step and for MD production runs we used the Parinello-Rahman[65] using the same pressure coupling parameters (isotropic at 1 bar, coupling constant of 12.0 $ps^{-1}$, and compressibility at $3x10^{-4}$). For both equilibration and production runs, we used the velocity-rescalling[57] thermostat at 303 K using a coupling constant of 1.0 $ps^{-1}$. For all simulations, including minimization, equilibration and production runs, the neighbor list was updated using the Verlet search algorithm with a van der Waals interaction cut-off of 1.1 nm[66]. The reaction-field method was used to treat Coulomb interactions using a 1.1 nm cut-off with a dielectric constant of the reaction field set to infinity[66].

| | **Forcefield** | **System** | **# Peptides** | **Pressure (bar)** | **Temperature (K)** | **Time (μs)** |
|---|---|---|---|---|---|---|
| Bilayer Membrane (AA simulations) | Amberff99sb-ildn-NMR (peptides)<br><br>SLipids (lipids) | POPC:POPG (1:1)<br><br>64 lipids per leaflet | 1 | 1 | 323 | 2 |
| Vesicle (CG simulations) | Martini3 | POPC:POPG (1:1)<br><br>(Outer: 1722 lipids)<br><br>Inner: 1106 lipids) | 28 | 1 | 303 | 10 |
| | | | 141 | | | 10 |
| | | | 283 | | | 50 |
| | | | 565 | | | 50 |
| | | | 848 | | | 50 |
| | | POPC<br><br>(Outer: 1701 lipids)<br><br>Inner: 1057 lipids) | 28 | | | 10 |
| | | | 138 | | | 10 |
| | | | 276 | | | 10 |
| | | | 551 | | | 10 |
| | | | 827 | | | 10 |

**Table 1:** All-atom (AA) and coarse-graining (CG) simulation set-ups utilized in this work. For BP100, all the set-ups were utilized. For Decoralin, NK-1, and Temporin, we simulated the AA simulations and CG simulations with POPC:POPG vesicles.

# 4.4. Results

### 4.4.1. All-atom simulations of single peptides on anionic membranes

To facilitate the comparison of peptide/membrane interactions, results shown in Figures 2 and 3 use a nomenclature identifying the property being analyzed by referring to the respective row (A-D) and column (c). For example, "Fig 2C, c1" refers to the DSSP analysis of BP100 during the simulated time (See below in the legend of Figure 2).

Experimental results show that the four peptides (BP100, Decoralin, NK-1, and Temporin-L) selected for this work fold into an alpha-helix on negatively charged membranes and have no structure in water[38,42,52]. Secondary structure analysis was performed using the DSSP algorithm (Fig. 2C), implemented in GROMACS. In all of the peptide/POPC:POPG atomistic simulations, we found a predominance of alpha-helical structure in all peptides except NK-1. On average, we found 75% of alpha-helix for BP100, 74% for Decoralin, 36% for NK-1, and 75% for Temporin-L throughout the simulations.

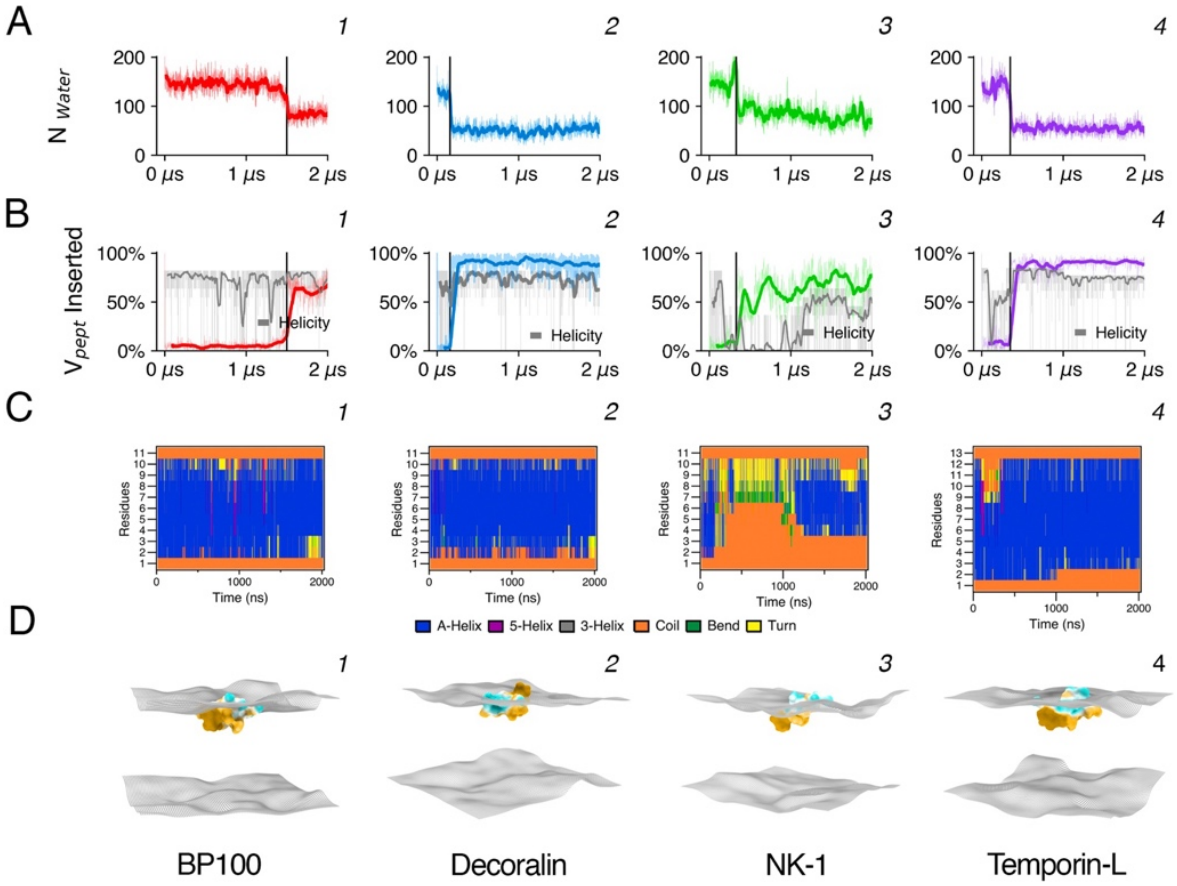


**Figure 2 - Peptide hydration, insertion, and structural analysis from atomistic simulations.** For peptide hydration (A), waters surrounding the peptide within a 0.5 nm cut-off ($N_{water}$) were computed for BP100 (column 1), Decoralin (column 2), NK-1 (column 3), and Temporin-L (column 4) throughout the simulations. Peptide flip occurred for all peptide:membrane simulations, at ~1.5 μs, ~0.16 μs, ~0.65 μs, and ~0.35 μs for BP100, Decoralin, NK-1 and Temporin-L, respectively. Black vertical lines in column 1 indicate the approximate time when peptide flip was observed. Peptide flip is accompanied by peptide steep dehydration (A) and insertion (B, $V_{pep}$ Inserted). In (C), DSSP analysis show alpha helical structure (blue) favors peptide flip. Snapshots of the last frame of each simulation are shown in (D). Peptides are represented with their hydrophobicity surface, with hydrophobic areas in beige and hydrophilic regions in cyan. Surfaces were generated using SuAVE, using the phosphorus positions.

Similarly to our previous findings with saturated phosphatidylglycerol (DPPG) membranes, BP100 alpha helix was stable in POPC:POPG membrane (Fig. 2C, c1). The amino acid composition and helical projection of Decoralin is similar to BP100 (Fig. 1A, B) and, as expected, its secondary structure was predominantly alpha helical and stable along the simulation (Fig. 2C, c2). Though NK-1 has prolines residues in its N-

terminus (Arg-Pro-Lys-Pro), we found no polyproline helix when analyzing the ψ and φ backbone dihedral angles of NK-1 first 4 residues in a Ramachandran plot (Fig. S2). As expected, the residues closer to the N-terminus remained unstructured due to the presence of Prolines (Pro2, Pro4) and when inserted into the membrane, NK-1 recovered its alpha-helix content in the half part closer to its C-terminus (Gln5, Gln6, Phe7, Phe8, Gln9, Leu10) (Fig. 2C, c3). As for Temporin-L, our secondary structure findings are in line with experimental CD[42] and atomistic simulation data[67] of Temporin-L in POPE/POPG and POPG membranes, with an overall alpha-helical structure.

Peptide flip is related with the peptide structure on membranes[35]. When folded into an alpha-helix, most SCHAMPs have a clear separation of hydrophilic and hydrophobic moieties, providing its amphiphilic character and favoring peptide rotation and insertion into the membrane.

Trajectory analysis revealed peptide flip occurred for all the peptides investigated here (Fig. 2D). In this set of simulations the flipping times were ~1.5 μs (BP100), ~0.16 μs (Decoralin), ~0.65 μs (NK-1), and ~0.35 μs (Temporin-L) in POPC:POPG membranes (Fig. 2D). Similarly to our previous results with BP100 in DPPG bilayers[35], peptides approached the POPC:POPG membrane with their charged residues portion, showing that the initial interaction is determined by electrostatic interactions. In this initial electrostatic-determined interaction the helical peptides were oriented parallel to the membrane surface. After variable times the peptides rotated and their hydrophobic residues were inserted into the membrane core, burying the peptides inside the bilayer (Figure 2D). Peptide dehydration was coupled with peptide flip (Figure 2A). The number of water molecules in the first hydration shell (r = 0.5 nm) decreased *ca.* 50% after the flip (Fig. 2A) [35]. Using the SuAVE membrane analysis package[58], we generated surface grids based on the membrane phosphorus atom positions and calculated the percentage of peptide volume inserted ($V_{pept}$) between the grids (Figure 2B). $V_{pept}$ remained constant after the flip (Fig. 2B), showing the flipped-inserted state was stable during our simulations.

We also analyzed the effect of peptide binding on membrane properties. Previous simulation[36] and experimental[18] data shows that BP100 causes local thinning, evidenced by the matching of the concavity observed in 2D mappings with the peptide locations (Fig. 3A,B). Selectively calculating lipid lateral diffusion ($D_L$) for the first neighboring 10, 20, and 64 lipids on each monolayer, we found that the 10 closest lipids were those most affected by the peptide binding, confirming its local activity (Figure 3D). The $D_L$ for the 10 lipids neighboring the peptide decreased 69% (BP100), 62% (Decoralin), 55% (NK-1), and 72% (Temporin-L), respectively.

The number of lipids surrounding the peptides, computed using a 0.75 nm cut-off, shows the probability distribution of lipids in contact with the peptides (Fig. 3C). All peptides seem to cluster negatively charged phospholipids as observed for BP100 in DPPC:DPPG mixed bilayers[35]. Clustering of POPG was not a consequence of peptide flip as it can be observed even before the occurrence of the flip. Rather, it seems to be related to the relative number of positively charged residues in the antimicrobial peptide amino acid composition and its overall hydrophobicity <H> (Table S1). Peptides with lower <H> and/or with higher percentage of positively charged residues in its sequence segregated larger numbers of POPG lipids, such as BP100 (+6, <H> = 0.427) and NK-1 (+3, <H> = 0.501). Conversely, both Decoralin and Temporin-L possess an overall +3 charge, but their overall hydrophobicity is high (0.780 and 0.906, respectively) compared to BP100 and NK-1. The presence of hydrophobic residues would increase the number of non-polar contacts between peptide and membrane acyl chains regardless of the lipid charge while the cationic peptide residues would attract specifically anionic lipids into the peptide surroundings.

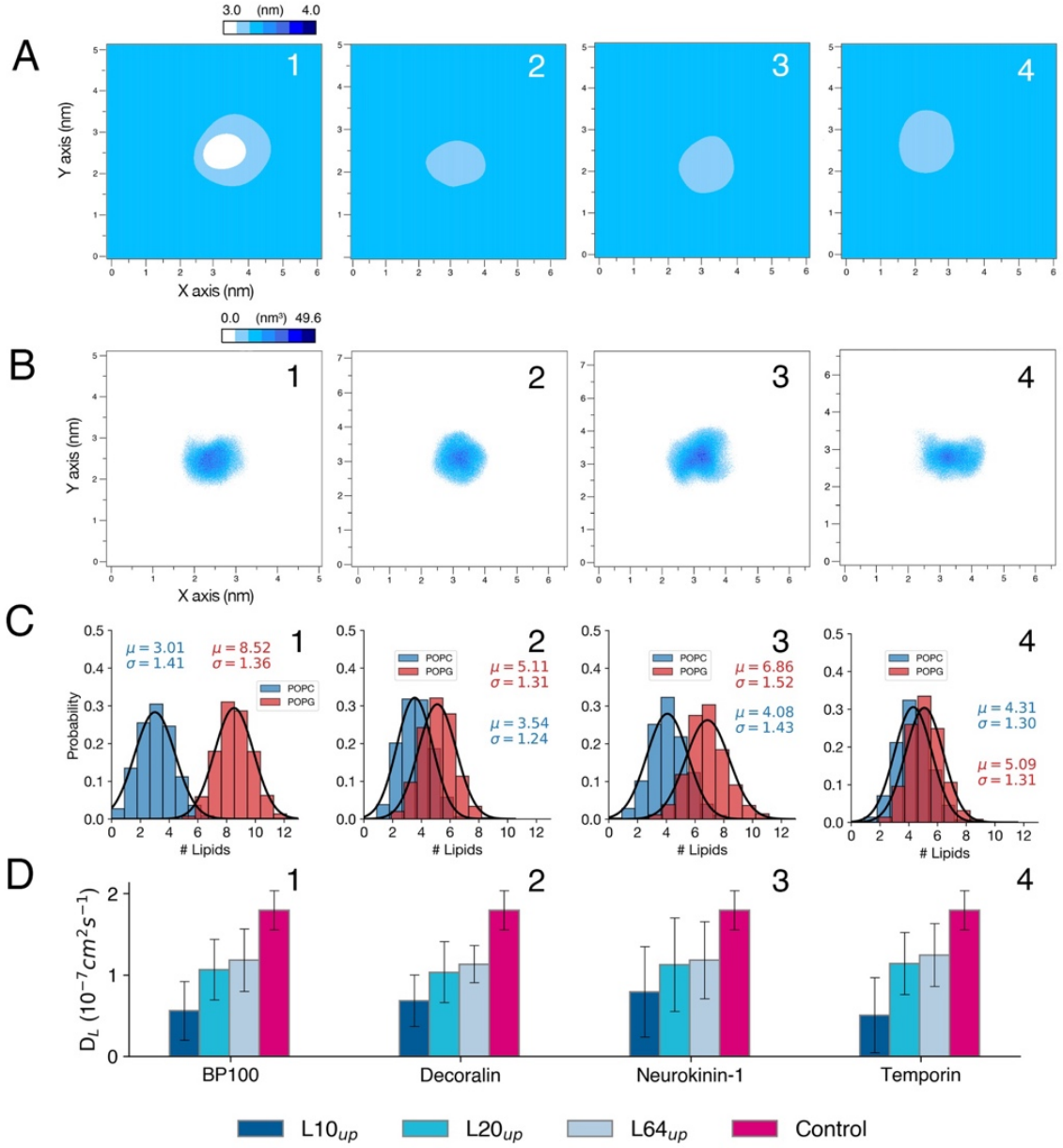


**Figure 3 - Antimicrobial peptides decrease membrane thickness and lipid diffusion locally.** (A) and (B) show respectively 2D thickness mappings and peptide density for BP100 (column 1), Decoralin (column 2), NK-1 (column 3), and Temporin-L (column 4) in POPC:POPG membranes. The same enumeration is applied for other data. The probability distribution of POPC and POPG lipids in contact with peptides with their respective average and standard deviation values are shown in (C). Lipid diffusion (D) was computed for all peptides selecting the first 10, 20 neighboring lipids and for the whole monolayer (upper). Control values are reported for comparison.

### 4.4.2. Higher P/L ratios with coarse-graining simulations

We simulated BP100 in POPC and POPC:POPG (1:1) vesicles using five peptide to lipid ratios (P/L): 0.01, 0.05, 0.10, 0.20, and 0.30. In all coarse-graining (CG) simulations with vesicles, peptide flip was observed for bound BP100 for both in POPC and in POPC:POPG vesicles.

Using vesicles of POPC, at any P/L ratio, we observed no vesicle shape alteration in the simulations with BP100 (Fig. S3). The average number of bound peptides to POPC vesicles reached a plateau around P/L=0.10 (Fig. S3B). At P/L=0.10, BP100 increased overall vesicle volume by 1.2% and membrane thickness by 1.1%, but no roundness or size change of the vesicle was evident in the simulations (Fig. S3 and Table S3).

The simulations of negatively charged vesicles (POPC:POPG, at 1:1 ratio) at low and medium P/L (0.01 to 0.10) reached equilibrium within 5 μs (Fig. S4). Virtually all peptides were bound and remained attached throughout the simulations (Fig. S4). Compared with control POPC:POPG vesicle, low and medium P/L simulations showed a proportional increase of the area per lipid (APL), total vesicle volume ($V_{total}$), membrane thickness ($D_{HH}$), and average radius (R) with peptide concentration (Fig. 4C,E-G, Table 2).

The overall vesicle shape can be monitored through sphericity (φ), an estimate of how closely the shape of an object resembles that of a perfect sphere[68]. At low P/L, BP100 binding did not significantly alter φ compared to control (Table 2). However, at higher peptide ratios (P/L = 0.10), we calculated a -5.7% variation in φ compared to control and at the end of the simulation, the vesicle adopted an ellipsoidal shape, with highly curved edges (Fig. 4A, P/L=0.10).

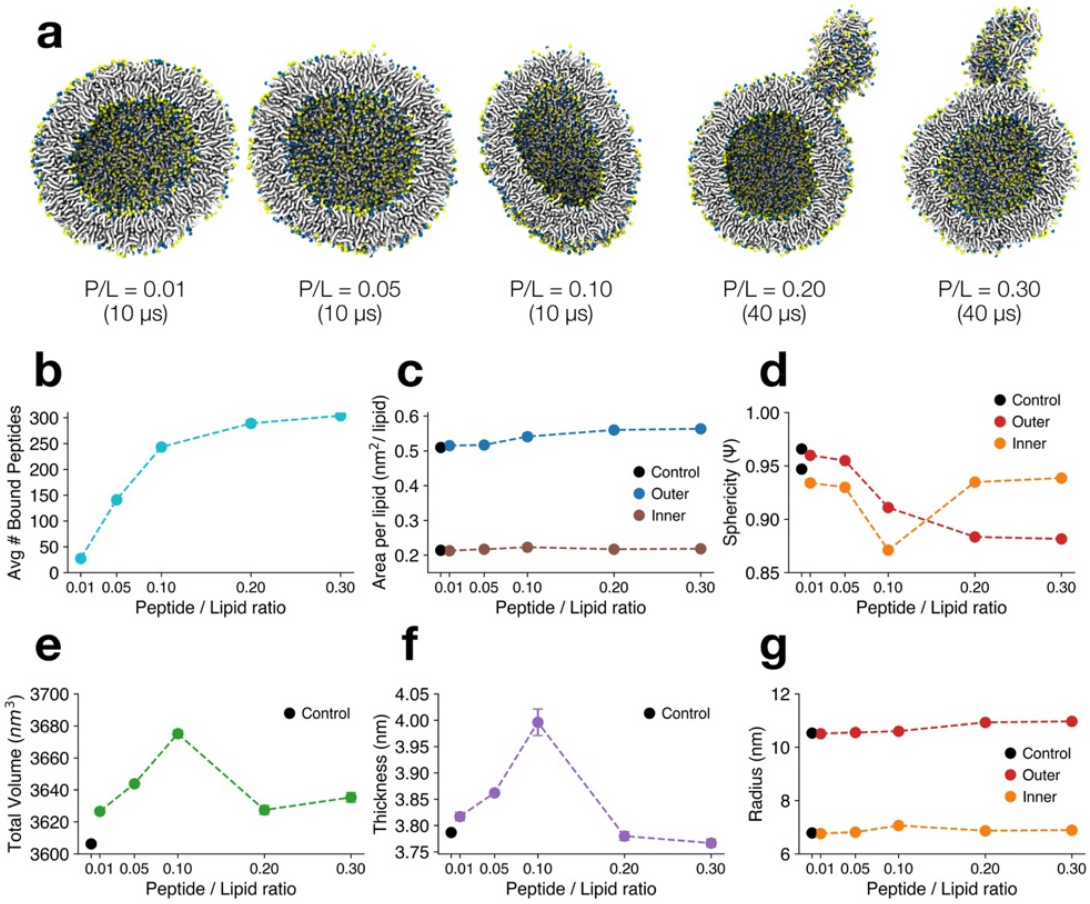


**Figure 4: Antimicrobial BP100 induces protrusion formation in vesicles at high peptide:lipid ratios.** (a) Cut-away cross-sectional last frame snapshots of POPC:POPG (1:1) vesicle/BP100 system at low (P/L = 0.01 and 0.05), medium (P/L = 0.10), and high (P/L = 0.20 and 0.30) concentrations. Peptides, water and ions are not shown for clarity. Obtained averaged peptide binding outcomes in vesicles according to the respective P/L are shown (b-g). Data points with no error bars had an error below 5%. Data points were obtained averaging the last 5 μs of each simulation. Errors are estimated by block averaging.

Such ellipsoidal shape is followed by the expansion of the outer and inner APL (Table 2). Although a 3.2% increment in the outer APL could seem irrelevant, aspiration experiments with giant unilamellar vesicles (GUV) with mellitin, revealed pore formation occurs at a 3.4% increase in GUV membrane area upon melittin binding[69]. BP100 binding into POPC:POPG vesicle thus caused vesicle swelling at P/L=0.10, with increase in the total vesicle volume (Fig. 4E, Table 2) and in membrane

thickness. The proportional increase in membrane thickness at low P/L can be explained by the binding of BP100 in the outer part of the vesicle. As atomistic simulations suggest, the binding and flipping of peptides into the membrane leads to a decrease in order parameter of lipid acyl chains leading to small membrane defects. In low concentrations (P/L $< 0.1$), such defects cause membrane thinning[36,70]. However, at low and medium concentrations, these voids can be filled with binding peptides leading to an asymmetry in lipid packing between the outer and inner monolayer.

BP100 induced vesicle budding at high concentrations (P/L = 0.20 and 0.30). We simulated both concentrations for 50 μs and vesicle budding was observed at ~10 μs and ~27 μs, respectively. In both simulations, the same pattern observed in P/L = 0.10 was observed. Initially, peptide binding alters the vesicle into an ellipsoidal shape as it increases the outer and inner APL (Fig. S4). Other vesicle properties increase proportionally, such as total vesicle volume, thickness and size (Fig. 5A, C)

| System | $APL_{outer}$ ($nm^2$/lipid) | $APL_{inner}$ ($nm^2$/lipid) | $V_{total}$ ($nm^3$) | $D_{HH}$ (nm) | R (nm) | φ |
|---|---|---|---|---|---|---|
| Control | 0.510 | 0.214 | 3606 | 3.79 | 10.5 | 0.966 |
| P/L = 0.01 | +1.0% | -0.5% | +0.6% | +0.8% | -0.2% | -0.6% |
| P/L = 0.05 | +1.4% | +1.9% | +1.0% | +2.0% | +0.2% | -1.1% |
| P/L = 0.10 | +6.1% | +3.2% | +1.9% | +5.5% | +0.6% | -5.7% |
| P/L = 0.20 | +9.8% | -2.8% | +0.6% | -0.2% | +3.8% | -8.5% |
| P/L = 0.30 | +10.4% | +1.0% | +0.8% | -0.5% | +4.2% | -8.7% |

Table 2: Variation in percentage of vesicle structural properties compared to control.

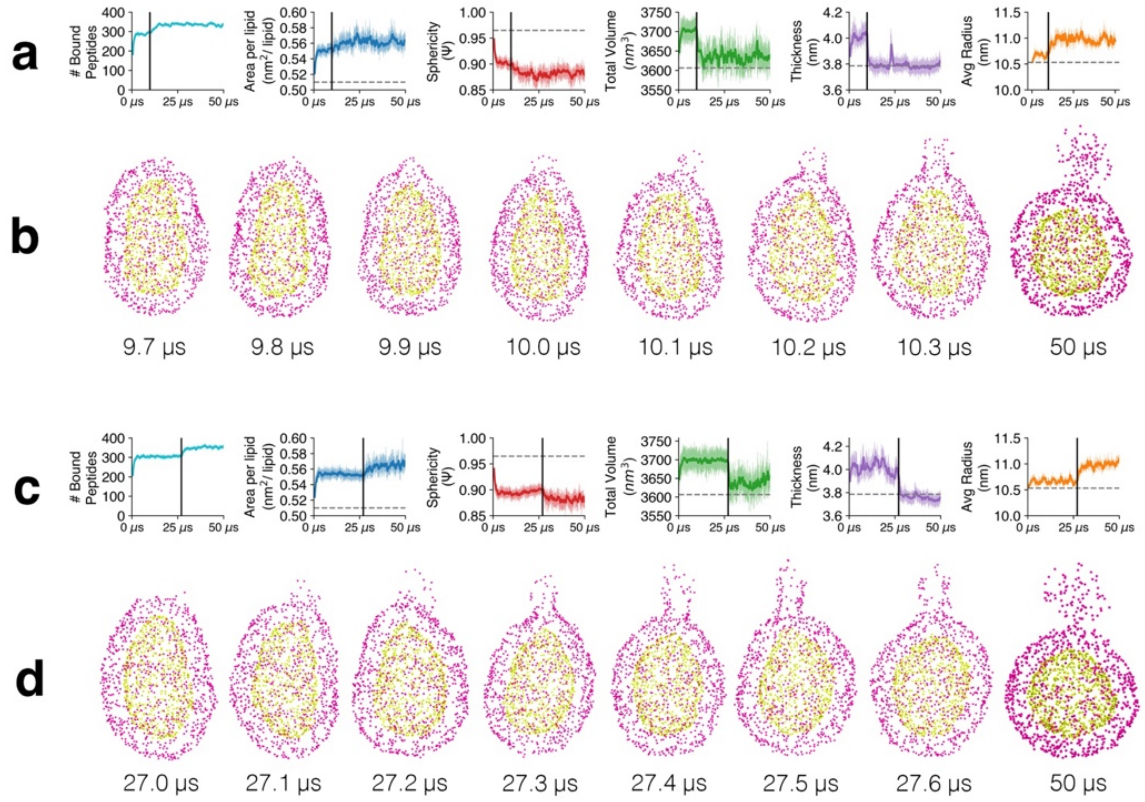


**Figure 5 - Antimicrobial peptide induce vesicle budding at high concentrations.** (A) and (C) show computed properties for POPC:POPG vesicles throughout BP100/vesicle simulation at P/L = 0.20 and P/L = 0.30, respectively. We show the number of bound peptides, outer area per lipid, outer leaflet sphericity, total vesicle volume, membrane thickness and average radius. Black vertical lines indicate the approximate time when budding started. (B) and (D) show snapshots of the vesicles of both simulations during membrane protrusion. Only phosphorus atoms are shown and are colored in magenta (outer) and yellow (inner).

The lateral tension generated at the peptide binding site in the outer membrane leaflet can be alleviated through membrane lateral expansion whilst the inner leaflet initially can accompany such expansion (Fig. S5), due to non-polar interactions between acyl chains of both leaflets. However, the continuous binding of peptides in the outer membrane may lead to an asymmetry of the membrane, due to the different surface lateral pressure between inner and outer monolayers. Such imbalance in membrane area and volume caused by peptides can produce budding in highly curved regions of the vesicle (Fig. 5B, D). Peptide-induced budding led to

detachment between acyl chains of the outer and inner monolayer lipids, thus allowing the inner leaflet to stabilize its APL and regaining its spherical shape, reaching control values (Fig. S5). In contrast, in the outer leaflet, more peptides bound (Fig. 5A,B), increasing the outer APL, and thus growing the protrusion-body size along the simulation (Fig. 5, S5). Concomitantly with budding, the average vesicle thickness decreased as fewer lipids on the outer leaflet were available to counter-part the inner vesicle lipids (Table 2, Fig. 5). Such thinning could make the peptide-enriched vesicles more prone to pore formation or further induce inner content leakage. No lipid flip-flop between outer and inner vesicle lipids nor full separation between vesicle and protrusion were observed during our simulation time (Fig. 5B, D).

We also simulated Decoralin, NK-1, and Temporin-L in POPC:POPG vesicles at the same P/L ratios (0.01, 0.05, 0.10, 0.20, and 0.30). Following our secondary structure data from atomistic simulations (Fig. 2C) all peptides except NK-1 were assigned as full alpha-helical CG structure. As the first 4 residues of NK-1 had no secondary structure (Fig. 2C, c3), only residues 5 to 11 were assigned as alpha-helix in our CG simulations.

Such difference in secondary structure was proven to be key in the outcomes of our peptide/vesicle CG simulations. NK-1 had no effect on the vesicles shape in all P/L ratios simulated (Fig. 6, NK-1). Like BP100, Decoralin peptides (Fig. 6, Decoralin) had little effect on POPC:POPG vesicles at low P/L (0.01 and 0.05) . At medium P/L (0.10), Decoralin altered the vesicle into an ellipsoidal shape. At high P/L (0.20 and 0.30), it created highly curved regions in the vesicle and eventually membrane budding was observed. Simulations with Temporin-L showed the same pattern except that membrane budding occurred from P/L = 0.10.

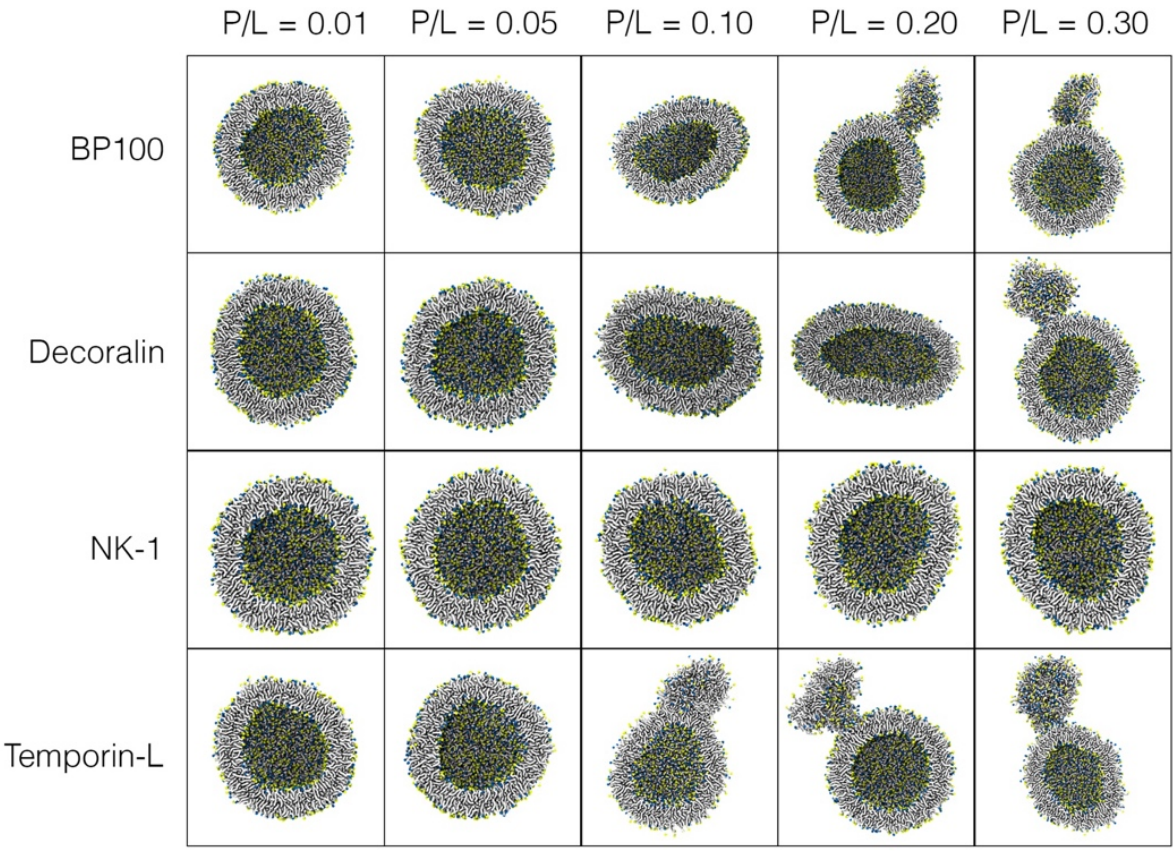


**Figure 6 – Short cationic alpha-helical peptides follow same vesicle budding at high concentrations.** Cut-away cross-sectional last frame snapshots of POPC:POPG (1:1) vesicles with BP100, Decoralin, NK-1, and Temporin-L simulations. Water, counter-ions, and peptides are not shown for clarity.

## 4.5. Discussion

Overall, our simulation results suggest SCHAMPs act on model membranes via the carpet mechanism at high peptide:lipid ratios. Such finding was suggested for BP100 experimentally[17,18,21,24,71], but our simulation data show it can be expanded for other peptides that share similar folding and length. Our CG results using the latest Martini3, are similar with those obtained by Woo et al, which first reported a budding or buckling effect on membranes by magainin-2, using Martini 2.2[72]. More recently, similar peptide-induced membrane budding was reported by Zhang et al[73], when simulating Temporin B and L on POPC:POPG (7:3) planar bilayers. Using the pSPICA CG forcefield, Miyazaki and Shinoda[74] conducted melittin simulations on POPC planar membranes and vesicles and reported identical budding and lipid extraction at P/L ~ 0.10 (when considering melittin's double length compared to SCHAMPs). The authors also described the alteration in the vesicle morphology into an ellipsoidal shape upon peptide binding, and further pore formation.

Peptide flip seems to be crucial for budding or buckling mechanism, as it defines how many peptides will interact with vesicles. For such, a conjuncture of factors is to be present. First, antimicrobial peptides amino acid composition should produce fully alpha-helical, positively charged, and amphiphilic peptides in negatively charged membranes. And second, bacterial membranes or model membranes ought to have negatively charged regions for initial peptide binding via electrostatic interactions.

Our atomistic simulations showed all four peptides caused membrane thinning and negative curvature (Fig. 3A). At the individual level, SCHAMPs bind and flip on the membrane, the peptide buries into the membrane and the hydrophobic facet can deeply insert into the membrane core and consequently, the higher conformational freedom of the lipid acyl chains creates empty pockets in the membrane which causes the upper and lower monolayer lipids to squeeze in order to occupy these void spaces, causing local membrane thinning[18,36]. However, at higher P/L, the steady and continuous binding and flipping of SCHAMPs into the

membrane creates an imbalance in the overall membrane volume and APL between the outer and inner leaflets. Such imbalance first promotes vesicle swelling, increasing outer and inner APL and membrane thickness, and thus, positive curvature is created (Table 2). When enough peptides are bound and highly curved regions are produced in vesicles (Fig. 5B,D), membrane budding starts. We observed that after budding, more peptides bound to the vesicle (Fig. 5A, D), increasing the outer APL and the protrusion size, while membrane thickness decreased. Such outcome could lead to pore-formation or complete dissociation between the protrusion and vesicle. It is worth noting that we simulated small vesicles (~20 nm in diameter), in larger vesicles, possibly SCHAMPs could induce more drastic outcomes such as vesicle fission or inner content leakage via pore-formation.

The differences between the studied peptides in their binding and membrane outcomes can be explained with the "wedge" model[75] (see reference for detailed description). In this model, SCHAMPs have a cross-sectional wedge shape, specific to their amino acid composition. Peptides featuring a wide polar face of charged residues and a narrow non-polar face are denominated as wedge-shaped peptides. SCHAMPs with a wider hydrophobic face and an apex consisting of a smaller cluster of cationic residues, are the inverted wedge-shaped peptides. At low P/L, wedge-shaped peptides can generate positive curvature while inverted wedge-shaped peptides produce negative curvature on membranes[76–78]. However, at high P/L, both types of peptides could generate positive curvature as bound peptide volume contribution increases.

Inverted wedge-shaped SCHAMPs, such as Temporin-L, are more hydrophobic than wedge-shape peptides, leading to higher percentage of bound peptides to the membranes even at lower and medium P/L. And thus, peptide-induced budding could occur even at P/L = 0.10 (Fig. 6).

The number of non-polar amino acids with large side-chains seem to have a key role in SCHAMPs activity. Leucine, phenylalanine, tyrosine, and tryptophan are found in many AMPs[79]. In the case of Temporin-L, when substituting both Phe3 and Phe5 with leucines, the modified

Temporin-L has no activity against *E. coli* and *P. aeruginosa*[80]. When folded into an alpha-helix, Temporin-L has a clear spatial segregation between hydrophobic and hydrophilic residues and the aromatic amino acids are concentrated in the hydrophobic portion (Fig. 1D). A similar behavior was reported in an alanine-scan study with BP100[71]. While substituting BP100 positively charged residues produced little to no effect in minimum inhibitory concentrations against Gram positive and negative bacteria, replacing hydrophobic residues with larger side groups with Alanine, such as Leucine, Phenylalanine, and Tyrosine, drastically reduced BP100 antimicrobial activity[71].

NK-1 contains proline amino acids which destabilize alpha-helix folding on the water/membrane interface, and although NK-1 has 2 aromatic amino acids (Phe), the hydrophobic/hydrophilic facets are not clearly separated, decreasing its hydrophobic moment and consequently decreasing its affinity with the membrane and peptide flip occurrence. Decoralin and BP100 have similar features in terms of amino acid composition, folding behavior in water and membranes, and clear hydrophobic/hydrophilic facet separation when in alpha-helical conformation. Moreover, both peptides possess residues with medium to large side-chains in their hydrophobic moiety (BP100 – Leu, Phe,Tyr ; Decoralin – Leu, see Fig. 1A,B).

The wedge model, is a convenient way to characterize some of the peptide effects observed here. We recognize, however that this model should not be the only parameter when ranking suitable antimicrobial peptides for pharmaceutical use. Inverted wedge-shaped SCHAMPs are likely to be more toxic towards human cells, such as Temporin-L[40], due to their higher affinity toward membranes.

Although our CG findings indicate SCHAMPs act via the carpet mechanism, one should be mindful of the limitations of AA and CG simulations. AMPs pore formation phenomena are in the microsecond scale[27,28], and therefore longer AA simulations with increased SCHAMP concentrations could reveal a different outcome. Moreover, Martini overestimates the energy cost for pore formation compared to AA

forcefields[81], probably due to the implicit screening of charges in Martini[59] and thus, the budding observed in our simulations could be the result of the current inability of Martini of simulating the formation of pores[33]. Finally, the role of peptide folding on the membrane interface is absent in Martini, in which peptide secondary structure is pre-determined and fixed into an alpha-helix[60]. Another interpretation of our results could be the possible occurrence of a simultaneous (with pore and budding formation) or a sequential membrane disruption mechanism, with budding as a short-lived intermediate state before pore formation.

In summary, our results suggest that BP100, Decoralin, NK-1, and Temporin-L share common mechanism steps when destabilizing anionic membranes. Our atomistic simulations revealed all 4 SCHAMPs flipped on anionic membranes at low peptide concentration, and were accompanied by peptide dehydration and insertion into the membrane core. All peptides perturbed the bilayers locally, with membrane thinning, anionic lipid aggregation and decreasing lipid lateral diffusion. In our CG vesicle simulations with higher peptide concentrations (PL=0.20 and 0.30), full alpha-helical peptides (BP100, Decoralin, and Temporin-L) deformed vesicles and induced the budding in highly curved regions of the vesicles. The inverted wedge mechanism coupled to the contributions of large hydrophobic aminoacids can explain the formation of by SCHAMPs. Future work on SCHAMPs, such as with improved forcefield parameters, polarized water models, and even with pre-formed larger pores could also shed light on other alternative mechanisms of SCHAMPs.

# 4.6. References

1. Antibiotic resistance. https://www.who.int/news-room/fact-sheets/detail/antibiotic-resistance.
2. Urban-Chmiel, R. *et al.* Antibiotic Resistance in Bacteria—A Review. *Antibiotics* vol. 11 Preprint at https://doi.org/10.3390/antibiotics11081079 (2022).
3. Bush, K. *et al.* Tackling antibiotic resistance. *Nature Reviews Microbiology* vol. 9 894–896 Preprint at https://doi.org/10.1038/nrmicro2693 (2011).
4. Murray, C. J. *et al.* Global burden of bacterial antimicrobial resistance in 2019: a systematic analysis. *The Lancet* **399**, 629–655 (2022).
5. O'Neill, J. Tackling drug-resistant infections globally: final report and recommendations. Preprint at (2016).
6. Mann, A., Nehra, K., Rana, J. S. & Dahiya, T. Antibiotic resistance in agriculture: Perspectives on upcoming strategies to overcome upsurge in resistance. *Current Research in Microbial Sciences* vol. 2 Preprint at https://doi.org/10.1016/j.crmicr.2021.100030 (2021).
7. Morris, S. & Cerceo, E. Trends, epidemiology, and management of multi-drug resistant gram-negative bacterial infections in the hospitalized setting. *Antibiotics* vol. 9 Preprint at https://doi.org/10.3390/antibiotics9040196 (2020).
8. Moretta, A. *et al.* Antimicrobial Peptides: A New Hope in Biomedical and Pharmaceutical Fields. *Frontiers in Cellular and Infection Microbiology* vol. 11 Preprint at https://doi.org/10.3389/fcimb.2021.668632 (2021).
9. Brogden, K. A. Antimicrobial peptides: Pore formers or metabolic inhibitors in bacteria? *Nature Reviews Microbiology* vol. 3 238–250 Preprint at https://doi.org/10.1038/nrmicro1098 (2005).
10. Turner, K. B., Dean, S. N. & Walper, S. A. Bacterial bioreactors: Outer membrane vesicles for enzyme encapsulation. in *Methods in Enzymology* vol. 617 187–216 (Academic Press Inc., 2019).
11. Sood, R. & Kinnunen, P. K. J. Cholesterol, lanosterol, and ergosterol attenuate the membrane association of LL-37(W27F) and temporin L. *Biochim Biophys Acta Biomembr* **1778**, 1460–1466 (2008).
12. Brender, J. R., McHenry, A. J. & Ramamoorthy, A. Does cholesterol play a role in the bacterial selectivity of antimicrobial peptides? *Front Immunol* **3**, (2012).
13. Torres, M. D. T. *et al.* Decoralin Analogs with Increased Resistance to Degradation and Lower Hemolytic Activity. *ChemistrySelect* **2**, 18–23 (2017).
14. Somma, A. di *et al.* Antibiofilm properties of temporin-l on Pseudomonas fluorescens in static and in-flow conditions. *Int J Mol Sci* **21**, 1–17 (2020).
15. Torres, M. D. T. *et al.* Natural and redesigned wasp venom peptides with selective antitumoral activity. *Beilstein Journal of Organic Chemistry* **14**, 1693–1703 (2018).
16. Ramesh, S., Govender, T., Kruger, H. G., de la Torre, B. G. & Albericio, F. Short AntiMicrobial Peptides (SAMPs) as a class of extraordinary promising therapeutic agents. *Journal of Peptide Science* **22**, 438–451 (2016).

17. Wadhwani, P. *et al.* Dynamical structure of the short multifunctional peptide BP100 in membranes. *Biochimica et Biophysica Acta (BBA) - Biomembranes* **1838**, 940–949 (2014).
18. Misiewicz, J. *et al.* Action of the multifunctional peptide BP100 on native biomembranes examined by solid-state NMR. *J Biomol NMR* **61**, 287–98 (2015).
19. Grau-Campistany, A., Strandberg, E., Wadhwani, P., Rabanal, F. & Ulrich, A. S. Extending the Hydrophobic Mismatch Concept to Amphiphilic Membranolytic Peptides. *Journal of Physical Chemistry Letters* **7**, 1116–1120 (2016).
20. Grau-Campistany, A. *et al.* Hydrophobic mismatch demonstrated for membranolytic peptides and their use as molecular rulers to measure bilayer thickness in native cells. *Scientific Reports 2015 5:1* **5**, 1–9 (2015).
21. Manzini, M. C. *et al.* Peptide:Lipid ratio and membrane surface charge determine the mechanism of action of the antimicrobial peptide BP100. Conformational and functional studies. *Biochim Biophys Acta Biomembr* **1838**, 1985–1999 (2014).
22. Melo, M. N., Ferre, R. & Castanho, M. A. R. B. Antimicrobial peptides: linking partition, activity and high membrane-bound concentrations. *Nature Reviews Microbiology 2009 7:3* **7**, 245–250 (2009).
23. Shai, Y. Mechanism of the binding, insertion and destabilization of phospholipid bilayer membranes by α-helical antimicrobial and cell non-selective membrane-lytic peptides. *Biochimica et Biophysica Acta (BBA) - Biomembranes* **1462**, 55–70 (1999).
24. Carretero, G. P. B. *et al.* Synthesis, biophysical and functional studies of two BP100 analogues modified by a hydrophobic chain and a cyclic peptide. *Biochim Biophys Acta Biomembr* **1860**, 1502–1516 (2018).
25. Mink, C. *et al.* Overlapping Properties of the Short Membrane-Active Peptide BP100 With (i) Polycationic TAT and (ii) α-helical Magainin Family Peptides. *Front Cell Infect Microbiol* **11**, 350 (2021).
26. Palmer, N., Maasch, J. R. M. A., Torres, M. D. T. & de La Fuente-Nunez, C. *Molecular Dynamics for Antimicrobial Peptide Discovery.* https://doi.org/10 (2021).
27. Leontiadou, H., Mark, A. E. & Marrink, S. J. Antimicrobial peptides in action. *J Am Chem Soc* **128**, 12156–12161 (2006).
28. Wang, Y., Chen, C. H., Hu, D., Ulmschneider, M. B. & Ulmschneider, J. P. Spontaneous formation of structurally diverse membrane channel architectures from a single antimicrobial peptide. *Nature Communications 2016 7:1* **7**, 1–9 (2016).
29. Bond, P. J., Parton, D. L., Clark, J. F. & Sansom, M. S. P. Coarse-Grained Simulations of the Membrane-Active Antimicrobial Peptide Maculatin 1.1. *Biophys J* **95**, 3802–3815 (2008).
30. Thøgersen, L., Schiøtt, B., Vosegaard, T., Nielsen, N. C. & Tajkhorshid, E. Peptide Aggregation and Pore Formation in a Lipid Bilayer: A Combined Coarse-Grained and All Atom Molecular Dynamics Study. *Biophys J* **95**, 4337–4347 (2008).
31. Rzepiela, A. J., Sengupta, D., Goga, N. & Marrink, S. J. Membrane poration by antimicrobial peptides combining atomistic and coarse-grained descriptions. *Faraday Discuss* **144**, 431–443 (2009).

32. Santo, K. P. & Berkowitz, M. L. Difference between magainin-2 and melittin assemblies in phosphatidylcholine bilayers: Results from coarse-grained simulations. *Journal of Physical Chemistry B* **116**, 3021–3030 (2012).
33. Su, J., Marrink, S. J. & Melo, M. N. Localization Preference of Antimicrobial Peptides on Liquid-Disordered Membrane Domains. *Front Cell Dev Biol* **8**, 350 (2020).
34. Badosa, E. *et al.* A library of linear undecapeptides with bactericidal activity against phytopathogenic bacteria. *Peptides (N.Y.)* **28**, 2276–2285 (2007).
35. Park, P. *et al.* Binding and Flip as Initial Steps for BP-100 Antimicrobial Actions. *Sci Rep* **9**, 8622 (2019).
36. Franco, L. R. *et al.* Simulations reveal that antimicrobial BP100 induces local membrane thinning, slows lipid dynamics and favors water penetration. *RSC Adv* **12**, 4573–4588 (2022).
37. Miao, X. *et al.* Enhanced cell selectivity of hybrid peptides with potential antimicrobial activity and immunomodulatory effect. *Biochim Biophys Acta Gen Subj* **1864**, (2020).
38. Woolley, G. A. & Deber, C. M. Peptides in membranes: Lipid-induced secondary structure of substance P. *Biopolymers* **26**, S109–S121 (1987).
39. Konno, K. *et al.* Decoralin, a novel linear cationic α-helical peptide from the venom of the solitary eumenine wasp Oreumenes decoratus. *Peptides (N.Y.)* **28**, 2320–2327 (2007).
40. Rinaldi, A. C. *et al. Temporin L : antimicrobial, haemolytic and cytotoxic activities, and effects on membrane permeabilization in lipid vesicles. Biochem. J* vol. 368 http://portlandpress.com/biochemj/article-pdf/368/1/91/710197/bj3680091.pdf (2002).
41. Carotenuto, A. *et al.* A different molecular mechanism underlying antimicrobial and hemolytic actions of temporins A and L. *J Med Chem* **51**, 2354–2362 (2008).
42. Zhao, H. & Kinnunen, P. K. J. Binding of the antimicrobial peptide temporin L to liposomes assessed by Trp fluorescence. *Journal of Biological Chemistry* **277**, 25170–25177 (2002).
43. Guerra, M. E. R. *et al.* MD simulations and multivariate studies for modeling the antileishmanial activity of peptides. *Chem Biol Drug Des* **90**, 501–510 (2017).
44. Wang, G., Li, X. & Wang, Z. APD3: The antimicrobial peptide database as a tool for research and education. *Nucleic Acids Res* **44**, D1087–D1093 (2016).
45. Van Der Spoel, D. *et al.* GROMACS: Fast, flexible, and free. *J Comput Chem* **26**, 1701–1718 (2005).
46. Hess, B., Kutzner, C., van der Spoel, D. & Lindahl, E. GROMACS 4: Algorithms for Highly Efficient, Load-Balanced, and Scalable Molecular Simulation. *J Chem Theory Comput* **4**, 435–447 (2008).
47. Abraham, M. J. *et al.* GROMACS: High performance molecular simulations through multi-level parallelism from laptops to supercomputers. *SoftwareX* **1**, 19–25 (2015).
48. Beauchamp, K. A., Lin, Y. S., Das, R. & Pande, V. S. Are protein force fields getting better? A systematic benchmark on 524 diverse NMR measurements. *J Chem Theory Comput* **8**, 1409–1414 (2012).

49. Jämbeck, J. P. M. & Lyubartsev, A. P. Derivation and Systematic Validation of a Refined All-Atom Force Field for Phosphatidylcholine Lipids. *J Phys Chem B* **116**, 3164–3179 (2012).
50. Jämbeck, J. P. M. & Lyubartsev, A. P. Another Piece of the Membrane Puzzle: Extending Slipids Further. *J Chem Theory Comput* **9**, 774–784 (2013).
51. Jämbeck, J. P. M. M. & Lyubartsev, A. P. An extension and further validation of an all-atomistic force field for biological membranes. *J Chem Theory Comput* **8**, 2938–2948 (2012).
52. Konno, K. *et al.* Decoralin, a novel linear cationic α-helical peptide from the venom of the solitary eumenine wasp Oreumenes decoratus. *Peptides (N.Y.)* **28**, 2320–2327 (2007).
53. Kim, S. J. *et al.* Structural characterization of de novo designed L5K5W model peptide isomers with potent antimicrobial and varied hemolytic activities. *Molecules* **18**, 859–876 (2013).
54. Martinez, L. *et al.* PACKMOL: A package for building initial configurations for molecular dynamics simulations. *J Comput Chem* **30**, 2157–2164 (2009).
55. Hess, B., Bekker, H., Berendsen, H. J. C. & Fraaije, J. G. E. M. LINCS: A Linear Constraint Solver for Molecular Simulations. *J Comput Chem* **18**, 1463–1472 (1997).
56. Essmann, U. *et al.* A smooth particle mesh Ewald method. *J Chem Phys* **103**, 8577 (1995).
57. Bussi, G., Donadio, D. & Parrinello, M. Canonical sampling through velocity rescaling. *Journal of Chemical Physics* **126**, (2007).
58. Santos, D. E. S., Pontes, F. J. S., Lins, R. D., Coutinho, K. & Soares, T. A. SuAVE: A Tool for Analyzing Curvature-Dependent Properties in Chemical Interfaces. *J Chem Inf Model* (2019) doi:10.1021/acs.jcim.9b00569.
59. Vries, A. H. De. The MARTINI Force Field: Coarse Grained Model for Biomolecular Simulations. 7812–7824 (2007) doi:10.1021/jp071097f.
60. Monticelli, L. *et al.* The MARTINI Coarse-Grained Force Field : Extension to Proteins. 819–834 (2008).
61. Souza, P. C. T. *et al.* Martini 3: a general purpose force field for coarse-grained molecular dynamics. *Nat Methods* **18**, 382–388 (2021).
62. Kroon, P. C. *et al.* Martinize2 and Vermouth: Unified Framework for Topology Generation. (2022).
63. Jo, S., Kim, T., Iyer, V. G. & Im, W. CHARMM-GUI: A web-based graphical user interface for CHARMM. *J Comput Chem* **29**, 1859–1865 (2008).
64. Qi, Y. *et al.* CHARMM-GUI Martini Maker for Coarse-Grained Simulations with the Martini Force Field. *J Chem Theory Comput* **11**, 4486–4494 (2015).
65. Parrinello, M. & Rahman, A. Polymorphic transitions in single crystals: A new molecular dynamics method. *J Appl Phys* **52**, 7182–7190 (1981).
66. De Jong, D. H., Baoukina, S., Ingólfsson, H. I. & Marrink, S. J. Martini straight: Boosting performance using a shorter cutoff and GPUs. *Comput Phys Commun* **199**, 1–7 (2016).
67. Manzo, G. *et al.* Temporin L and aurein 2.5 have identical conformations but subtly distinct membrane and antibacterial activities. *Sci Rep* **9**, (2019).

68. Wadell, H. Volume, Shape, and Roundness of Quartz Particles. *https://doi.org/10.1086/624298* (1935) doi:10.1086/624298.
69. Lee, M. T., Hung, W. C., Chen, F. Y. & Huang, H. W. Mechanism and kinetics of pore formation in membranes by water-soluble amphipathic peptides. *Proc Natl Acad Sci U S A* **105**, 5087–5092 (2008).
70. Grage, S. L., Afonin, S., Kara, S., Buth, G. & Ulrich, A. S. Membrane thinning and thickening induced by membrane-active amphipathic peptides. *Front Cell Dev Biol* **4**, (2016).
71. Zamora-Carreras, H. *et al.* Alanine scan and 2H NMR analysis of the membrane-active peptide BP100 point to a distinct carpet mechanism of action. *Biochimica et Biophysica Acta (BBA) - Biomembranes* **1858**, 1328–1338 (2016).
72. Woo, H. J. & Wallqvist, A. Spontaneous buckling of lipid bilayer and vesicle budding induced by antimicrobial peptide magainin 2: A coarse-grained simulation study. *Journal of Physical Chemistry B* **115**, 8122–8129 (2011).
73. Zhang, S. *et al.* Structure and formation mechanism of antimicrobial peptides temporin b-and l-induced tubular membrane protrusion. *Int J Mol Sci* **22**, 11015 (2021).
74. Miyazaki, Y. & Shinoda, W. Cooperative antimicrobial action of melittin on lipid membranes: A coarse-grained molecular dynamics study. *Biochim Biophys Acta Biomembr* **1864**, (2022).
75. Safinya, C. R. & Rädler, J. O. *Handbook of Lipid Membranes; Molecular, Functional, and Materials Aspects*.
76. Zemel, A., Ben-Shaul, A. & May, S. Modulation of the spontaneous curvature and bending rigidity of lipid membranes by interfacially adsorbed amphipathic peptides. *Journal of Physical Chemistry B* **112**, 6988–6996 (2008).
77. Tytler, E. M. *et al.* Reciprocal effects of apolipoprotein and lytic peptide analogs on membranes. Cross-sectional molecular shapes of amphipathic alpha helixes control membrane stability. *Journal of Biological Chemistry* **268**, 22112–22118 (1993).
78. Epand, R. M., Shai, Y., Segrest, J. P. & Anantharamiah, G. M. Mechanisms for the modulation of membrane bilayer properties by amphipathic helical peptides. *Biopolymers* **37**, 319–338 (1995).
79. Decker, A. P., Mechesso, A. F. & Wang, G. Expanding the Landscape of Amino Acid-Rich Antimicrobial Peptides: Definition, Deployment in Nature, Implications for Peptide Design and Therapeutic Potential. *Int J Mol Sci* **23**, (2022).
80. Srivastava, S., Kumar, A., Tripathi, A. K., Tandon, A. & Ghosh, J. K. Modulation of anti-endotoxin property of Temporin L by minor amino acid substitution in identified phenylalanine zipper sequence. *Biochemical Journal* **473**, 4045–4062 (2016).
81. Bennett, W. F. D. & Tieleman, D. P. Water defect and pore formation in atomistic and coarse-grained lipid membranes: Pushing the limits of coarse graining. *J Chem Theory Comput* **7**, 2981–2988 (2011).
82. Humphrey, W., Dalke, A. & Schulten, K. VMD: Visual molecular dynamics. *J Mol Graph* **14**, 33–38 (1996).
83. Pettersen, E. F. *et al.* UCSF ChimeraX: Structure visualization for researchers, educators, and developers. *Protein Science* **30**, 70–82 (2021).

# 4.7. Supplementary Material

| | | **BP100** | **Decoralin** | **NK-1** | **Temporin** |
|---|---|---|---|---|---|
| Sequence | | KKLFKKILKYL | SLLSLIRKLIT | RPKPQQFFGLM | FVQWFSKFLGRIL |
| Amino acids | | 11 | 11 | 11 | 13 |
| Overall charge | | +6 | +3 | +3 | +3 |
| <H> Hydrophobicity | | 0.427 | 0.780 | 0.501 | 0.906 |
| Amino acid composition | Polar | 5 (45.45%) | 5 (27.78%) | 5 (27.78%) | 5 (27.78%) |
| | Non-Polar | 6 (54.54%) | 6 (33.33%) | 6 (33.33%) | 8 (44.44%) |
| | Charged | 5 (45.45%) | 3 (27.27%) | 2 (18.18%) | 3 (27.27%) |
| | Aromatic | 2 (18.18%) | 0 (0%) | 2 (18.18%) | 4 (30.76%) |

**Table S1:** Structural properties of the antimicrobial peptides studied. The hydrophobicity <H> was calculated using the Fauchere-Pliska scale[1].

## Secondary Structure in Water

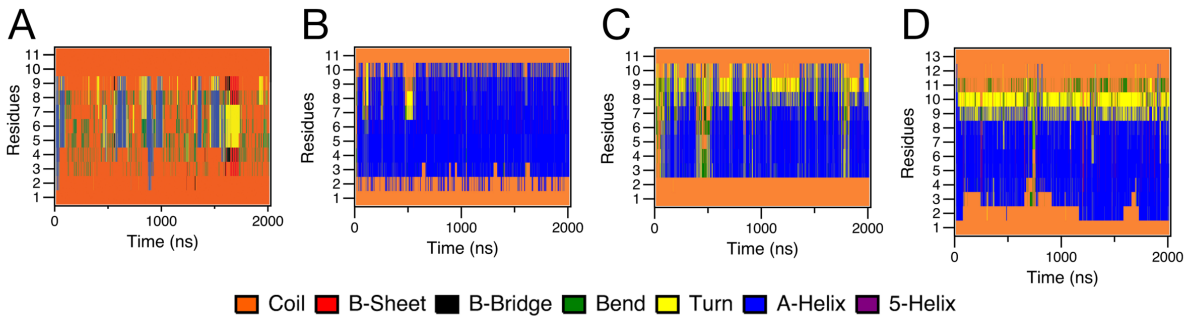


| BP100 | Decoralin | Neurokinin-1 | Temporin |
|---|---|---|---|
| Helicity (%) | | | |
| 9 | 65 | 49 | 49 |
| Random Coil (%) | | | |
| 67 | 29 | 36 | 36 |

**Figure S1:** Secondary structure analysis (DSSP) of peptides in water from atomistic simulations. BP100 (A), Decoralin (B), NK-1 (C), and Temporin-L (D). The table below shows the respective percentage of helicity obtained from the DSSP analysis.

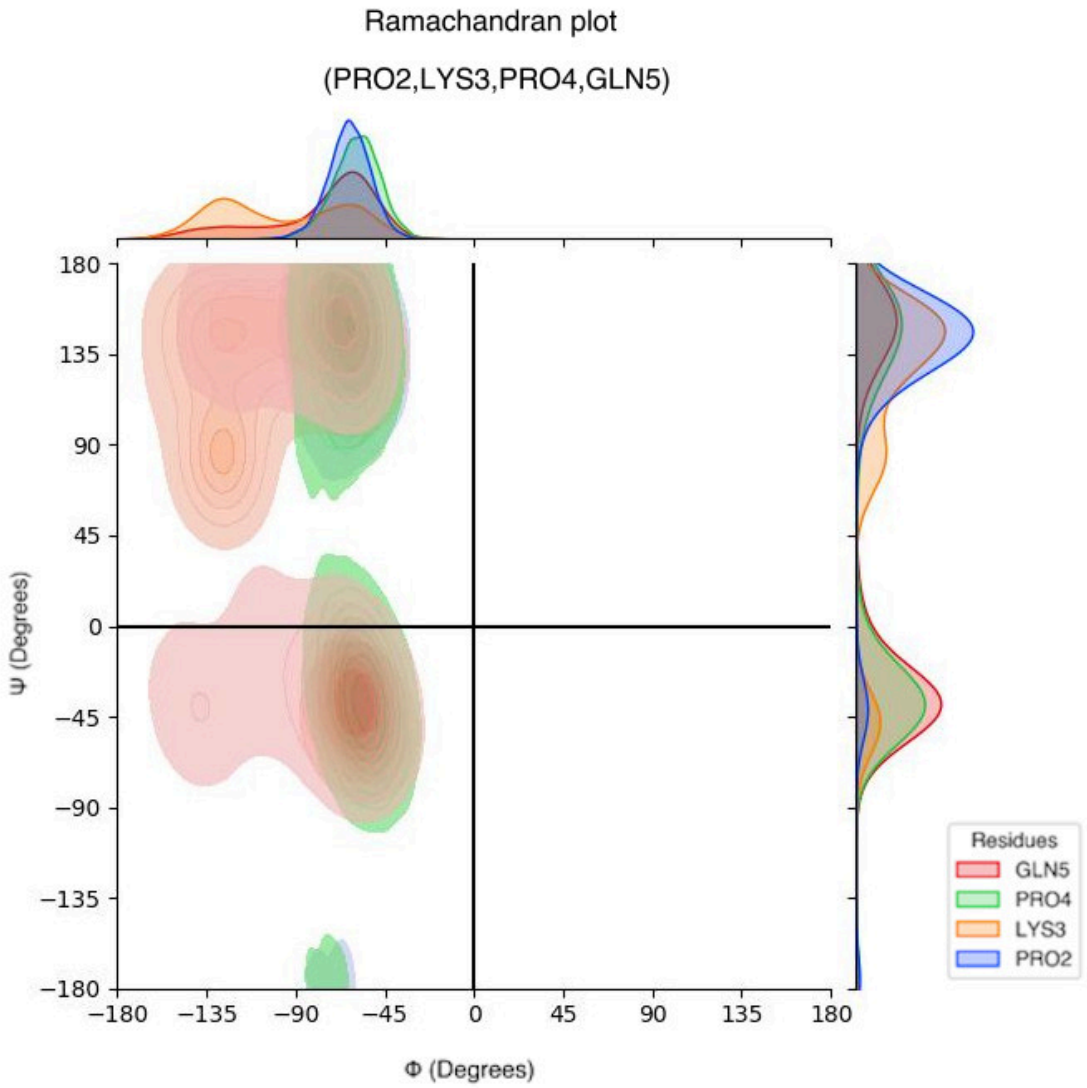


**Figure S2:** Ramachandran plot and respective histograms for NK-1 N-terminus region from the atomistic simulation in POPC/POPG membrane. The plot reveals the region has higher flexibity, as in a random coil conformation, which means residues can occupy randomly different regions of the graph at different times[2], with some restrictions due to the more rigid nature of proline, given that it can only bend at a range of roughly -90 to -45 degrees along the $\phi$ axis[3]. For example, GLN5 occupies regions typically associated with beta sheets, PPII helices and alpha helices[4].

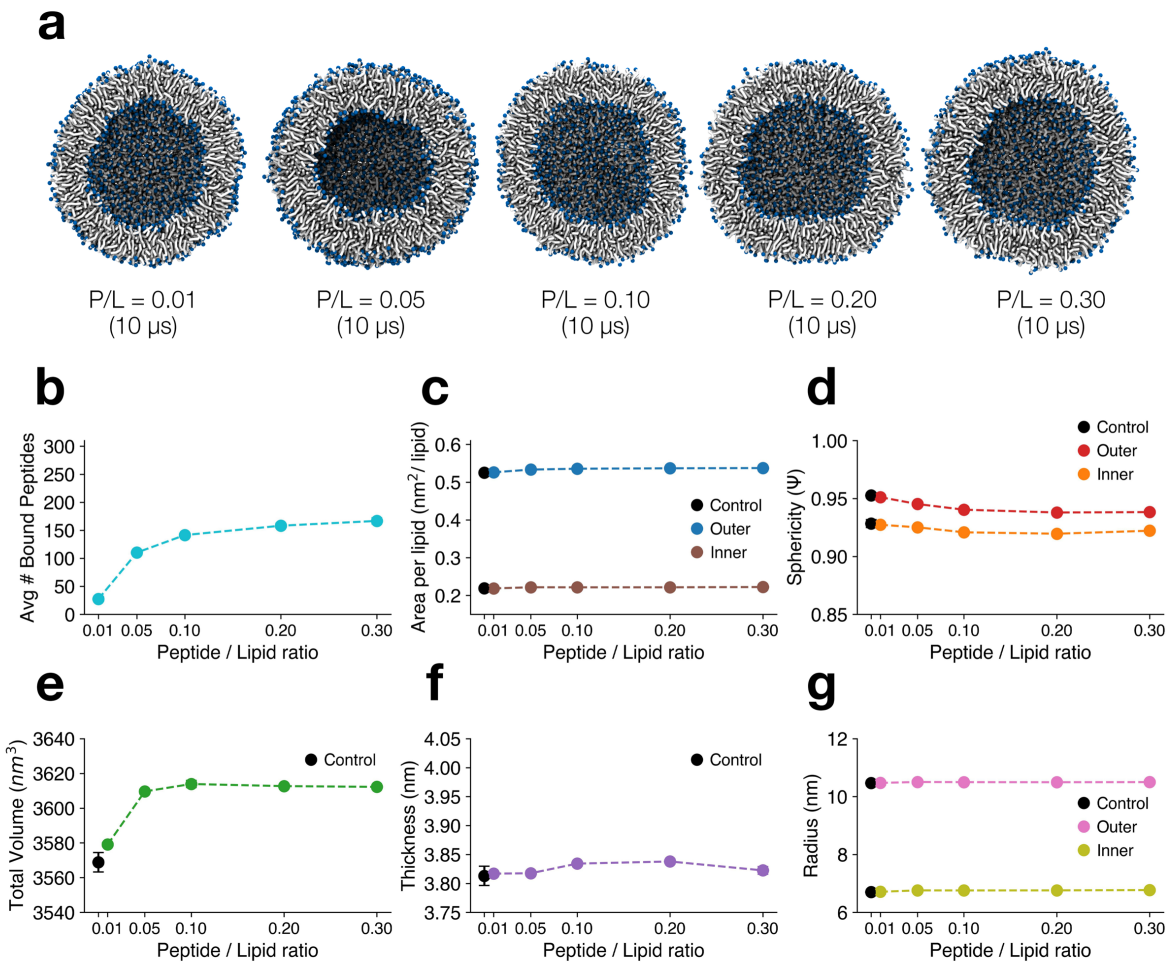


**Figure S3: Simulations of BP100 in POPC vesicles.**
(a) Cut-away cross-sectional last frame snapshots of POPC vesicle/BP100 system at low (P/L = 0.01 and 0.05), medium (P/L = 0.10), and high (P/L = 0.20 and 0.30) concentrations. Peptides, water and ions are not shown for clarity. Obtained averaged peptide binding outcomes in vesicles according to the respective P/L are presented (b-g). Data points with no error bars had an error below 5%. Data points and error bars were obtained averaging the last 5μ of each simulation.

| System | $APL_{out}$ ($nm^2$/lipid) | $APL_{in}$ ($nm^2$/lipid) | $V_{total}$ ($nm^3$) | $D_{HH}$ (nm) | R (nm) | $\varphi$ |
|---|---|---|---|---|---|---|
| Control | 0.525 | 0.219 | 3568 | 3.81 | 10.4 | 0.952 |
| P/L = 0.01 | +0.19% | -0.17% | +0.29% | -0.17% | +0.07% | -0.15% |
| P/L = 0.05 | +1.54% | +1.24% | +1.14% | +1.24% | +0.37% | -0.78% |
| P/L = 0.10 | +1.99% | +1.16% | +1.26% | +1.16% | +0.32% | -1.29% |
| P/L = 0.20 | +2.20% | +1.18% | +1.23% | +1.18% | +0.30% | -1.54% |
| P/L = 0.30 | +2.32% | +1.52% | +1.22% | +1.52% | +0.34% | -1.50% |

**Table S2:** Summary of vesicle structural properties from BP100 in POPC vesicle simulations. Variation in percentage of POPC vesicle structural properties compared to control.

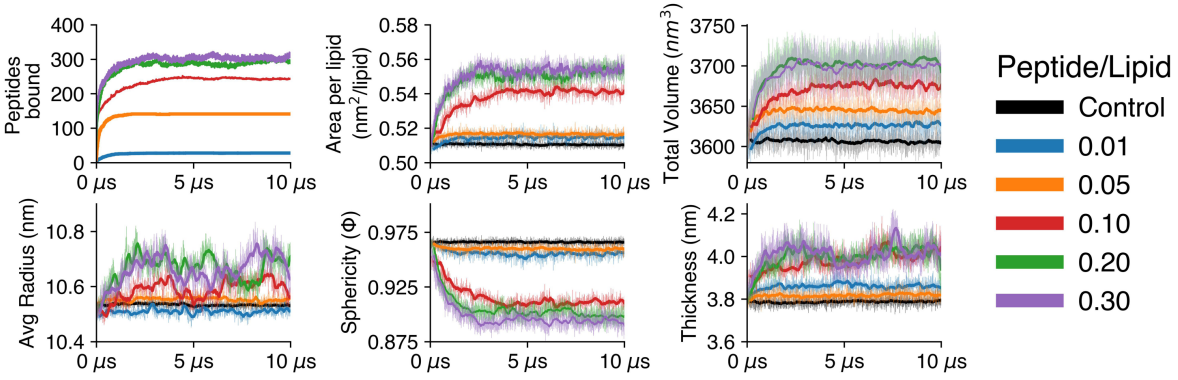


**Figure S4:** Temporal analysis of vesicle structural properties from BP100 in POPC:POPG (50:50) vesicle simulations.

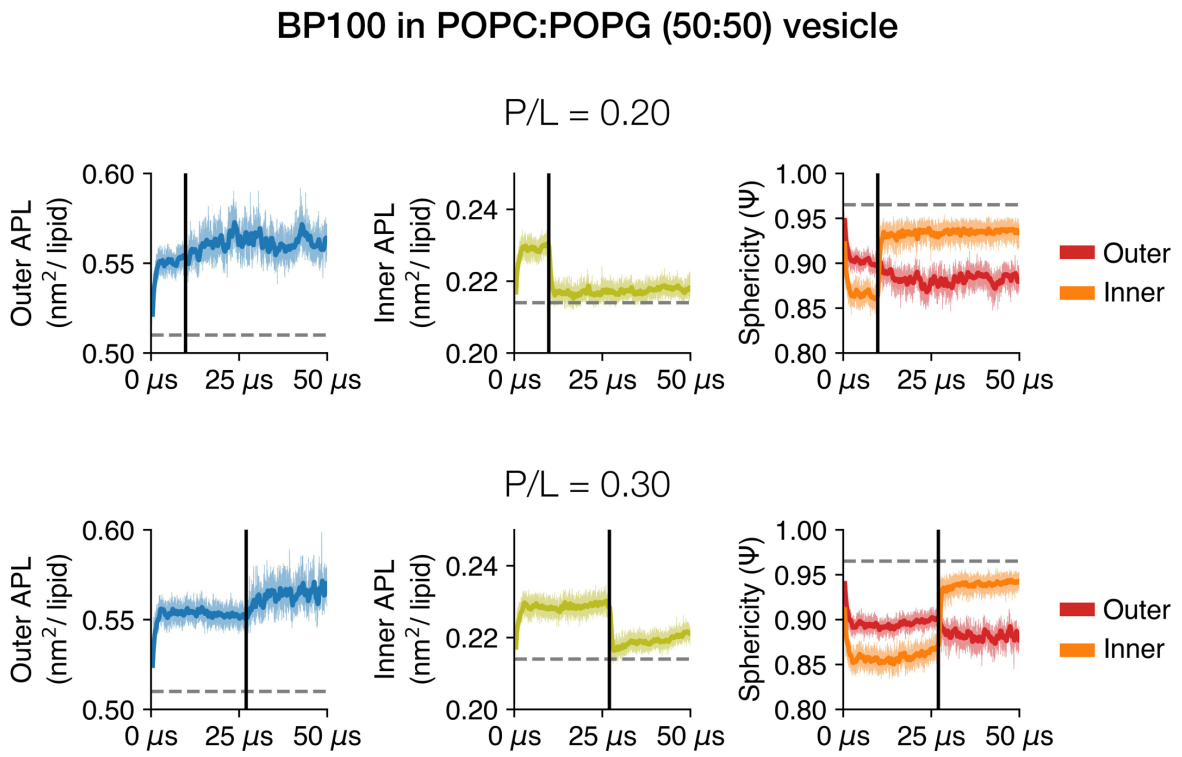


**Figure S5:** Vesicle outer and inner area per lipid and sphericity for P/L = 0.20 and P/L = 0.30 simulations (BP100 in POPC:POPG (50:50)). Black vertical lines mark when budding was detected and dotted horizontal lines indicate outer and inner control values for each property.

# 4.8. Supplementary Material References

1. Fauchere, J.-L. & Pliska, V. Hydrophobic parameters of pi amino-acid side chains from the partitioning of N-acetyl-amino-acid amides. *Eur. 1. Med. Chem. Chim. Ther.* **18,** 369-375 (1983).
2. Schweitzer-Stenner, R. (2012). Conformational propensities and residual structures in unfolded peptides and proteins. In *Molecular BioSystems* (Vol. 8, Issue 1, pp. 122–133). https://doi.org/10.1039/c1mb05225j
3. Adzhubei, A. A., & Sternberg, M. J. E. (1993). Left-handed Polyproline II Helices Commonly Occur in Globular Proteins. *Journal of Molecular Biology*, *229*(2), 472–493. https://doi.org/10.1006/jmbi.1993.1047
4. Hollingsworth, S. A., & Karplus, P. A. (2010). A fresh look at the Ramachandran plot and the occurrence of standard structures in proteins. In *Biomolecular Concepts* (Vol. 1, Issues 3–4, pp. 271–283). De Gruyter Mouton. https://doi.org/10.1515/bmc.2010.022

# Chapter 5

# Other projects

## Violacein Targets the Cytoplasmic Membrane of Bacteria

This article can be found in
https://doi.org/10.1021/acsinfecdis.8b00245

## Abstract

Violacein is a tryptophan-derived purple pigment produced by environmental bacteria, which displays multiple biological activities, including strong inhibition of Gram-positive pathogens. Here, we applied a combination of experimental approaches to identify the mechanism by which violacein kills Gram-positive bacteria. Fluorescence microscopy showed that violacein quickly and dramatically permeabilizes *B. subtilis* and *S. aureus* cells. Cell permeabilization was accompanied by the appearance of visible discontinuities or rips in the cytoplasmic membrane, but it did not affect the cell wall. Using in vitro experiments, we showed that violacein binds directly to liposomes made with commercial and bacterial phospholipids and perturbs their structure and permeability. Furthermore, molecular dynamics simulations were employed to reveal how violacein inserts itself into lipid bilayers. Thus, our combined results demonstrate that the cytoplasmic membrane is the primary target of violacein in bacteria. The implications of this finding for the development of violacein as a therapeutic agent are discussed.

# Position matters in ester thiolysis by cysteine-containing peptides in micelles and vesicles

*Submitted*

## Abstract

**Hypothesis.** The interaction of peptides with nanoaggregates is an active research topic. Cysteine (Cys)-containing peptides open opportunities for developing low molecular weight compounds with interesting properties and potential applications. Knowledge of the relationship between the position of the Cys in the peptides and the aggregate interface is essential. **Experiments.** We synthesized a series of Cys-containing peptides having variable number of glycines (Gly) as spacers between the hexadecyl amide chain at their N-terminal portion and Cys at their carboxy-terminal. The apparent pKa of the Cys-thiol group of each peptide was measured in micelles of CTAC (hexadecyltrimethyl ammonium chloride) and vesicles of DHDAC (dihexadecyldimethyl ammonium chloride). No clear correlation existed between the pKa´s and the number of Gly in the peptides. However, the rate of p-nitro-phenyl-octanoate (NPO) thiolysis by the peptides in micelles and vesicles decreased regularly with peptide length. Molecular Dynamics (MD) analysis of the peptides in CTAC micelles was carried out. **Findings.** pKa determinations and rate dependance of the peptides in a thiolysis reaction and MD analysis strongly suggested that the higher rates observed with shorter peptides can be attributed to an increased probability of Cys be located below the micellar surface, where the carbonyl reaction center of NPO resides.

# Acknowledgements

Agradeço a Deus pelo dom da vida.
Por ser Ele o meu bom pastor e castelo forte.

A meus queridos e amados pais, Han Jin e Seung Oui.
Por serem meus fiéis conselheiros, ouvintes e apoiadores.

A meus orientadores, "psora" Iolanda e "psor" Hernan.
Por terem me lapidado num pequeno cientista.
O aprendizado e crescimento que obtive durante meus anos no laboratório foram excepcionais e de grande proveito.
Foi uma honra e privilégio ter sido aluno dos senhores.

A meu co-orientador, prof. Filipe da Silva Lima.
Por ter me proporcionado a base teórica e prática em Dinâmica Molecular.
E pelas conversas e amizade.

A meus colegas que estiveram presentes nessa jornada:
Laura Mortara, Gustavo Battesini, Valdomiro Vagner, Carol Lacerda, Matheus Cortez e Leandro Rezende.
Foi um prazer conviver com vocês e obrigado pela companhia e amizade.

Ao prof. Siewert Marrink,
Pela oportunidade de realizar estágio em seu laboratório durante o BEPE.

A FAPESP, pelo apoio financeiro por meio dos grants 2019/03023-8 e 2019/26557-8.

À Superintendência de Tecnologia da Informação da USP, pelos recursos computacionais disponibilizados.

Ao IQUSP e à USP e a todos os seus funcionários.

A todos, os meus sinceros agradecimentos.

# Peter Park

São Paulo, Brazil
+55 11 99968-2827
peterprk0@gmail.com

## Education

**(2017 - 2023)** **Ph.D., Biochemistry**
University of São Paulo, Brazil

**(Sep 2020 - Oct 2021)** **Visiting Researcher**
The University of Groningen, the Netherlands

**(2011 - 2016)** **B.Sc. Pharmacy**
University of São Paulo, Brazil

**(Sep 2013 - Oct 2014)** **Visiting Student**
Seoul National University, South Korea

## Research Experience

**(2017 - Present)** **Ph.D. project**
Supervisor: Prof. Iolanda Midea Cuccovia (University of São Paulo, Brazil)

***Elucidating antimicrobial peptide BP100 initial interaction with membranes using Molecular Dynamics***
Based on experimental results obtained in our lab, I performed all-atom simulations of BP100 on bilayers at low peptide concentration. I have successfully described the initial steps of the peptide binding to membranes on a molecular level, which included initial electrostatic interaction, peptide rotation, dehydration and insertion into the membrane (ref 2). Membrane analysis confirmed the local activity of the peptide, with membrane thinning and negative curvature (ref 3).

**(Sep 2020 -Oct 2021)** **Visiting Researcher**
Supervisor: Prof. Siewert Jan Marrink (University of Groningen - Netherlands)

***Coarse-graining analysis of the interaction of BP100 with lipid vesicles***
Using the Martini3 forcefield I explored the effects of higher concentrations of BP100 on lipid vesicles, exploring the vesicle shape alterations and peptide binding. Through the simulations, I could suggest that BP100 and possibly similar peptides act via the carpet mechanism at medium and high concentrations. Simultaneously, I contributed in developing the enhanced GoMartini model in MARTINI3 to better sample the secondary structure of Intrinsically Disordered Proteins, resulting in publication (ref 4).

## Languages

| Portuguese | English | Spanish | Korean |
|---|---|---|---|
| Native | Fluent | Proficient | Intermediate |

## Key skills

**Computational**

I use **Python** for the analysis of both experimental and computational data. I have designed and written my analysis code. I am particularly familiar with MDAnalysis, Numpy, Pandas, Seaborn, and Matplotlib libraries.

I use **Bash** scripting for various UNIX tasks and data analysis

I use **Gromacs** for simulating and analyzing my simulations. I have used all-atom (ff99sb-ildn-NMR and SLipids) and coarse-grained (Martini) forcefields.

I use the Visual Molecular Dynamics (**VMD**) software for simulation visualization and image rendering.

**High-performance computing:** I am a regular user of the Dutch National Supercomputer Snellius, the University of São Paulo cluster (LINCE), and the University of Groningen cluster (Peregrine).

**Teaching**

Supervision of undergraduate project students working in our lab for computational projects. I carried out the students' project design, development, computational training, and thesis review.

From 2014 to 2020, I worked as a private Portuguese language tutor for international students, preparing them for the CELPE-Bras certificate of proficiency.

## Other professional skills and experience

**Communication**

- Biochemistry Department Seminars at IQUSP (2019) - *Oral presentation*
- CNRE, Institut de Biologie et Chimie des Protéines, Lyon, France (2021) - *Oral presentation*
- Best poster award - SBBq, Brazilian Society for Biochemistry and Molecular Biology (2017)
- First author publications (refs 2,3,6,7)
- Worked with external collaborators leading to publications (refs 1-7)

**Courses attended**

- Programming with Python for Life Sciences (2021) - University of Groningen
- Martini3 online workshop (2021)
- São Paulo School of Advanced Science of Colloids (SPSAS on Colloids - 2018)

**Extras**

- Experience with image and video editing
    - Adobe Photoshop, Lightroom, and Premiere Pro
    - Final Cut Pro
    - VMD, UCSF ChimeraX, and Blender

## Publications

1. Cauz, A. C. G.; Carretero, G. P. B.; Saraiva, G. K. V.; **Park, P.**; Mortara, L.; Cuccovia, I. M.; Brocchi, M.; Gueiros-Filho, F. J. *Violacein Targets the Cytoplasmic Membrane of Bacteria. ACS Infect. Dis.* (2019)

2. **Park, P.**; Franco, L.R.; Chaimovich, H; Coutinho, K.; Cuccovia, I.M.; Lima, F.S. *Binding and Flip as Initial Steps for BP-100 Antimicrobial Actions. Sci. Rep, 9 (1), 8622. (2019)*

3. Franco, L. R.*; **Park, P.***; Chaimovich, H.; Coutinho, K.; Cuccovia, I. M.; Lima, F. S. *Simulations Reveal That Antimicrobial BP100 Induces Local Membrane Thinning, Slows Lipid Dynamics and Favors Water Penetration*. RSC Adv. 12 (8), 4573–4588. (2022)

* Authors contributed equally

4. Souza, P.C.T.; Moreira, R.A.; **Park, P.**; Poma, A.B.; Thallmair S., Marrink, S.J. *Virtual-Site Implementation of an Enhanced GōMartini Model: From Local to Large-Scale conformational Changes in Proteins.* **(In preparation)**

5. Lacerda, C.D.; Juliano, M.A.; Liria, C.W. , Machini, M.T.; **Park, P.**; Matsubara, D.K.; Barzotto, D.R.; Lima, F.S., Chaimovich, H.; Cuccovia, I.M. *Position matters in ester thiolysis by cysteine-containing peptides in micelles and vesicles. Colloids and Surfaces A* **(Submitted)**

6. **Park, P.**; Chaimovich H.; Cuccovia, I.M.; Lima, F.S. *Antimicrobial BP100 induces membrane budding and membrane rupture at high peptide:lipid ratio*. **(In preparation)**

7. **Park, P.**; Barzotto, D.R.; Matsubara, D.K.; Chaimovich H.; Cuccovia, I.M.; Lima, F.S. *Simulations suggest common carpet mechanism for short amphiphilic antimicrobial peptides*. **(In preparation)**